LOT project
-
Long Term Test of Buffer Material

Parcel A2 field and laboratory draft report

Main Report

Ola Karnland, Siv Olsson, Ann Dueck, Martin Birgersson, Ulf Nilsson,

Clay Technology AB, Lund

Appendices

Bacteria: Karsten Pedersen, Micans Laboratory AB and Göteborgs University

Tracer diffusion: Sara Eriksson and Trygve Eriksen, KTH

Copper corrosion: Bo Rosborg, Stockholm University and Rosborg consulting

Water analyses: Arto Muurinen, VTT

Mineralogy ANDRA: D. Rousset, R. Mosser-Ruck, M. Cathelineau, G2R
F. Villiéras, M. Pelletier, LEM

Mineralogy BGR: Stephan Kaufold, BGR

Mineralogy NAGRA: Raúl Fernández, Urs Mäder, Margarita Koroleva, University of Bern

September 2008

Key words: Bacteria, Bentonite, Buffer, Clay, Copper corrosion, Diffusion, Field experiment, LOT, Mineralogy, Montmorillonite, Physical properties, Radioactive waste, Repository, Äspö.

Table of Contents

List of Figures

List of Tables

1 BACKGROUND

1.1. General

Bentonite clay has been proposed as buffer material in several concepts for HLW repositories. In the Swedish KBS-3 concept the demands on the bentonite buffer are to serve as mechanical support for the canister, reduce the effects on the canister of a possible rock displacement, and minimize water flow over the deposition holes. The transport through the buffer is expected to be reduced principally to diffusion, both with respect to corrosive components in the groundwater and to corrosion products and escaping radionuclides in case of a canister failure.

Comprehensive research and development work has been carried out during the last twenty years in order to determine the basic behavior of unaltered bentonite material. The results have been reported in technical reports, and tentative computer codes concerning both unsaturated and saturated buffer conditions are at hand /e.g. Börgesson et al. 1995/. The models are believed to well describe the function of an unaltered MX-80 bentonite buffer after water saturation with respect to physical properties, e.g. swelling pressure, hydraulic conductivity and rheological behavior. Further, techniques for bentonite block production and application have been developed in order to fulfill the requirements concerning density, homogeneity, handling etc. /Johannesson 1995/.

The decaying power from the spent fuel in the HLW canisters will increase temperature and initially give rise to a thermal gradient over the bentonite buffer by which original water will be redistributed parallel to an uptake of water from the surrounding rock. A number of laboratory test series, made by different research groups, have resulted in various buffer alteration models /Karnland & Birgersson, 2006/. According to these models no significant alteration of the buffer is expected to take place at the prevailing physico-chemical conditions in a KBS3 repository neither during, nor after water saturation. The models may to a certain degree be validated in long term field tests. Former large scale field tests in Sweden, Canada, Switzerland and Japan have in different respects deviated from possible KBS-3 repository conditions and the testing periods have generally been dominated by initial processes, i.e. water uptake and temperature increase.

The present test series is consequently focused on the long term performance of the bentonite buffer, i.e. the conditions after water saturation, and on buffer related processes in a water saturated bentonite buffer concerning microbiology, cation transport, and copper corrosion. Long term in this context does of course not refer to the full time span of a repository. However, a considerable part of the heating period in a KBS3 repository is being covered with respect to kinetic reactions by the use of adverse conditions in the present A2 test parcel.

This report concerns the A2 parcel with respect to:

- background
- construction
- field results
- results from laboratory analyses of field exposed material concerning
    - physical properties
    - mineralogy

- bacterial activity
- tracer element diffusion
- copper corrosion

The mineralogical processes are not discussed in detail in this report, but will be reported separately within the separate LOT modeling project.

The project was initiated and is financed by SKB (Sweden). Posiva have contributed from project start by financing clay water analyses performed by VTT. As from the present A2 parcel also ANDRA (France), BGR (Germany) and Nagra (Switzerland) has joined the project by financing parallel independent mineralogical analyses performed by laboratories in these countries, respectively.

2 OBJECTIVES

2.1. General

The bentonite buffer material in the KBS-3 concept is a natural mixture of montmorillonite and several common accessory minerals, e.g. quartz, feldspar, calcite, siderite and pyrite. A fundamental demand on the buffer is that the desirable physico-chemical properties are preserved to a large extent during the lifetime of the repository. These properties e.g. low hydraulic conductivity, swelling ability and suitable rheological behavior, are mainly determined by the interaction between water and the smectite component in bentonite, which usually is montmorillonite. The stability of the montmorillonite mineral is therefore of vital importance for the buffer performance and is of main interest in this study. Also possible changes of the accessory minerals may be important though they may dissolve and precipitate and thereby change the rheological properties of the buffer material.

Main aspects of the previously accomplished LOT one year tests were to check that compaction, placement and water saturation did not significantly change the physical properties of the buffer. In this part of the project, i.e. medium term exposure to repository conditions, the main aspects are to check that the repository temperature and geochemical conditions after water saturation do not significantly change the physical properties of the buffer.

The test layout also makes it possible to study other important processes in the canister-buffer-rock system, bacteria activity, tracer element transport, copper corrosion and gas transport. A brief description of specific issues of interest is given in the following sections. The general objectives in the LOT test series may be summarized in the following items:

- Collect data for validation of models concerning buffer performance under quasi-steady state conditions after water saturation, e.g. swelling pressure, hydraulic conductivity and rheological properties.
- Check of existing models concerning buffer degrading processes, e.g. mineral redistribution and montmorillonite alteration.
- Produce data concerning “critical gas penetration pressure” and gas transport capacity. This option has not been used in the present A2 test parcel.
- Check of existing models concerning cation diffusion in bentonite.
- Collect information concerning survival, activity and migration of bacteria in bentonite under repository-like conditions.
- Check of calculated data concerning copper corrosion, and information regarding the character of possible corrosion products.
- Information, which may facilitate the realization of the full-scale test series (e.g. the Prototype project) with respect to clay preparation, instrumentation, data handling, termination, retrieval and evaluation.

2.2. Physical buffer properties

The clay/water system in a KBS-3 repository is expected to have well known physical properties. Vital properties for the buffer function are swelling pressure, hydraulic

conductivity and plasticity. These properties are basically determined by the interaction between the montmorillonite part of the buffer and water, and the properties may be expressed as a function of the final density of the buffer. A large number of data from laboratory tests are available in reports produced by SKB and corresponding organizations in other counties (e.g., AECL, ANDRA, ENRESA, NAGRA, PNC and Posiva).

A main hypothesis in this project is that the initial swelling pressure, hydraulic conductivity and plasticity of the water saturated bentonite material are well described and possible to predict for a KBS-3 construction by present laboratory results and models.

2.3. Buffer stability

2.3.1. General

One reason for choosing bentonite as buffer material is its long term stability in nature. It is frequently found in very old geological formations also in relation to the lifetime of a HLW repository. As an example, the Wyoming formation from which the commercial MX-80 bentonite is produced is from the Cretaceous period (~65 million years ago). However, in a future repository the bentonite will be exposed to a new environment with respect mainly to temperature and ground-water chemistry (Figure 2-1).

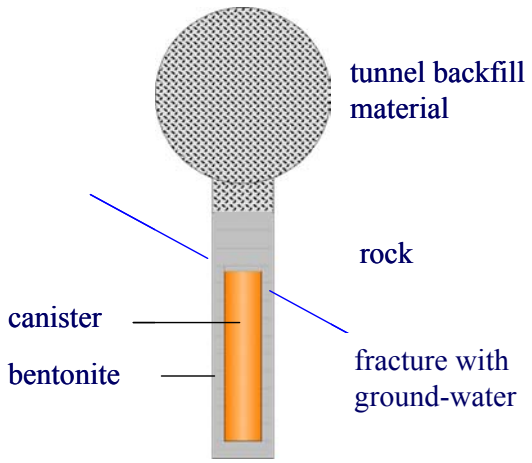

Figure 2-1 Schematic view of a cross section through a deposition tunnel and deposition hole in a KBS-3 repository.

The design criteria for the KBS-3 repository stipulate that the temperature should not exceed 100°C at any time or position in the buffer, including a safety margin of 10°C.

The expected temperature evolution has been calculated for the present repository layout to lead to a maximum temperature below 90°C, and a maximum temperature gradient below 24°C over the 0.35 m thick buffer material. (Figure 2-2), /Hökmark and Fälth, 2003/).

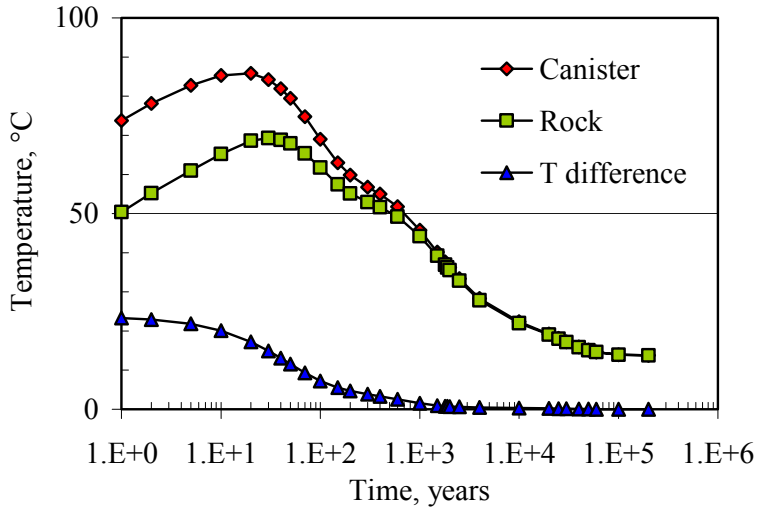

Figure 2-2 Calculated temperature evolution in a typical KBS-3 deposition hole showing the buffer temperatures at the interfaces to the canister and the rock, and the temperature gradient over the buffer. Calculated from data in /Hökmark and Fälth, 2003/.

Consequently, different alteration processes have been studied with respect to repository conditions. Further, and to a larger extent, much work has been made mainly in relation to oil exploration. A large number of articles concerning measured natural alteration and alteration models have been published over the last 50 years in scientific clay literature, e.g Clay Minerals, Clays and Clay Minerals, and Applied Clay Science, and several books have been written on this subject /Karnland and Birgersson, 2006/.

Chemical/mineralogical changes of possible importance in a KBS-3 repository may be listed as follows:

- Enrichment of substances emanating from the saturating groundwater
- Dissolution and precipitation of accessory minerals
- Montmorillonite surface reactions
  - ion exchange, e.g. from sodium to calcium
  - pH buffering of the montmorillonite
- Montmorillonite structural alteration,
  - in situ alteration e.g. into illite
  - incongruent dissolution, e.g. release of silica
  - congruent dissolution

Depending on the overall conditions and to what extent all these types of alterations may result in significant changed of the buffer physical properties.

2.3.2. Dissolution and precipitation of accessory minerals

Different enrichment processes of dissolved substances may take place due to the temperature gradient which prevails over the KBS-3 buffer during the first part of the deposition period. Precipitations may cement the buffer and change mainly the rheological properties of the buffer functions /Pusch et al., 1992/. One such possible

process is ion transport parallel to water uptake from the outer cooler parts of the bentonite, or from the surrounding groundwater, to the wetting front in the originally unsaturated bentonite. The transport is assumed to take place by a cyclic evaporation/condensation process in which water is sucked in from cooler parts, evaporates at the wetting front, and is partly redistributed in the form of steam. Dissolved salts will thereby be deposited at the wetting front.

A second possible process is precipitation of specimens, which have lower solubility at higher temperature, e.g. calcium sulfate (gypsum/anhydrite) and calcium carbonate (calcite). This process may take place also in a fully water saturated bentonite and the potential problem is consequently larger. The process will come to a standstill after limited enrichment if the buffer material alone is the source of the original pore water concentration. The total maximum effect will then be possible to calculate. On the other hand, if the surrounding groundwater is the source of substances then the enrichment process may continue until the precipitation stops due to spatial limitations.

According to laboratory experiments the following conditions reduces enrichment of easily dissolved minerals in a bentonite buffer /Karnland 1995:2/.

- High buffer density, no enrichment at KBS-3 buffer conditions,
- Low content of accessory minerals in the buffer,
- Low electrolyte content in the surrounding water,
- High water pressure.

The use of water pre-saturated bentonite blocks, supply of low electrolyte water in open slots, and a fast restoration of the hydrostatic pressure may consequently reduce mineral redistribution and enrichment in a KBS3-repository. No such preventive techniques were used in the present test series since the present tests aim to study the magnitude and consequences of such reactions. Instead, the initial water content was low and the slots were filled with groundwater in order to have conservative test conditions, i.e. to maximize the effects. Further, the processes were enhanced in the current A2 parcel by elevated temperature compared to KBS-3 conditions, and by placing reactive substances in specified positions in the parcel.

The hypothesis is that precipitation will be small and that no major cementation processes will take place at normal repository conditions.

2.3.3. Smectite-to-illite conversion

Depending on the conditions, alteration of minerals in the smectite group may take place and form a number of related minerals, e.g. illite, chlorite or zeolites. In nature the most common smectite alteration at elevated temperature is transformation into illite. This type of conversion has also been considered as the most probable, or rather least improbable, under repository conditions. Fortunately the smectite-to-illite reaction has been extensively studied for several decades because of its relevance to oil prospecting. Different parameters have been proposed as kinetic controlling factors but there is no basic consensus on the reactions involved in the conversion. Based on geological analogues and laboratory experiments i.a. the following factors have been proposed as kinetic controlling factors (no ranking):

- Overburden pressure /Weaver 1959/
- Temperature /Perry and Hower 1970/

- Potassium activity /Hower et al.,1976/
- Aluminum activity /Boles and Frank, 1979/
- pH /Eberl et al.,1993/
- Dehydration /Couture, 1985/, /Karnland et al.,1994/
- Silica activity /Abercrombie et al.,1994/

According to the Huang model /Huang et al.,1993/, the overall kinetics of the smectite-to-illite reaction can be described by the equation:

$$-dS/dt = A\cdot[K+]\cdot S^2 \exp(-Ea/RT) \quad \text{Equation 1}$$

where S is the smectite fraction in the illite/smectite material, A is frequency factor, Ea is activation energy and R is the universal gas constant, and T is temperature. After integration of $-dS/dt = A\cdot[K+]\cdot S^2 \exp(-Ea/RT)$, Equation 1, the smectite content at a certain time can be calculated if the temperature and potassium concentration in the pore water are known.

The potassium concentrations in the Äspö groundwater are measured to be in the range of a few ppm up to 80 ppm /Nilsson 1994/. According to the model, practically no clay conversion will take place in a KBS-3 repository at these conditions as shown in Figure 2-3 Remaining smectite part for different temperatures in a hydrothermal system with [K+] = 0.002 mole/litre (80 ppm) according to the Huang et al. kinetic model and laboratory determined constants (Ea = 27.4 kcal/mole and A = 8.5E4).

However, the reaction relationship and the constants are determined from relatively short-term laboratory experiments at temperatures significantly higher than repository conditions (250-325°C), and from geological analogues, which differ from repository conditions in several aspects. The uncertainty in calculated conversion increases with the difference in temperature between test condition and calculated condition /Karnland et al., 1995/, /Karnland and Birgersson, 2006/.

The Lot test series aim at checking the model constants (activation energy and frequency factor) in experiments performed at ”as repository like conditions” as possible. No changes are expected and the main aim is to check that the reaction is not substantially faster than predicted by the model by use of moderate temperature increase (130°C) and high potassium concentration. The test technique is conservative in that sense that the transport of potassium, which is considered as one of the major hindrances for illitisation /Hökmark 1995/, is leaped over by the potassium placed in the adverse condition tests.

2.3.4. Effects of cement pore water

Possible effects on the bentonite of an exposure to cement pore water are believed to give the following reactions /Eberl et al., 1993/, /Karnland et al., 200/, Karnland and Birgersson, 2006/:

- Replacement of the original charge balancing cation, e.g. sodium against calcium.
- Cementation of the bentonite due to precipitation of cement matter (e.g. calcium-silica-hydrates and calcite) in clay pore space.
- Attack on the accessory minerals (e.g. cristobalite) in the bentonite.
- Alteration of clay mineral lattice due to the induced high pH.

The hypothesis is that bentonite under repository conditions resists short-term attack from cement pore water without major alteration. The main aspects of this part of the project are is to confirm/reject results from former laboratory experiments, which showed ion exchange, minor mineral dissolution/neo-formation and no or minor clay lattice alteration.

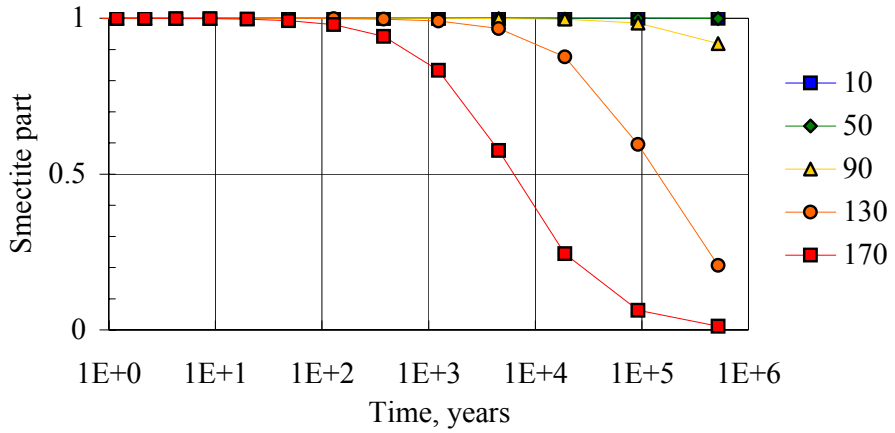

Figure 2-3 Remaining smectite part for different temperatures in a hydrothermal system with [K+] = 0.002 mole/litre (80 ppm) according to the Huang et al. kinetic model and laboratory determined constants (Ea = 27.4 kcal/mole and A = 8.5E4).

2.4. Microbiology

The survival of bacteria in bentonite has been suggested to depend on the water activity. Laboratory tests have shown that two different species of sulfate reducing bacteria were killed when the water activity was decreased to 0.96, corresponding to the conditions in an un-pressurized and fully saturated clay at a density of 2000 kg/m3 /Motamedi et al, 1995/. It may, however, be argued that other, more halo-tolerant sulfate reducing bacteria could survive and be active.

The main hypothesis is that bacterial survival is governed by water activity/induced swelling pressure. The low water activity/high swelling pressure in compacted bentonite around waste canisters is expected to act as a strong limiting factor for bacterial survival and activity, thereby reducing or eliminating the risk for bacterial production of gas and corrosive metabolic products.

Further, it has been argued that bacteria should be able to colonize the buffer from the groundwater. The presence of viable bacteria in deep clay sediment is usually interpreted as if the bacteria were mixed in with the clay during burial. Theoretically, the pore size of compacted bentonite is much smaller (nanometers), compared to microorganisms (microns), which makes migration into the buffer from groundwater, improbable.

2.5. Cation migration

The diffusion of radionuclides in compacted bentonite has been studied rather extensively in laboratory experiments with synthetic groundwater. The pore water diffusion model, generally used to interpret the experimental data, is based on the assumption that diffusion takes place in pore water and is retarded by sorption of the diffusing species on the solid phase. This model may be adequate for cations sorbed on the solid phase by surface compexation mechanisms, e.g. Co^{2+}. For cationic species present in the clay due to ion exchange, e.g. Cs^{+} and Sr^{2+}, experimental data indicate an additional diffusion mechanism

in which migration takes place within the nano-sized interlayer space between the montmorillonite surfaces. The diffusivities of Cs^+ and Co^{2+} in compacted bentonite saturated with groundwater of different ionic strength (salinity) are rather well documented at room temperature and, in principle, it should be possible to model the diffusive transport of these cations in the actual bentonite system.

A common theory is that cation transport may take place by two different transport mechanisms i.e. by diffusion in pore water which is not affected by the montmorillonite and by an additional migration between individual montmorillonite mineral layers next to the mineral surface. Recently it has been shown that the interlayer volumes play an important role in compacted bentonite, and that laboratory diffusion data may be explained to a large extent by two interlayer ion equilibrium processes; Donnan equilibrium and ion exchange (Birgesson and Karnland 2008).

A difference in diffusive transport is expected between cations sorbed by surface complexation mechanisms e.g. Co^{2+} and cationic species present as ion exchangeable ions e.g. Cs^+ and Sr^{2+}. A faster transport is therefore expected to take place for the latter cations. In the present A2 parcel the diffusive behavior of $^{60}Co^{2+}$ was studied.

2.6. Copper corrosion

The corrosion rate of the canister is in principle determined by the chemical reactivity at the canister surface and the mass transfer from and to this surface. For a specific canister, the corrosion rate depends on the geochemical conditions of the close vicinity of the copper surface, i.e. the type, content and mobility of dissolved constituents in the surrounding bentonite buffer. Thermodynamic calculations show that alteration products of copper are stable and that the corrosion process is expected to be affected by the redox conditions of the clay medium /Wersin et al., 1993/.

In general there are different types of uncertainties associated with estimation of the corrosion rate of copper in bentonite:

- Model validity
- Time scale of oxic/anoxic transition
- Pitting factor
- Transport properties of the clay

Modeling which takes into account diffusive transport in addition to flow, equilibrium reactions and kinetic processes at the bentonite-canister interface has been made /Wersin et al., 1994/. The results indicate conservative corrosion rates of $2 \cdot 10^{-8}$ and $7 \cdot 10^{-6}$ m/y for anoxic and oxic conditions, respectively. A sensitivity analysis indicates that the main uncertainties arise from the diffusion properties of the clay.

The present test aims at determining the mean corrosion rate, and identifies possible pitting and corrosion products. The main hypothesis is that the mean corrosion rate under the initial oxic conditions will be less than $7 \cdot 10^{-6}$ m/y.

2.7. Gas transport

No gas pressure test was included in the A2 parcel test, mainly because the focus has been on the ongoing full scale Lasgit project at the Äspö HRL.

3 EXPERIMENTAL CONCEPT

3.1. General

3.1.1. Principles

The LOT test series may be described as a multi-task experiment in which relatively small test parcels are exposed to conditions similar to those in a KBS-3 repository and to conditions, which accelerate alteration processes, respectively. The test parcels contain prefabricated bentonite blocks placed around a copper tube, which are placed in vertical boreholes in granitic rock. At tests termination the parcels are extracted by overlapping core drilling outside the original borehole, and the whole test parcels are lifted and partitioned. Material from defined positions in the parcels and reference material are thereafter examined by well-defined tests and analyses in order to provide data for the different objectives.

The dimensions of the parcels are kept considerably smaller, especially the diameter, compared to a KBS3 deposition hole in order to:

- Shorten the water saturation period and thereby have saturated condition during a substantial part of the test period
- Get a higher temperature gradient over the buffer material
- Facilitate sampling, i.e. release and up-lift of the exposed test parcel in one piece

3.1.2. Adverse conditions

Mineralogical stability of the bentonite clay is one of the grounds for the choice of bentonite as buffer material. Nevertheless, alteration processes will take place in the buffer but are predicted to be very slow under KBS-3 repository conditions. The following accelerating conditions compared to KBS-3 conditions were therefore used in order to make it possible to study slow alteration processes in the relatively short duration time of the experiments:

- Higher temperature,
- Higher temperature gradient,
- Higher content of accessory minerals (calcite, gypsum, K-feldspar),
- Introduction of new substances (Portland cement).

The expected effect of these accelerating conditions (buffer adverse conditions) may be summarized in the following discussion.

The initial reaction rate of a reaction

$aA + bB \rightarrow$ products Equation 2

can be described by the standard rate law

$Rate = k [A]^n [B]^m$ Equation 3

where n and m are constants, and k is a rate constant which can be expressed by the Arrhenius relationship

$k = zp \cdot \exp(-Ea /RT)$, Equation 4

where z is the collision frequency factor, p is the steric factor, and Ea is activation energy and R is the gas constant.

This reaction rate theory consequently implies:

- The reaction rate increases with increasing concentration of a reactant
- The reaction rate increases with increasing temperature
- The temperature effect increases with increasing activation energy
- The temperature increase effect is reduced with increasing temperature

For the case of illitization the high activation energy measured by Huang et al. (114700 J/mole), and a temperature increase of 10 K results in a close to tripled reaction rate. Consequently, the increase from 90°C, which is the upper limit temperature in the KBS-3 buffer, to the maximum temperature in the adverse conditions parcels (130°C) leads to an increased illitization reaction rate of around 40 times according to the Huang et al. model. The calculated maximum temperature hundred years after fuel deposition is around 70°C and the corresponding temperature after 1000 years is 50°C (Figure 2-2) The temperature in the outermost part of the bentonite will initially be around 20°C lower (Figure 2-2). A comparison between the 130°C in the adverse condition parcel and the maximum bentonite temperature after 100 years (70°C) gives a reaction rate factor of almost 400 times. A 5-year test at 130°C consequently represents a significant part of the thermal load in a KBS-3 repository with respect to kinetically controlled slow processes.

Consequently, the LOT A2 test is expected to show mineralogical effects of processes governed by the kinetics of the involved reactions. The introduction of additional substances will accelerate also processes, which in a repository are governed by the transport of reactants, e.g. potassium for illitization.

However, reactions governed by the removal of reaction products cannot be generally accelerated in a simple way in this kind of field tests. The adverse conditions in the present A2 parcel do not accelerate such processes generally, although the increase in temperature will increase e.g. the precipitation rate of quartz.

3.2. Experimental configuration

3.2.1. Test program

In total, the LOT test series includes seven test parcels (Table 3-1 Test program for the ”Long Term Test of Buffer Material” series. A = adverse conditions, S = standard conditions, T = temperature, [K+] = potassium concentration, pH = high pH from cement, am = accessory minerals added) of which three have been exposed to standard KBS-3 conditions, and four test parcels which are exposed to adverse conditions. The present report concerns the A2 parcel.

Table 3-1 Test program for the ”Long Term Test of Buffer Material” series. A = adverse conditions, S = standard conditions, T = temperature, [K+] = potassium concentration, pH = high pH from cement, am = accessory minerals added

Type	No.	max T, °C	Controlled parameter	Time, years	Remark
A	1	130	T, [K+], pH, am	1	pilot test
A	0	120-150	T, [K+], pH, am	1	main test
A	2	120-150	T, [K+], pH, am	> 5	main test

Type	No.	max T, °C	Controlled parameter	Time, years	Remark
A	3	120-150	T	>> 5	main test
S	1	90	T	1	pilot test
S	2	90	T	>5	main test
S	3	90	T	>>5	main test

3.3. Test site

3.3.1. General

The LOT main test series are run in the G tunnel situated in the western part of the present Äspö hard rock laboratory (Figure 3-1). The depth from surface is around 450 m and the rock consists mainly of Äspö diorite, which is crossed by some pegmatite and bands of fine-grained granite. A few water-bearing fractures are visible, but the tunnel may be considered dry relative to the average Äspö rock volume.

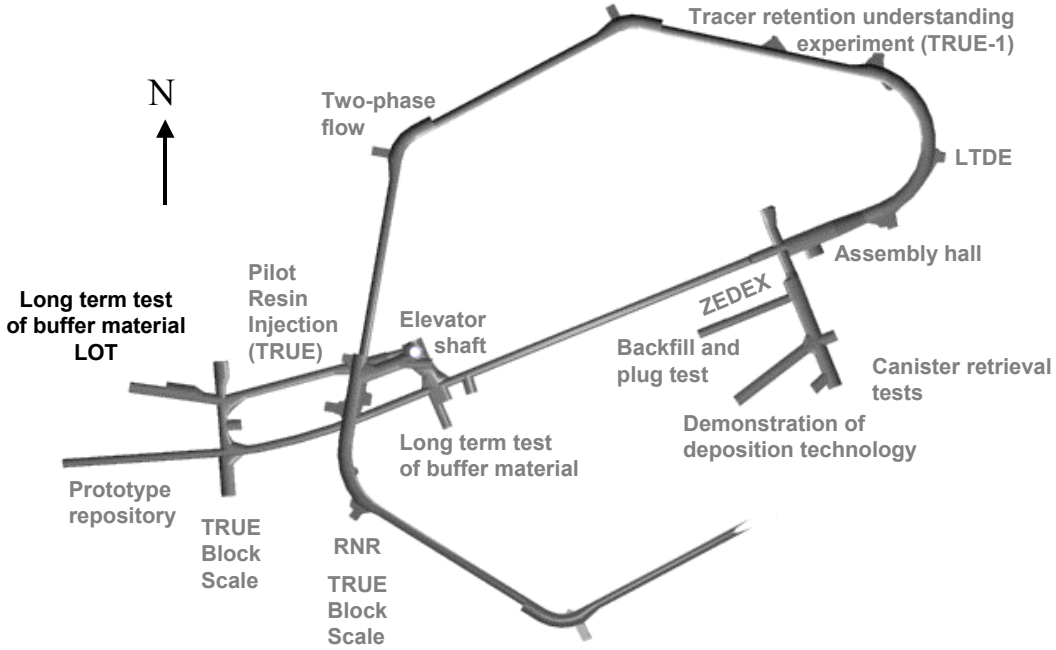

Figure 3-1 Test present LOT test site is located in the G-tunnel in the western part of the research area, and close to the lowest part of the Äspö tunnel.

3.3.2. Pilot holes

Five 76 mm vertical pilot holes were drilled in line on the northern side of the G-tunnel between March 2nd and March 4th 1999. The holes were approximately 8 m deep and with a relative distance of 4.5 m. The holes were termed KG0033G01, KG0037G01, KG0042G01, KG0046G01 and KG0051G01, where K denotes core-drilled, G denotes the G-tunnel, 0033 denotes the length in meters from tunnel entrance, G denotes floor position. The KG0037G01 hole was used for the present A2 test.

No definite suitability criteria were defined for the test holes, but the water pressure in the holes generally has to be higher than the vapor pressure at the chosen test temperature. Further, water inflow had to be sufficiently low to allow the placement of the test parcels and to exclude the risk of piping and erosion after closure.

Shortly after drilling, mechanical packers were installed. The boreholes were shut in and kept closed until the start of flow and pressure measurements were performed. The flow measurements were made by use of double packers with 1 m spacing in the upper 4 m and a single packer was used for bottom part (4 m to 8 m). The results of the flow measurements are presented in Table 3-2

Table 3-2 Flow rates (ml/min) measured in intervals of the five pilot boreholes for the LOT tests in the G-tunnel of ÄSPÖ HRL, April 1999.

	Borehole:				
Section	KG0033G01	KG0037G01	KG0042G01	KG0046G01	KG0051G01
1.4 - 8.05	0.025	0.02	-0.12	1.3	0.025
1.00 – 2.00	0.07	0.09	± 0	0.1	0.07
2.00 – 3.00	0.07	0.07	0.04	0.14	0.01
3.00 – 4.00	0.06	0.14	0.05	0.08	0.07
4.00 - 8.05	0.01	0.06	0.01	0.60	0.01

The general conclusions from the pilot hole characterization program were that the water inflow was low, and that the water inlet points were few in all holes. The test time was thereby expected to be much longer than acceptable. Instead of abandon the site it was decided to add external ground-water into the test holes during the test period. A water supply hole (HG0038B01) was drilled into the northern wall where a water-bearing fracture was found a few meters into the rock. The water pressure was determined to be around 1.2 MPa and the flow was more than sufficient to support all test holes. The water supply hole was packed off and a system of titanium tubes was used to inject water into the test holes.

The ground-water composition has repeatedly been measured in bore-hole HG0038B01 by use of the “class 5” quality (highest) according to the Äspö HRL nomenclature and the typical composition of main elements is given in ()

Table 3-3 Main composition of the the ground-water in water supply bore hole HG0038B01 (in mg/L):

pH	Na^+	K^+	Ca^{2+}	Mg^{2+}	Cl^-	SO_4^{2-}	HCO_3^-
6.9 ± 0.1	100	0.28	47.3	2.4	178	4.6	0.44

3.3.3 Test holes

The five pilot holes were enlarged to a diameter of 300 mm to a depth of 4 m. The enlargement was made by percussion drilling because this technique was thought to best simulate the core TBM-type drilling with respect to surface damage and thereby to water conductivity. The test holes were named according to the standard Äspö database nomenclature; HG0033G01, HG0037G01, HG0042G01, HG0046G01 and HG0051G01. The test hole HG0037G01 was used for the present A2 parcel.

The diameter and the straightness of the test holes were checked and the test holes diameter was estimated to exceed 300 mm by up to 10 mm in some parts.

3.4. Test parcel construction

3.4.1. General

The basic demand for the test parcel construction was to keep a defined maximum temperature in the central part of the clay column during the test time span. An important part of the system was therefore the temperature measurement and power regulation system. A central heater inside an open tube was chosen, as this allows for heater change during the test period in case of a failure. The central tube was made of copper in order to simulate the KBS-3 copper canister, and thereby keep as realistic chemical conditions as possible. The A2 test parcel contained heater, central tube, bentonite blocks, sensors and additives, which are individually described in the following sections.

3.4.2. Heater

Specially designed electric heater from Backer Elektro-värme AB, Sösdala, Sweden were used. The total length was 4650 mm, and the active bottom part had a length of 2000 mm. Three individual stainless steel (SS2348) elements with a diameter of 14 mm were brazed into a stainless steel (SS2343) flange, which was designed in order to let the heater hang down from the support of the top of the copper tube. The maximum power was decided to be 2 kW (230/400 V, AC), i.e. each element has a maximum power of 667 W (230 V) corresponding to 0.7 W/cm2. The expected power need was based on the previously performed pilot tests A1 and S1, which were in agreement with scoping calculations made by MICROFIELD finite element computer code performed by Harald Hökmark, Clay Technology AB.

3.4.3. Central tubes

The canister simulating copper tube (SS 5015-04) had a length of 4700 mm, an inner diameter of 100 mm and a wall thickness of 4 mm. At the bottom end a copper plate and 4 copper reinforcement parts were brazed by use of soldering silver. A detachable lifting device was placed at the top of the tube during the placement. The maximum possible external pressure acting on the outside of the central tube was expected to be less than 10 MPa (bentonite swelling pressure plus hydrostatic water pressure), which correspond to a maximum compression stress of 140 MPa acting at the inner radius. The used hard-drawn copper quality has a yield point exceeding 200 MPa, which consequently was sufficient.

No water/steam leakage into the tube could be accepted with respect to both the heater function and the mass transport conditions. The impenetrability was therefore tested after the soldering by use of a helium source inside the copper tube and an external detector.

3.4.4. Blocks

Wyoming bentonite with the commercial name MX-80 was the source material for all bentonite components in the system. It was delivered by Askania AB and manufactured by Volclay LTD, Mersyside, UK. The material was delivered in 25 kg sacks in one consignment.

The material is dominated by natural mainly sodium montmorillonite clay (~ 80 % by weight). Accessory minerals are quartz (~4 %), tridymite (~4 %), cristobalite (~3 %), feldspars (~4 %), muscovite/illite (~4 %) sulphides (~0.2 %), and small amounts of

several other minerals and organic carbon (~0.4 %). Dispersed in distilled water the clay fraction (grain size < 2 μm), make up around 80%. The mean mineralogical composition of the montmorillonite part is given by:

$(Si_{7.92}\ Al_{0.08})\ (Al_{3.10}\ Fe^{3+}_{0.4}Fe^{2+}_{0.02}\ Mg_{0.48})\ O_{20}(OH)_4 \qquad Na_{0.48}\ Ca_{0.04}\ Mg_{0.02}$

The cation exchange capacity is around 0.75 eq/kg bulk material and around 0.85 eq/kg clay in the minus 2 μm fraction. The natural exchangeable cations are sodium (~70 %), calcium (~20 %), magnesium (~ 6 %) and small amounts of potassium (~2 %). The specific surface area is around $5.5 \cdot 10^5$ m^2/kg material and the grain density is around 2750 kg/m^3 /Karnland et al., 2006/.

The various blocks and plugs produced for the A2 parcel may be divided in the following groups:

- Standard blocks with maximum original diameter of 281 mm and a height of 100 mm.
- Special blocks, which were prepared from standard blocks, with excavations for reinforcements, instruments, copper plates or 20 mm test plugs.
- 20 mm diameter bentonite plugs with or without different additives, used in the tracer tests, the bacteria tests, and accessory mineral enrichment tests.

The choice of block compaction technique was based on experiences from previous SKB projects concerning block production /Johannesson et al., 1995/. A uniaxial compaction device was constructed in order to make it possible to produce blocks with the accurate dimensions, density and composition. A slight axial conic form and chamfered edges between mantle and end sides were used in order to facilitate the expulsion after compaction and to avoid subsequent stress induced cracks. A small amount of molybdenum sulfide grease was used to smear the mantel surfaces in order to reduce friction.

The bentonite material was compacted without pre-treatment. Water content was measured in each 25 kg sack in order to determine the amount of solid bentonite in each block batch. The governing figure for the production was the final density in the test hole after expansion by water uptake. The reference KBS-3 bentonite bulk density is 2000 kg/m^3 with an accepted divergence of ± 50 kg/cm^3. The accomplished calculations were made by use of a bentonite solid density of 2750 kg/m^3, a mean block radius of 139.3 mm and an inner radius of 56 mm, a borehole radius of 150 mm and copper tube radius of 54 mm. Extra blocks were made in the production series in order to be dissected and analyzed with respect to homogeneity. For each produced block, approximately 250 g of the same material, i.e. from the same 25 kg sack, was marked and stored as reference material for background analyses.

The blocks predestined for gauges or plugs were made from standard blocks by drilling and carving out the necessary volume. The bentonite material is well suited for this technique and the produced unintentional gaps between the gauges and the bentonite are small and insignificant with respect to the final buffer density

The special blocks produced for the A2 parcel had the following modifications:

block no.	**modifications/excavations for**
01	copper bottom-plate reinforcements
02	3 thermocouples

05	20 mm cylindrical holes for tracer tests, 2 filters/tubes
08	5 thermocouples, 1 total pressure gauges, 1 water pressure gauge, 1 relative humidity gauge
10	4 plugs of 10% of and 1 water sampling cup
12	4 plugs of 10% CaSO4 and 1 water sampling cup
14	5+1 thermocouples, 1 total pressure gauges, 1 water pressure gauge, 2 relative humidity gauge
16	3*4 plugs of 50% K-feldspar and 1 water sampling cup
18	3 water sampling cups and 2 tubes with filters
20	5 thermocouples, 1 total pressure gauge, 1 water pressure gauge, 1 relative humidity gauge
22	2 copper plates
24	2*3 cement plugs
26	3 thermocouples
28	2 tubes with filters
30	2 copper plates
32	1 thermocouple, 3 water sampling cups, 1 tube with filter
36	1 water sampling cup
38	1 thermocouple

All blocks were devoted to defined positions in the test parcels and given a specific denomination. The blocks were theoretically partitioned in 9 sections in order to get a system for instrumentation and sampling. The first section ranging from the inner mantel surface and 2 cm outwards was termed section 1, and the following volume, i.e. between 2 and 4 cm from the inner mantel surface, was termed section 3, etc. The last section was consequently 9, and this section only had an initial extension outwards of ~1 cm. After swelling, due to water uptake, section 9 represented the volume between 8 and ~10 cm (rock wall). Furthermore, the point of the compass was used to describe the horizontal orientation. The denomination of a specific point (centre of a volume) is according to the example 08ASE3 where

08	block number (counted from the bottom of the parcel),
A	vertical level in the block,
SE	direction of compass in the test hole,
3	radial distance in centimeter from the inner mantel surface to the centre of the specimen.

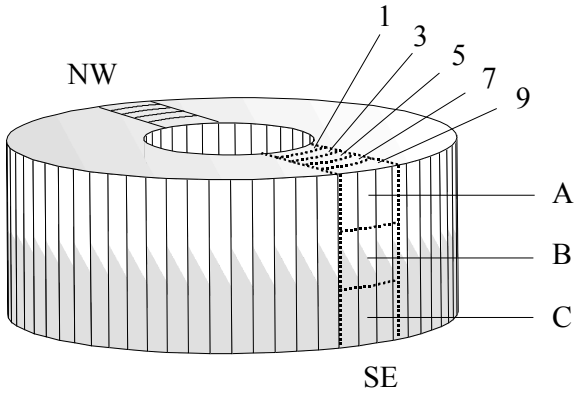

Figure 3-2 Schematic block partition. SE and NW denote the directions of compass in the test-hole, figures denote the centre of the specimens expressed in centimeters measured from the block inner mantel surface, and A, B and C denotes the analyzed three vertical position in the blocks.

The reference material was related to an imaginary point. Reference material from a specific block was termed according to the example RA209 where

R reference material,

A2 parcel type and number,

09 block number (counted from the bottom of the parcel).

The layout of all special blocks are schematically shown in Appendix 1.

3.4.5. Test plugs

All bentonite-containing plugs had a cylindrical form with a length and diameter of 20 mm. They were compacted in a laboratory compaction device working by the same principle as the block compaction device, but no grease was used. The plugs were compacted to a density corresponding to the standard density of 2000 kg/m^3 after full water saturation regardless of the additives. The compaction was accordingly controlled by the final sample volume and not by the maximum compaction pressure.

The plugs were placed in cylindrical holes, which were drilled from the mantle surface into the specified blocks halfway between, and parallel to, the end surfaces. The hole diameter was constantly 21 mm, while the depth depended on the purpose of the test. The outer plugs were sprayed with a small amount of deionized water before they were inserted in order to let the bentonite swell slightly and thereby seal the slots. The positions of the plugs were marked by millimeter thick titanium wires inserted into drilled holes placed 20 mm above the centre of the plugs. Two wires marked the northern position, and one wire marked the other three main directions of compass. The positions of all test plugs are shown schematically in Figure 3-3 Scaled schematic drawing of the A2 test parcel and Appendix 8.

The calcite plugs had a 10w-% content of calcite. The calcite material was a finely ground pure quality which was thoroughly mixed with the bentonite and compacted to a density of 2000 kg/m^3. Cylindrical holes were drilled from the mantle surface into block A210 to a depth of 40 mm and from 4 sides. All four holes were sealed with a slightly wetted bentonite plug without additives in the outer 10 mm.

The gypsum plugs had a 10w-% content of gypsum. The used CaSO4 (0.5 hydrate) material was a finely ground pure quality which was thoroughly mixed with the bentonite

and compacted to a density of 2000 kg/m^3. Cylindrical holes were drilled from the mantle surface into block A224 from 4 sides to a depth of 30 mm. All four holes were sealed with a slightly wetted plug without additives in the outer 10 mm.

The cement plugs were cast to a cement water ratio (cwt) of 0.8 by use of an Aalborg white Portland cement and de-ionized water. The cement was allowed to harden in water for 14 days before the emplacement. Two cylindrical holes were drilled into block A224, A234 from the north and from the south side to a depth of 80 mm. Four plugs were placed in each hole. Titanium marks were used in the A0 blocks. No bentonite plugs were used for sealing.

The ^{60}Co-tracer doped plugs. A few cubic millimeters of bentonite were ion-exchanged to contain 1 MBq of ^{60}Co. The prepared material was placed in the centre of two bentonite plugs. Cylindrical holes were drilled from the north and south side into the mantle surface in block A205. The diameter of the holes was 21 mm and the depth was 50 mm, meaning that the doped part was placed close to the centre of the bentonite, halfway between the rock and the copper tube. The tracer-doped plugs were placed into the block during the submerging of the parcels.

The copper samples were placed in tiny slots drilled and sawed from the upper side of the blocks. The copper coupons were placed in the blocks during the pile up of the bentonite column. The samples were pre-characterized and marked with letters, for identification, and with smaller marks for localization during the post test investigation.

3.5. Instrumentation

3.5.1. General

The basic aim for the field activity in the LOT tests is to expose the bentonite clay to conditions similar to those in a KBS-3 repository, and to expose the clay to adverse physico-chemical conditions, mainly by an increased temperature. A fundamental demand was therefore to measure the temperature in order to regulate power, and to register the obtained temperature distribution in the whole A2 parcel. Relative humidity, porewater pressure and swelling pressure reveal the state of saturation and were therefore also measured. An additional objective with the LOT series was to test equipment for the subsequent full scale buffer tests at Äspö. These demands in combination with the relatively limited volume in the clay and the potential risk for artifacts due to the instrumentation led to the following compromise concerning instrumentation of the A2 parcel:

- 24 thermocouples
- 3 total pressure gauges
- 3 water pressure gauge
- 7 water filters of ,which some are equipped with external pressure gauges
- 4 relative humidity sensors

The gauges and sensors were placed in the parcels as shown in Figure 3-3 Scaled schematic drawing of the A2 test parcel and Appendix 1. The equipment was termed in accordance with the following example:

A2084P where

A2 parcel type and the number of the test,

08 block number counted from the bottom,

4 position in the block (according to section 3.4.4),

P type of measuring equipment.

The following abbreviations of measuring equipment was used:

E temperature in the pressure gauges,

M relative humidity sensors,

P total pressure gauges,

T thermocouples,

W water pressure gauges.

3.5.2. Thermocouples

Temperature was generally measured by thermocouples with a hot junction type J according to IEC 584 standard. Additional temperature information was given by the pressure and humidity sensors, which had thermistors and Pt-100 sensors built-in, respectively. The thermocouples were delivered by BICC Thermoheat Limited, Hedgeley Road, Hebburn, Tyne & Wear NE31 1XR, England. The soldering spots were isolated by cupro-nickel alloy, which also jackets the wires up to the tunnel and into the measuring cabinet.

The placing strategy was to concentrate the thermocouples in the clay volume around the heater in order to monitor the temperature gradient over the bentonite in detail. Thermocouples were placed in position 1, 3, 5, 7, and 9 in the blocks 08, 14, and 20. In block 14 there was an additional sensor on the copper surface. Below the most interesting sections, three thermocouples were placed in position 1, 5 and 9 in block 02. And above, three thermocouples were placed in position 1, 5 and 9 in blocks 26. One thermocouple was placed in position 4 in block 32 and 38, respectively. All measuring soldering points were placed from the upper surface of the blocks, into pre-drilled holes, down to a depth of 35 mm.

Calibration is generally not needed for thermocouples, however, a function control was made by connecting all thermocouples to the actual data collecting system and a check was made that the thermocouples showed the prevailing temperature before installation.

3.5.3. Pressure gauges

Two quite different types of pressure gauges were used in order to make the pressure measurements redundant. The placing strategy was to place the optical gauges in block 08 and 20, and in between the vibrating wire gauges in block 14.

The optical gauges, model FOP, were manufactured and delivered by Roctest Ltd, 665 Pine Avenue, Saint-Lambert, Canada. The gauges were delivered with signed individual calibration data sheets and traceability numbers.

The vibrating wire gauges, model no. 4500TI-1500, were manufactured and delivered by Geokon Inc., 48 Spencer St. Lebanon, N.H. 03766, USA. The gauges were delivered with signed individual calibration data sheets and traceability numbers according to ANSI Z540-1.

The water pressure transferred by titanium tubes was measured by external gauges place in the tunnel above the parcels. The gauges were produced by Druck Limited, Fir tree

Lane, Groby, Leicester LE6 0FH, and delivered by AMTELE AB Box 66, SE-12722 Skärholmen, Sweden. Individual data sheets, including gauge serial no, were delivered with the sensors.

The factory calibrations and temperature compensations were used for all three types of pressure gauges in the following presentation of results.

3.5.4. Moisture gauges

The measuring principle for the humidity sensors was electrical capacity change which gives a large measuring span and sufficient accuracy in order to follow the water uptake. The sensors were manufactured by Vaisala Oyj, Vanha Nurmijärventie 21, Fin-01670 Vantaa, Finland. The gauges were delivered with signed individual calibration data sheets. Traceability is guaranteed by the Vaisala Oyj.

The sensors were individually calibrated in order to check the delivery calibration data both with respect to relative humidity and to temperature dependence. The sensors were connected to the actual data collecting system, including all cables etc. The gauges were placed in specially designed plastic boxes, which were partly filled with different saturated salt solutions. Saturated solutions of $(NH_4)_2SO_4$, KCl, $BaCl_2$ and KH_2PO_4 were used. The temperature was kept at 22°C and the equilibrium relative humidity 81.2, 84.8, 90.4 and 94 %, respectively, were used for the calibration.

The $BaCl_2$ solution was also used for the temperature compensation calibration, since the humidity equilibrium is relatively stable in the examined temperature range. Temperatures close to 40, 50 and 60°C were used and a linear function, describing apparent dRH as a function of T, was determined for each sensor. No significant differences between the factory calibration and the Clay Technology laboratory calibration were noticed with respect to relative humidity. The factory calibration and temperature compensation were therefore used in the following presentation of results.

3.5.5. Data collection and registration system

All measuring sensors and gauges were connected to DATASCAN units, which in turn were connected to computer working under Windows NT placed in a cabin close to the test site. The software was named Orchestrator and was manufactured by Eurosoft Technology, UK. MSS AB, Åkersberga, delivered the software and DATASCAN units. The program has a range of output/input drivers and real time data acquisition which i.a. admitted the use of event-governed logging in addition to periodic logging and alarm functions. The standard logging interval was set to 1 hour during the entire test period. The alarm system was used in order to detect overheating, and the system was connected to the control room at the CLAB facility at the nearby nuclear power plant for 24 h supervision.

A standard interval of 1 hour was used for all collection of data since the course of events was expected to be relatively slow. In addition, an event governed data collection was programmed for each type of measuring equipment. The triggering measuring event was exceeding or falling short of a fixed value, or a fixed interval related to the previous measured value. The configuration was made in such a way that all channels related to the test was read off if an event-triggered measurement was started by a single instrument.

The recording and real time handling of data may be divided in three levels of importance. The handling of data used for regulating the system was of course most important since a malfunction may have lead to a fast destruction of the system. Of second most importance

were the data needed for the evaluation of the test conditions, and finally there is a group of data which is of general interest but which is not necessary for the accomplishment of the test. In consequence, several levels of alarm function were used in the monitoring system. Depending on the type of released alarm different measures were stipulated, ranging from simple notes to immediate actions from the safety guard at the nuclear power plant.

All recorded data were stored in the specific project computer and backup was regularly made at the Äspö HRL. The standard recorded data concerning temperature, pressure and humidity were copied approximately once a month from Clay Technology and stored in an SQL-database. The data were processed by means of MS EXCEL and thereafter stored in the SICADA database at Äspö.

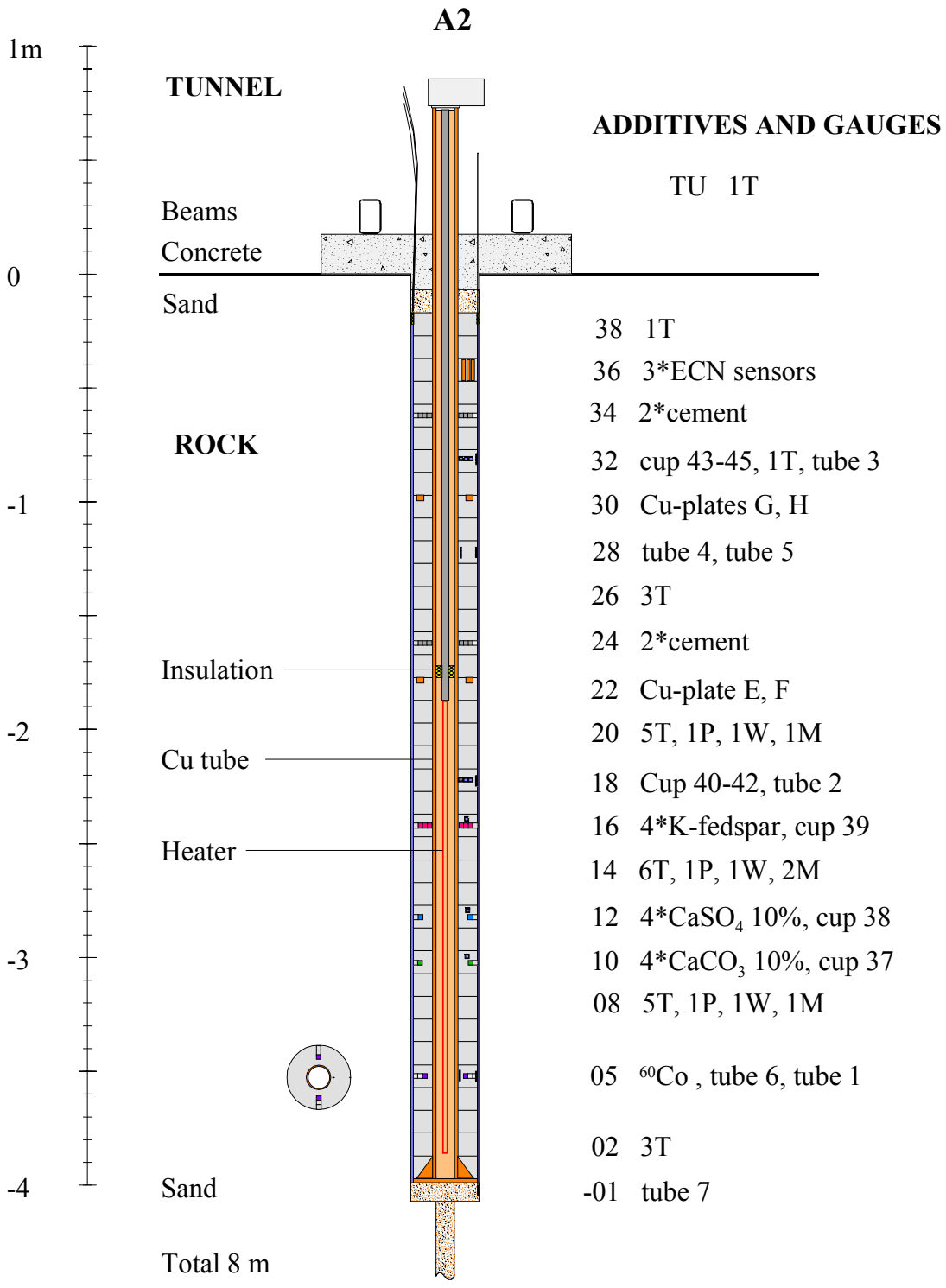

Figure 3-3 Scaled schematic drawing of the A2 test parcel. Abbreviations are explained in section 3.4.4 to section 3.5.4.

4 FIELD OPERATION

4.1. Preparation

4.1.1. Parcel assembly

The entire parcel systems were prepared and checked in laboratories in Lund, dismantled and loaded on to a lorry for transport to Äspö HRL. At the test site, the water in the test hole was pumped and the bottom part was filled with sand up to approximately 10 cm from the bottom. The central 8 m deep pilot hole with a diameter of 76 mm was thereby also filled with sand. The test hole was covered with a building board and the copper tube was vertically fixed at a bottom support right on top of the test hole. The predestined blocks were thread onto the copper tube from above one by one from a scaffold (Figure 4-1 Left: Finalizing the construction of the A2 parcel at test site, note the large number of tubes from sensors. Right).

Figure 4-1 Left: Finalizing the construction of the A2 parcel at test site, note the large number of tubes from sensors. Right: Insertion of the ^{60}Co containing plug during lowering the parcel into the test hole. Note the lack of disturbing sensor tubing in the lower hot section.

The gauges and sensors were placed in the prepared cavities before the successive block was placed. The instruments were fixed in position only by overlying blocks without additional equipment. The tubes from each instrument were placed in tracks excavated in the outer mantle surface of the blocks above the instrument. The tubes were fixed during the construction of the parcels, but released during the parcel submerge in order to admit movements during the subsequent swelling of the bentonite. A few thin copper wires were though left to keep the tubes in place during the placement (Figure 4-1 Left: Finalizing the construction of the A2 parcel at test site, note the large number of tubes from sensors. Right). The various plugs were placed in position after all bentonite blocks

were in position. The plugs were fixed and sealed by adding a small amount of water on the outer plug surface before they were pressed into position. The tracer test plugs were the lasts to be placed in order to minimize the risk for contamination with ^{60}Co. The entire mounting procedure of the A2 parcel at the test site was achieved within two day (although quite long days) since the parcel was constructed as a ”building kit”.

4.1.2. Installation

The A2 parcel was installed into test hole HG0037G01 on October 29,1999. The top of the copper tube was connected to the lift device mounted in the roof above the test hole. The parcel was slightly heaved and the bottom support and building board were removed. The test hole was again emptied on water and the parcel was carefully centered and slowly lowered into the test hole. The total submergence procedures took approximately 15 minutes. The upper slot between the bentonite and the rock was caulked with mineral insulation (Rockwool) in order not to let sand penetrate downwards. An approximately 10 cm thick sand layer was placed on top of the clay column and the tubes from all gauges and filters were brought together above the bentonite and fixed. The uppermost 10 cm of the test-hole and a square-formed reinforced concrete top plug were cast. After hardening, the plug was prevented from heaving, due to bentonite swelling and water pressure, by use of two steel beams, which in turn were fixed by 4 rock bolts (Figure 4-2 Left: Picture of the test site with parcel A2 in the front. Right: Schematic drawing of the final appearance of the A2 test after installation.). The sensor and heater cables were connected to measuring and regulating equipment placed in cabinets on top of the test hole, and the cabinets were covered by a simple drip shelter. The measuring equipment was connected to computers in a hut at about 10 m distance. These computers were in turn connected to the general backup system at the Äspö HRL.

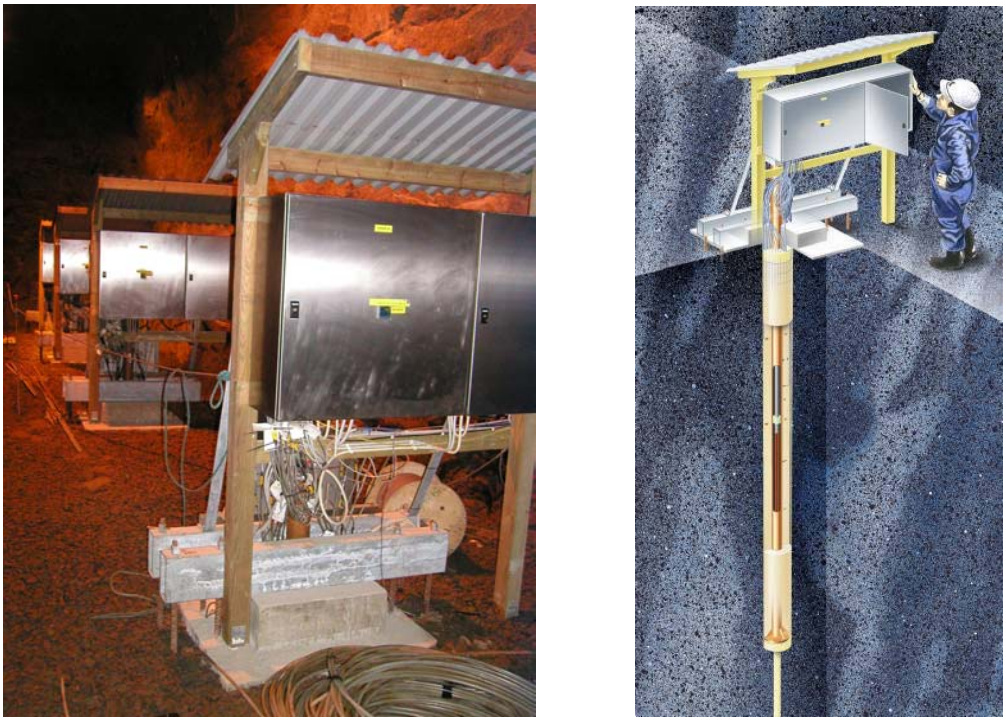

Figure 4-2 Left: Picture of the test site with parcel A2 in the front. Right: Schematic drawing of the final appearance of the A2 test after installation.

4.2. Heating phase

4.2.1. Temperature control

There are in principle two main options to control the temperature in this kind of tests, i.e. regulation of the heater power to a fixed value, or to regulate the power to give a defined temperature at a certain position. The former method best simulates the real conditions of spent fuel and the latter ensures a defined maximum temperature. The power was first turned on February 2, 2000, and regulated to give a constant maximum temperature of 50°C. A mean value of the three thermocouples A208T1, A214T1 and A220T1 were initially used to govern the power in order to ensure that no overheating took place. The maximum temperature target was thereafter increased in steps of 10°C. On April 19, 2000 the regulation was changed to a fixed power of 480 W. The power was thereafter increased in steps to a final power of 850 W which was reached on June 17, 2000..

4.2.2. Water supply

The slot between the clay column and the rock was slowly water filled on February 2, 2000 in parallel with the onset of the heater. The filling was made with ground-water from the adjacent borehole (HG0038B01) by use of the fixed installed titanium tube and bottom filter (filter no 7) placed in the sand below the parcel and close to the rock wall. The valve connected to the bottom filter was closed at the time when the ground-water had reached the upper most filter (Filter 3 in block 32), which so far was open against air. This filter was instead connected to the ground-water supply, and the intension was to leave it open to ensure saturated in the upper cold part of the parcel in order to prevent steam to leave along the copper tube. However, the system did not seal completely, likely due to the large number of tubes intersecting in the uppermost part, (Figure 4-1 Left: Finalizing the construction of the A2 parcel at test site, note the large number of tubes from sensors. Right). The supply of ground-water was therefore moved to the next lower filter in order to ensure a sufficient ground-water pressure and thereby prevent boiling.

4.3. Field Results

4.3.1. General

The field regulating and measuring systems worked very well during the entire six years of operation, and no malfunction of importance occurred. Most important was that no overheating or temperature drops took place. Minor incidents with logging units and service stops in logging can be seen in the various results.

4.3.2. Temperature

The temperature recordings were of special importance as this parameter is of such importance for the reaction rate of chemical processes. The large number of sensors gave a clear picture of the temperature distribution within the parcel. Figure 4-3 shows the measured temperature evolution in the warmest section (block 14). Uppermost curve shows the temperature at the copper tube surface, and the underlying curves show the temperatures of point successively 2 cm closer to the rock. The lowest curve consequently represents a point approximately 1 cm from the rock.

A certain annual cyclic variation is noticed, which can be correlated to the temperature in the ventilated tunnel, and represents the combined effect of the thermal conductivity of the bentonite, copper tube and surrounding rock. A minor temperature decrease in the

inner most positions over the first 3 years is noticed in all warm positions, and is a strong indication of the water saturation course. Figure 4-4 (left) shows the temperature distribution in the parcel during the major part of the field exposure, and Figure 4-4 (right) shows the distribution in the cooled parcel seven days after power termination.

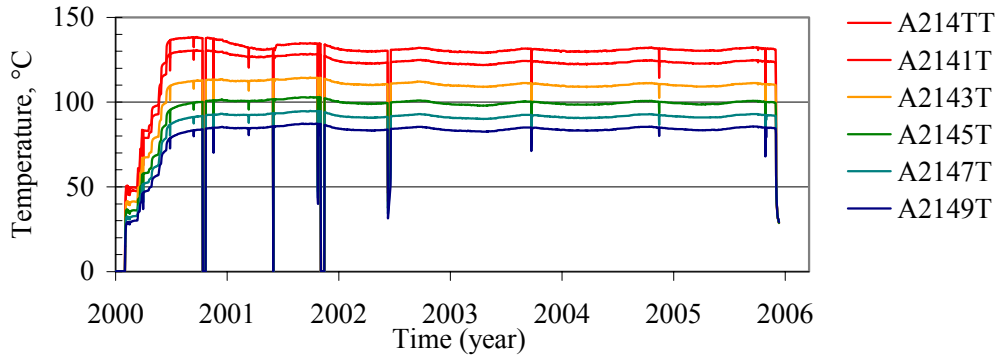

Figure 4-3 Temperature results from the thermocouples in block no. 14. Uppermost curve shows the temperature at the copper tube surface, and the underlying curves show the temperatures of point successively 2 cm closer to the rock. The lowest curve represents a point approximately 1 cm from the rock.

4.3.3. Total and water pressure

The two types of pressure sensors, i.e. optical sensors in block 08 and 20 and vibrating wire sensors in block 14 show similar results, both with respect to total pressure and water pressure (Figure 4-5). The results shows that the sensors worked quite good, but still one has to be careful with the absolute values, because of the high temperature and long time after calibration. Qualitatively, it is clear that the bentonite was fully water saturated after less than 2 years at the measuring points, which is in agreement with the temperature indications. The measured maximum water pressure is close to the applied ground-water pressure (~1.2 MPa) in the supply filter, indicating the accuracy of the measurements. An unintended closure of the valve on the supplying water in January 2002 led to a significant pressure drop in all three positions, both of total and water pressure. The valve was thereafter deliberately left close until September 2002 in order to study the natural pressure evolution. A quick response was noticed after opening the valve.

4.3.4. Moisture

High quality moisture measurements are difficult to perform over long time, especially in the very harsh environment in high temperature bentonite. At full water saturation of the bentonite the fragile moisture sensors normally get contaminated of the saline water. This commonly leads to subsequent erroneous results, which however is a good indication of full water saturation. Figure 4-6 shows the results from three moisture and accessory temperature sensors from block A208, A214 and A220, respectively. All moisture sensors indicate a rather fast increase in humidity to over 90% within the first half year. A complete failure of both the moisture and temperature sensors took place around mid 2001 for all sensors, which indicates full water saturation. These results are consequently well in agreement with the indications from the pressure sensors and thermocouples with respect to water saturation.

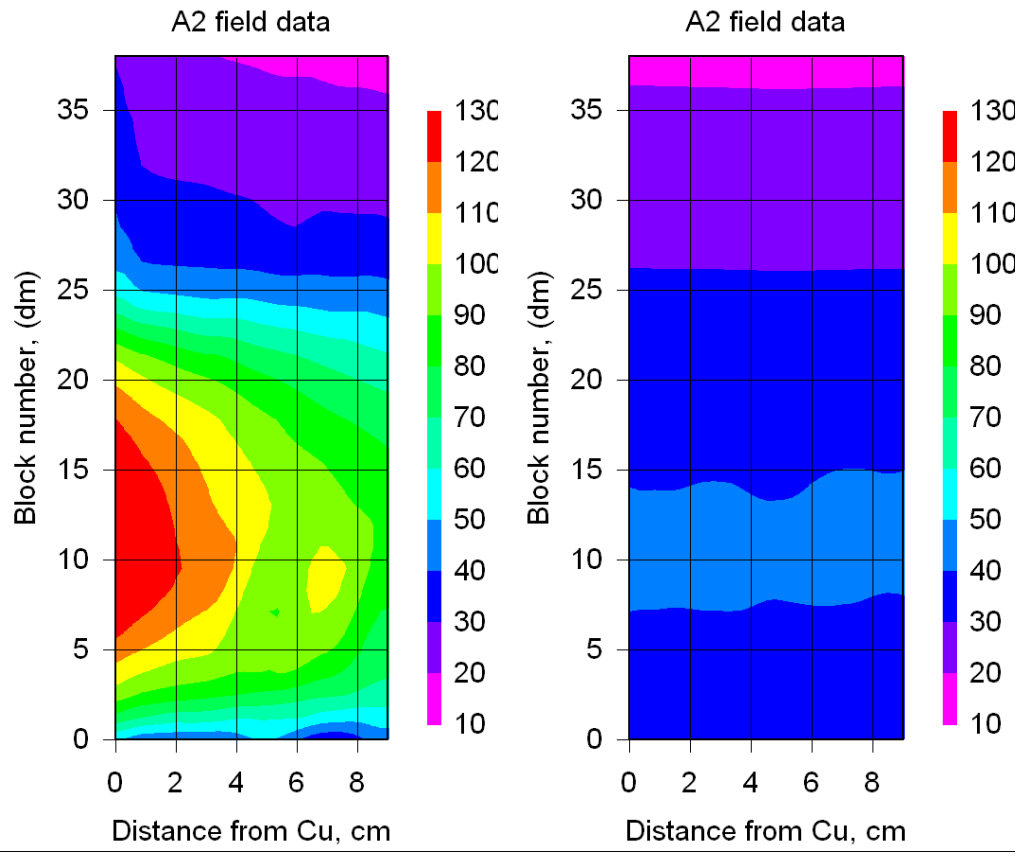

Figure 4-4 Temperature distribution at termination of the power, which also represents the major part of the field exposure time(left), and temperature distribution one week after termination of power(right).

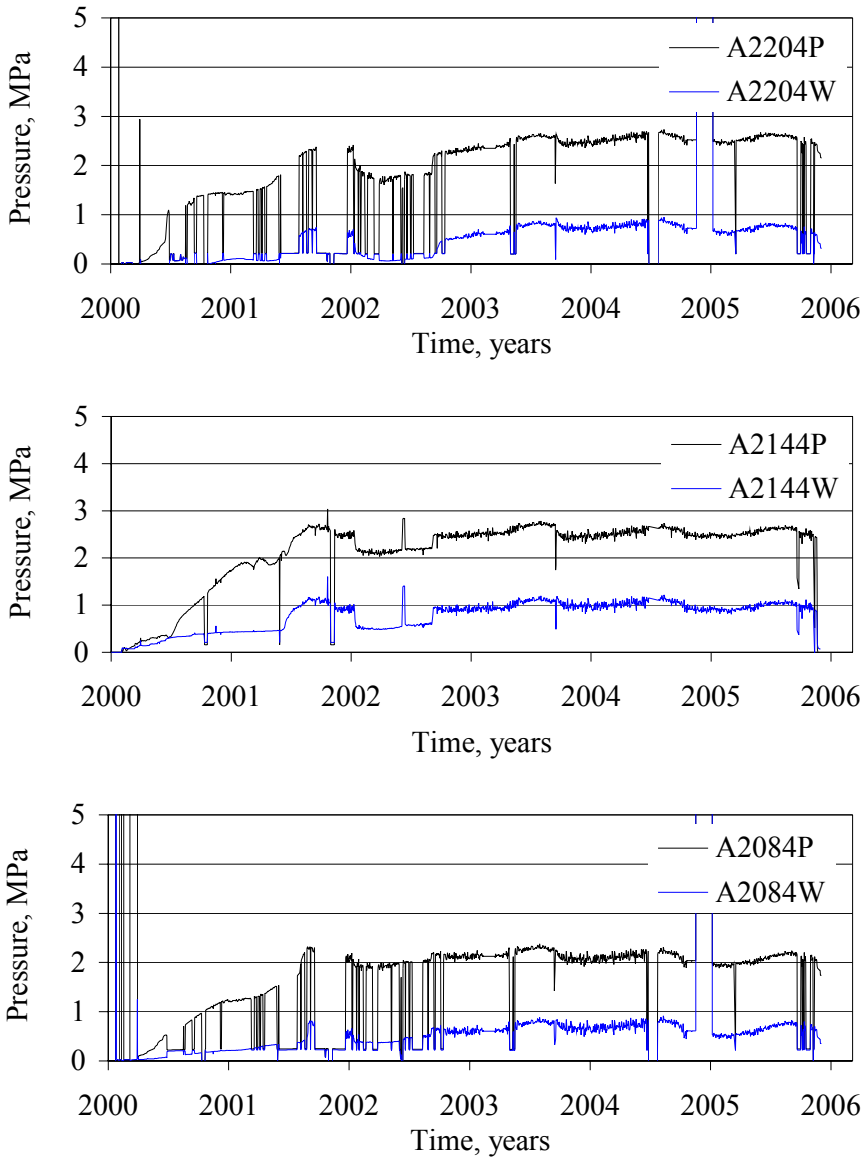

Figure 4-5 Total pressure (black lines) and water pressure (blue lines) versus time in block 20 (upper), 14 (mid) and in block 8 (lower) at mid position between the copper tube and the rock.

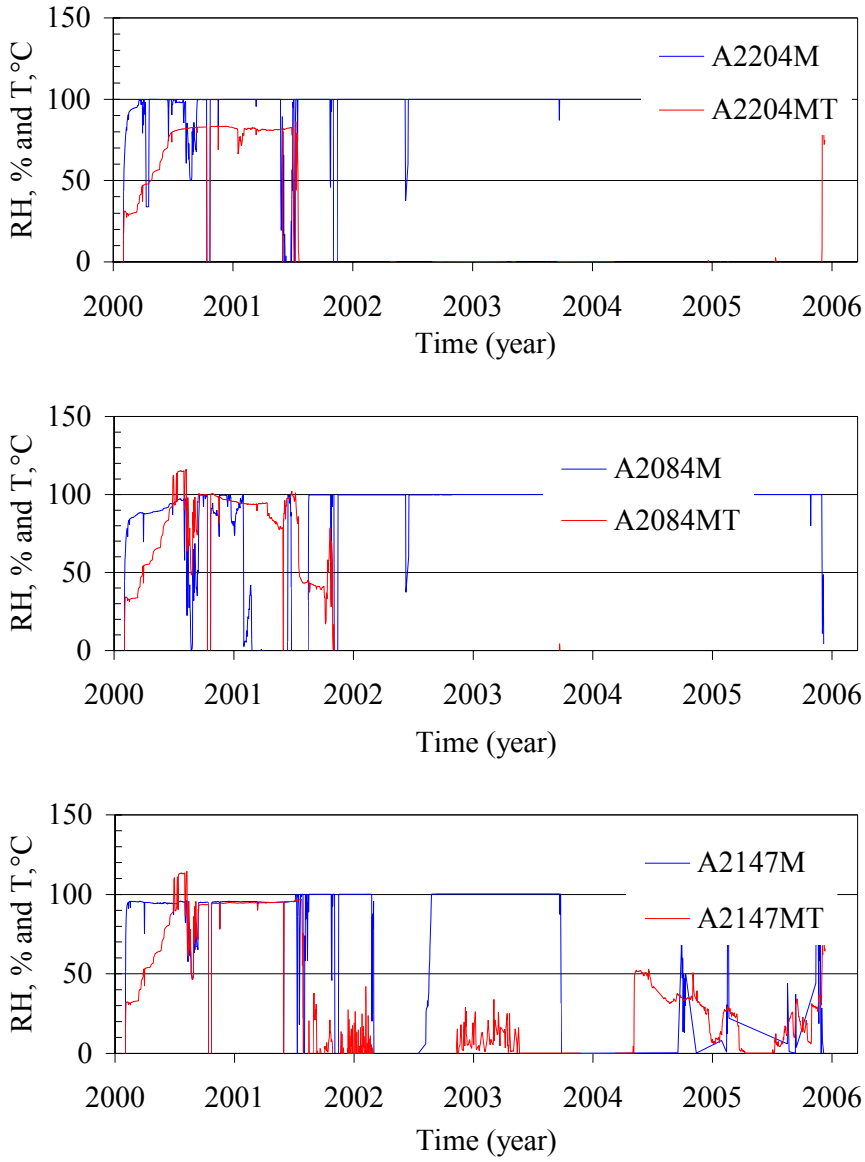

Figure 4-6 Results from the Vaisala moisture sensors showing temperature (red lines) and the in situ relative humidity (blue lines) in equilibrium with the bentonite in block A208, A214 and A220.

4.4. Termination of the field activity

4.4.1. Termination, drilling and uplift

The heater power was reduced to zero on December 6, 2005. The temperature drop was relatively fast and below 50°C within one week (Figure 4-4, right). The uncovering drilling operation is described in the Äspö HRL activity plan AP TD F62-05-023.

In short, the test parcel was partly released by overlapping percussion drilling in the surrounding rock. The diameter of the boreholes was 89 mm diameter and the depth was around 4.5 m. The final part of the circumference was core drilled with a diameter of 280 mm (Figure 4-7). The choice of percussion technique was motivated partly by economic

reasons, but mostly by the fact that no cooling water was necessary. The core drilling technique was used to finalize the slot around the parcel, since the rock support normally is poor at this stage which makes the steering of a percussion boring head cumbersome. The large diameter of the core drilled holes was motivated by the wire sawing equipment which was used to release the bottom of the rock column. The resulting free block containing parcel and covering rock was lifted by a crane lorry and transported to a dry niche for examination and sampling. The total weight of the rock/parcel block was around 4000 kg, and the diameter was around 65 cm. i.e. the rock cover of the test parcel was of a good size.

Figure 4-7 Left: Top part of the parcel with attached lifting device. Note the surrounding slot made by overlapping percussion drill holes and the larger core drilled holes. Right: Entire A2 test parcel with rock cover to be placed on the lorry for transport.

4.4.2. Partitioning of the parcel

The uncovering of rock and subsequent sampling operation started on January 17, 2006 and was finalized after two days of intense work. The operation is described in the Äspö HRL activity plan AP TD F62-06-001, and the course of events is described in detail in the appurtenant Daily log.

In short, the covering rock was successively removed approximately half a meter by sawing, wedges, and by use of natural weaknesses in the rock (Figure 4-8). The approximate position of the original block interfaces were identified in the exposed bentonite by use of the tubes going in to defined positions and by measuring. The bentonite blocks were cut by sawing and successively removed from the copper tube. The blocks were market in various ways and placed in plastic bags. Air was evacuated by use of a vacuum pump, and the bags were sealed and placed in plastic boxes which were closed. The main material was transported to Clay Technology laboratory in Lund for analyses and further distribution to the involved laboratories. Special care was taken to the blocks aimed for water analyses at VTT, mineralogical analyses performed by University of Bern, bacterial analyses by Micans laboratory, copper coupon analyses, and the bottom 6 blocks aimed for ^{60}Co tracer analyses at KTH. The VTT blocks were place in metal containers and air was replaced by an argon atmosphere in order to reduce redox reaction due to contact with air. The Uni Bern block was transported directly after release to the Äspö surface laboratory for partitioning and storing. The blocks aimed for bacterial activity analyses were quickly brought to an anaerobic box at the nearby underground bacterial test site at Äspö. The blocks containing copper coupons were sealed and transported directly for analyses at e.g. Studsvik AB. Finally, the KTH bottom part of the parcel was placed in a special box for prompt transport to the department of nuclear chemistry at KTH, Stockholm.

Figure 4-8 Left: Photo taken just after the removal of the first piece of rock from the upper part of the parcel. Note the well covered sensor tubes and the tight interface between bentonite and the covering rock. Right: Sawing cuts were made approximately at the original block interfaces and the released blocks were successively removed from the copper tube.

5 LABORATORY ANALYSES - GENERAL

5.1. Test philosophy

Reference material and material from defined positions in the A2 parcel material were tested and analyzed. The results were compared with respect to changes in physical properties and mineralogy. The present Lot A2 parcel material was analyzed with respect to mineralogy/chemisty not only by SKB and Posiva, but also by the four additional independent laboratories BGR in Germany, University of Bern in Switzerland, G2R and LEM from Nancy University in France, which were financed by BGR, NAGRA and ANDRA respectively.

The large number of performed physical tests and mineralogical/chemical analyses of the material were made without close contact between the different laboratories. The purpose was to get independent results based on the techniques normally used by the different laboratories, which to some extent differs by tradition. The most striking example is the cation exchange capacity, which was determined without using the same technique in two laboratories. The risk for systematic artifacts and resolution limitations are thereby believed to be reduced significantly.

Since absolute quantitative data are difficult to procure for some of the properties, the aim has been to reveal possible systematic discrepancies between parcel material from different positions and the reference material.

5.2. Test material

The six bottom blocks devoted for the ^{60}Co tracer analyses were only analyses at KTH, Stockholm and the results are presented in Appendix 2. Block 13 was only analyzed by the University of Bern and the results are presented in Appendix 7. One part of block 15 was analyzed by BGR, and the results are presented in Appendix 6, and another part of the same block was analyzed by the G2R and LEM laboratories and their results are presented in Appendix 5.

The main part of the blocks was transported to Clay Technology's laboratory, and selected blocks were divided by use of an electric band saw in order to produce test material according to Figure 5-1 Schematic block partition. SE and NW denote the directions of compass in the test-hole, figures denote the centre of the specimens expressed in centimeters measured from the block inner mantel surface, and A, B and C denotes the analyzed three vertical position in the blocks.. The rough partition of the clay at the test site enabled a relatively fast and precise sampling of the bentonite and the various additives was fairly easily localized. The partition was made within a few days in order to reduce redistribution of elements in the material. The sawn samples were made large enough to supply several planned tests from a specific position. In other words, material with the same specimen denomination was used for several different kinds of tests and analyses. The denomination of a specific point (centre of a volume) was according to the following example:

08ASE3 where

08 block number (counted from the bottom of the parcel),

A vertical level in the block,

SE direction of compass in the test hole,

3 radial distance in centimeters from the inner mantel surface to the centre of the specimen.

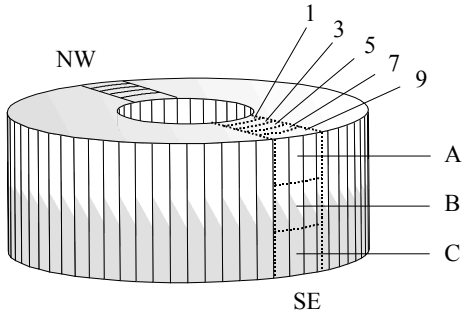

Figure 5-1 Schematic block partition. SE and NW denote the directions of compass in the test-hole, figures denote the centre of the specimens expressed in centimeters measured from the block inner mantel surface, and A, B and C denotes the analyzed three vertical position in the blocks.

6 BASIC GEOTECHNICAL PROPERTIES

6.1. Test principles

Basic geotechnical properties were determined for a large number of positions in the test material in order to give a general picture of especially density and the water distribution. Block no. 7, and every second block above, except block 13, were analyzed with respect to water ratio (w) and bulk density (D_b) from which the degree of saturation (S_r) was calculated. No specific preparation of the test material was made except for sawing specimens to a size corresponding to approximately 20 grams. The relatively large samples and quick handling after sawing were used in order to minimize drying artifacts.

All samples were taken at the mid height (B position) of the western side of the blocks in order to minimize interference from gauges and other test devices. An exception is block 19 where the south section was used. The sample bulk density (D_b = total mass/total volume) determined by weighing the material in air and submerged in paraffin oil. The bulk density was thereafter calculated according to:

$$D_b = \frac{m \cdot D_{paraffin}}{m_{paraffin}} \qquad \text{Equation 5}$$

where m is the mass of the specimen, $D_{paraffin}$ is the density of the paraffin oil, and $m_{paraffin}$ is the mass of displaced paraffin oil. All bulk density results are compiled in (Table 6-1 Measured bulk density of blocks 07 to 38 in parcel A2).

The water ratio (w) was determined by drying the material in a laboratory furnace at 105°C for 24 h, and the water ration was calculated according to:

$$w = \frac{m - m_d}{m_d} \qquad \text{Equation 6}$$

where m_d is the mass of the dry sample. All water ratio results are compiled in (Table 6-2).

The degree of saturation (S_r) was calculated from sample density (D_b) and water ratio (w) according to:

$$S_r = \frac{w \cdot D_b \cdot D_s}{D_w(D_s(w+1) - D_b)}$$ Equation 7

where D_s is the mean grain density, D_w is the water density. A mean grain density of 2750 kg/m^3 was used for the bentonite /Karnland et al., 2006/. All results of calculated degree of saturation are compiled in (Table 6-3).

Dry densities (D_d) were also calculated, but not presented here, from the saturated densities (D_m) assuming a water density of 1000 kg/m^3 according to:

$$D_d = \frac{D_m - D_w}{1 - \frac{D_w}{D_s}}$$ Equation 8

6.2. Results

The results show that there was a significant density distribution in the parcel bentonite mass. One extreme being the denser lower part close to the hot copper tube with a density around the KBS-3 target density, and the other extreme was the uppermost outer part close to the rock. The variations may still be considered quite small, taking into account the geometry and the temperature distribution in the parcel. Further all samples were fully water saturated within the accuracy of the measurements, which by definition means that the saturated densities were equal to the measured bulk densities.

The raw and calculated data are stored in Excel files and transferred to the SICADA database. The individual specimens were denominated according to the general description scheme. A typical denomination of a specimen is consequently A238BW1b, where A2 is the parcel, 38 is the block number, B is the mid height in the block, W is the western direction, 1 is the radial position, and finally the b denotes that it concerns the bulk material.

Table 6-1 Measured bulk density of blocks 07 to 38 in parcel A2

	Position, in cm from Cu tube				
Block no.	1	3	5	7	9
38	1864	1876	1859	1862	1847
33	1923	1922	1920	1918	1897
31	1941	1948	1943	1930	1898
29	1955	1962	1954	1941	1912
27	1954	1962	1957	1945	1912
25	1965	1960	1953	1916	1890
23	1977	1971	1964	1943	1917
21	1982	1978	1969	1955	1928
19	1979	1981	1962	1940	1921
17	1983	1987	1948	1951	1928
15	1977	1985	1959	1942	1919
11	1987	1993	1979	1950	1933
09	1990	1988	1975	1951	1934
07	2000	1991	1975	1954	1936

Table 6-2 Measured water ratios in parcel A2

	Position, in cm from Cu tube				
Block no.	1	3	5	7	9
38	0.376	0.380	0.374	0.393	0.408
33	0.321	0.321	0.320	0.325	0.337
31	0.309	0.305	0.309	0.316	0.336
29	0.301	0.299	0.304	0.314	0.331
27	0.309	0.303	0.304	0.312	0.333
25	0.299	0.301	0.304	0.320	0.340
23	0.293	0.293	0.299	0.313	0.332
21	0.285	0.289	0.293	0.304	0.326
19	0.287	0.285	0.303	0.317	0.333
17	0.282	0.278	0.295	0.308	0.324
15	0.280	0.279	0.300	0.316	0.330
11	0.268	0.271	0.279	0.297	0.316
09	0.269	0.271	0.282	0.303	0.318
07	0.275	0.274	0.283	0.298	0.314

Table 6-3 Calculated degree of saturation (S_r) in parcel A2

	Position, in cm from Cu tube				
Block no.	1	3	5	7	9
38	1.00	1.02	1.00	1.02	1.02
33	0.99	0.99	0.99	0.99	0.99
31	0.99	1.00	1.00	0.99	0.99
29	1.00	1.00	1.00	1.00	1.00
27	1.01	1.01	1.00	1.00	1.00
25	1.00	1.00	1.00	0.98	0.98
23	1.01	1.00	1.00	1.00	1.00
21	1.00	1.00	1.00	1.00	1.00
19	1.00	1.00	1.01	1.01	1.01
17	1.00	1.00	0.98	1.00	1.00
15	0.99	0.99	1.00	1.01	1.00
11	0.98	0.99	0.99	0.98	1.00
09	0.98	0.98	0.99	1.00	1.00
07	1.01	0.99	0.99	0.99	1.00
Mean	1.00	1.00	1.00	1.00	1.00

7 SEALING PROPERTIES

7.1. Test principles

The hydraulic conductivity and swelling pressure were determined in combined tests on material chosen from strategic positions within the test parcel and on the corresponding reference material. The test series includes the following sub-series and the all samples are summarized in Table 7-1 Results from swelling pressure and hydraulic conductivity tests.:

- reference material, air-dry preparation, Äspö-water, 6 samples
- parcel material, air-dry preparation, Äspö-water, 6 samples
- parcel material, naturally saturated, Äspö-water, 6 samples

Five purpose-built swelling pressure test cells made of acid-proof stainless steel were used (Figure 7-1). The samples were confined by cylinder rings with a diameter of 20 mm and stainless steel filters at the top and bottom. The test volumes were sealed by o-rings placed between the bottom plates and the cylinder rings and between the pistons and the cylinder rings. At test start the height of the test volumes were fixed to 10 mm by the flanges on the moveable pistons. The axial force from a sample was determined by the transducer placed between the piston and the upper lid. The displacement of the piston due to transducer deformation is 100 μm at maximum force, which consequently correspond to 1% of the sample height and is considered insignificant

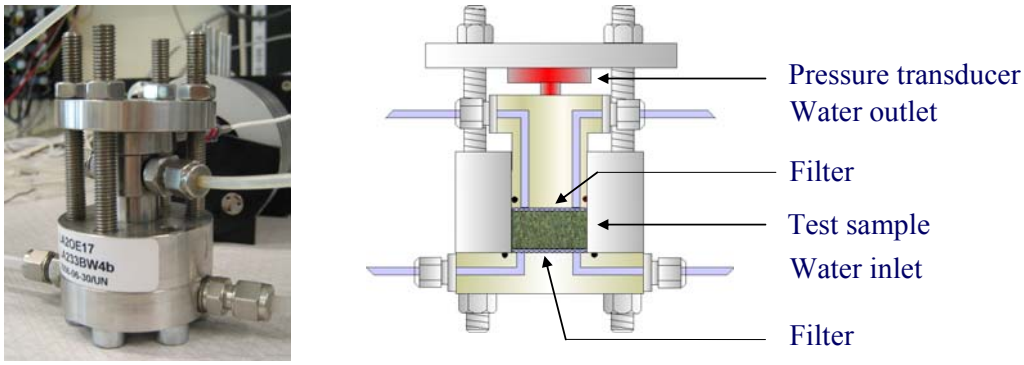

Figure 7-1 Schematic drawing of the swelling pressure oedometer which was used for determination of swelling pressure and hydraulic conductivity.

The reference samples were prepared from reference material saved from the block production, and the parcel material was prepared in to ways;

- air-dried and crushed to a grain size similar to the original MX-80 powder and re-compacted to a density of 2000 kg/m^3
- sawed and trimmed to fit the sample holders and thus have a density close to the field value.

Air was evacuated from the test volumes by use of a vacuum pump (approximately 2 kPa) and the test solution was allowed to enter the specimen from both filters. A minor water pressure (10 kPa) was applied and the water uptake was indirectly monitored by the force transducer (Figure 7-1). Stable force conditions were reached within 1 week. At this point the water pressure in the bottom inlet as increased to 50%, at a maximum, of the measured swelling pressure in order to start percolation. The volumes of the percolated water solution were registered daily by visual observations of the water/air interface meniscus.

The water pressure was thereafter reduced to zero and the tests were terminated when the recorded axial forces had stabilized. The two stable force conditions, i.e. before and after percolation, were used to evaluate the swelling pressure.

The swelling pressure *Ps* (Pa) was calculated from the measured force at zero water pressure according to:

$$P_s = \frac{F}{A} \qquad \text{Equation 9}$$

where F is the axial force (N) and A is the sample area acting on the piston (m^2). The accuracy of the measured values is governed by the force transducers which were calibrated against a standard force ring before and after each test.

The hydraulic conductivity k (m/s) was evaluated from the percolated water volume according to Darcy´s law:

$$k = \frac{V \cdot l}{A \cdot h \cdot t} \qquad \text{Equation 10}$$

where V is the percolated volume (m^3), l is the sample length (m), A is the sample area (m^2), h is the water pressure difference over the sample expressed as water column (m) and t is the time (s).

At test termination, the samples were split in two halves and the sample bulk density (D_b) and water ratio (w) were determined by the same technique as described in section 6.1

7.2. Results

The accuracy of both pressure and density determinations were good. The scatter in density of the trimmed samples are due to more or less good fit to the sample holders, and a small swelling has obviously took place in some samples, but with no tendency to give abnormal results (Figure 7-2 Measured swelling pressure results from the A2 parcel material compared with reference material and to the previous one year test material (A0).. No differences were found in the results from warm positions compared to those from the upper cool positions or from the reference material The results from the A2 parcel are also in good agreement with previously measured results, e.g. from the one year parcel and reference material.

The hydraulic conductivity of the trimmed samples generally showed a lower hydraulic conductivity compared to all other samples (Figure 7-3 Measured hydraulic conductivity results from the A2 parcel material compared with results from reference material and to the previous one year test material (A0).). There is however no difference between samples from different positions in the parcel. The somewhat lower conductivities in the trimmed samples can consequently not be related to temperature or temperature gradients.

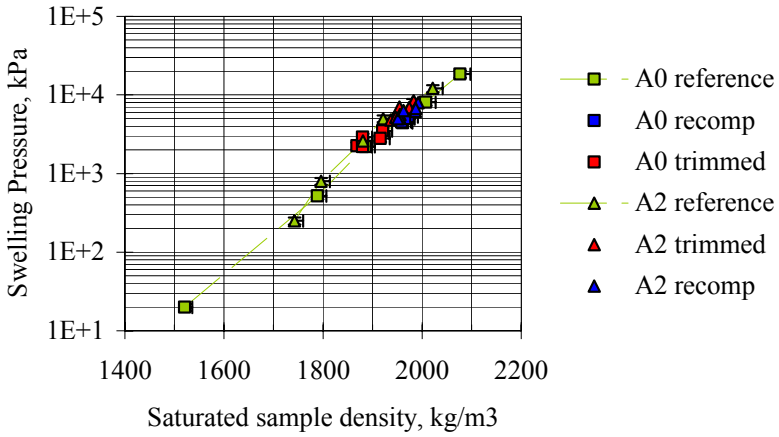

Figure 7-2 Measured swelling pressure results from the A2 parcel material compared with reference material and to the previous one year test material (A0).

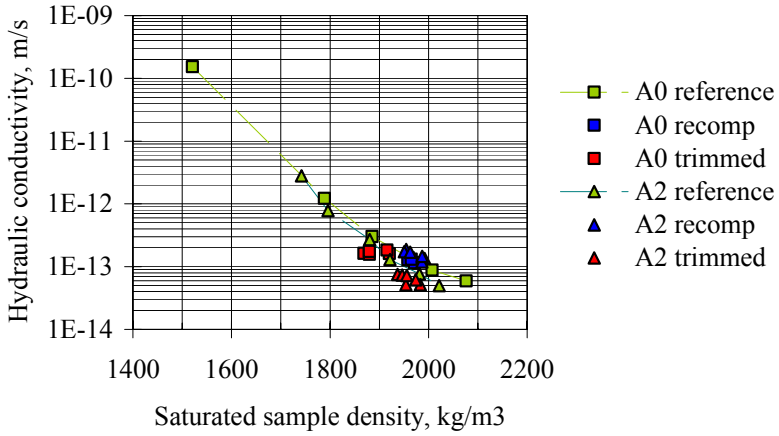

Figure 7-3 Measured hydraulic conductivity results from the A2 parcel material compared with results from reference material and to the previous one year test material (A0).

Table 7-1 Results from swelling pressure and hydraulic conductivity tests. Groundwater from bore-hole HG0038B01 was used in all tests

Test material	Preparation	Water ratio	Bulk Density,	Swelling pressure	Hydraulic conductivity
		%	kg/m^3	MPa	m/s
LA2R	air-dry	0.494	1742	0.25	2.8E-12
LA2R	air-dry	0.436	1796	0.80	7.8E-13
LA2R	air-dry	0.359	1881	2.60	2.7E-13
LA2R	air-dry	0.327	1922	5.0	1.3E-13
LA2R	air-dry	0.285	1981	8.1	7.7E-14
LA2R	air-dry	0.259	2022	12.1	5.0E-14
LA209BS4b	air-dry	0.303	1955	5.1	1.9E-13

LA209BS8b	air-dry	0.278	1992	7.9	1.4E-13
LA211BS4b	air-dry	0.306	1951	5.0	1.7E-13
LA211BS8b	air-dry	0.281	1987	6.2	1.2E-13
LA233BW4b	air-dry	0.281	1987	6.7	1.5E-13
LA233BW8b	air-dry	0.297	1963	6.3	1.7E-13
LA209BS4b	trimmed	0.284	1983	8.4	5.1E-14
LA209BS8b	trimmed	0.303	1954	7.0	5.1E-14
LA211BS4b	trimmed	0.290	1974	6.9	6.2E-14
LA211BS8b	trimmed	0.316	1937	4.8	7.5E-14
LA233BW4b	trimmed	0.309	1946	5.2	7.4E-14
LA233BW8b	trimmed	0.302	1955	5.6	7.2E-14

The samples may be considered fully water saturated due to the test conditions, and the dry density, void ratio and porosity can be calculated since the grain density is known.

The raw and calculated data have been stored in Excel files and transferred to the SICADA database. The test series was termed LA2OE (OE for oedometer test) and the individual specimens were denominated according to the general scheme, e.g. LA209BS2b

8 RHEOLOGICAL PROPERTIES

Ann Dueck, Clay Technology AB

8.1. Triaxial tests

8.1.1. Test principles

The strength properties of soil materials are preferably evaluated from triaxial tests. A description concerning technique and evaluation is given by Börgesson et al. (1995). The technique requires relatively large test specimens and is resource consuming, and since no major discrepancies between the reference material and parcel material were expected, only a few tests were planned for. Three samples from the parcel and one reference sample were tested.

Three tests were run on parcel material; two representing high temperature conditions (blocks 09 and 11), and one low temperature condition (block 33). The specimens were sawn from the inner part of the block cylinder ring (position 0 to 4 in the radial direction). (Table 8-1).

Table 8-1 The LOT A2 triaxial test series (LA2TL).

Test ID	Material	Preparation	Solution	Density	Max temperature of the parcel material
				kg/m^3	^{o}C
LA2TL01	LA209BS2b	sawn	LOT	parcel	125
LA2TL02	LA211BS2b	sawn	LOT	parcel	125
LA2TL03	LA233BS2b	sawn	LOT	parcel	30
LA2TL04	MX-80 LA2R	air-dry	LOT	1950	

8.1.2. Equipment

The test specimens were pre-saturated in a cylindrical saturation device equipped with an axial steel filter to achieve radial saturation. A piston allows for measurement of the axial swelling pressure parallel to the saturation. The device is axially divisible in order to enable removal of the specimens without use of axial force.

A high pressure triaxial cell was used for all tests. The cell is equipped with standard strain gauges, force transducers and pore-pressure transducers according to Figure 8-1.

8.1.3. Sample Preparation

Cylindrical specimens were prepared from the parcel material by sawing rough work pieces which were trimmed to a cylindrical form with a diameter of 35 mm and a height of 70 mm. The reference sample was compacted from air-dry powder to the same dimensions, and water saturated in the same saturating device as used for the parcel samples. After 4 weeks in the saturation device each sample was mounted in the triaxial cell (Figure 8-1), and a cell pressure corresponding to the measured swelling pressure was applied in the cell. The valve to the pedestal was kept closed during an equilibration period and the pore pressure (u) at the base pedestal was measured. Filter paper drains along the samples were used to accelerate the equalization of the pore pressure over the sample height.

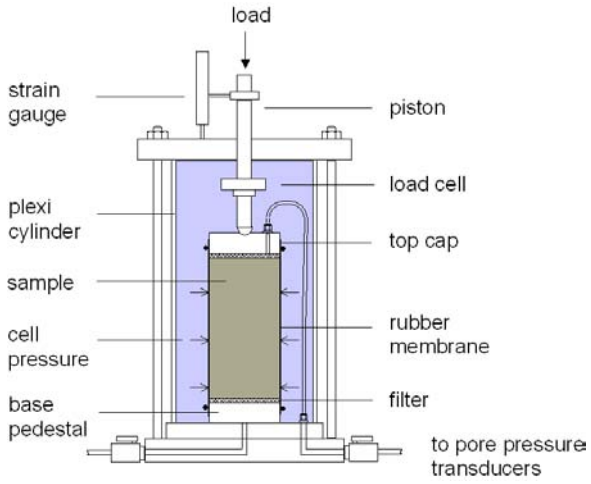

Figure 8-1 Triaxial test equipment.

8.1.4. Test procedure

The cell was placed in a mechanical press when pressure equilibrium was reached and the pore pressure was considered stable with time. A constant shear rate of 7.5 mm/week ($7.4 \cdot 10^{-4}$ mm/min) was applied. The sample was undrained during the course of shearing. After failure the water ratio and density of the specimens were determined. The water ratio and the density were determined according to section 6.1.

8.1.5. Data flow and evaluation

The cell pressure (σ_3), pore pressure (u), deformation (Δl), and axial force (F) were measured. The samples were considered as undrained during shearing and no volume change was taken into account. The deviator stress is calculated from:

$$q = \frac{F}{A_0}\left(\frac{l_0 - \Delta l}{l_0}\right) \qquad \text{Equation 11}$$

where A_0 is the specimen initial cross section area and l_0 the initial length of the sample. The contact area between load piston and top-cap is considered insignificant.

The vertical total stress (σ_1) is calculated from:

$$\sigma_1 = q + \sigma_3 \qquad \text{Equation 12}$$

The average effective stress (p') is calculated from:

$$p' = \frac{1}{3}(\sigma_1 + 2\sigma_3 - 3u) \qquad \text{Equation 13}$$

The strain (ε) is calculated from:

$$\varepsilon = \frac{\Delta l}{l_0} \qquad \text{Equation 14}$$

The measured cell pressure, pore pressure, deformation, and axial force versus time were stored together with the calculated stresses, strain, water ratio and density data in an Excel file. The test series are termed LA2TL (TL for triaxial test) and the individual specimens are denominated according to the general LOT scheme, e.g. LA209BS2b. In the result

section this individual specimen is denoted x_09_2 which means test number_block number_distance in cm from the canister.

8.1.6. Results

Deviatoric stress versus strain resulting from the triaxial tests are shown in Figure 8-2. The stress path is plotted as deviatoric stress vs. mean effective stress in Figure 8-3. In Results from the triaxial tests. final water content and density are noted for each sample together with the swelling pressure measured during saturation. Stresses and strain at maximum deviatoric stress during shearing are also noted in Table 8-2.

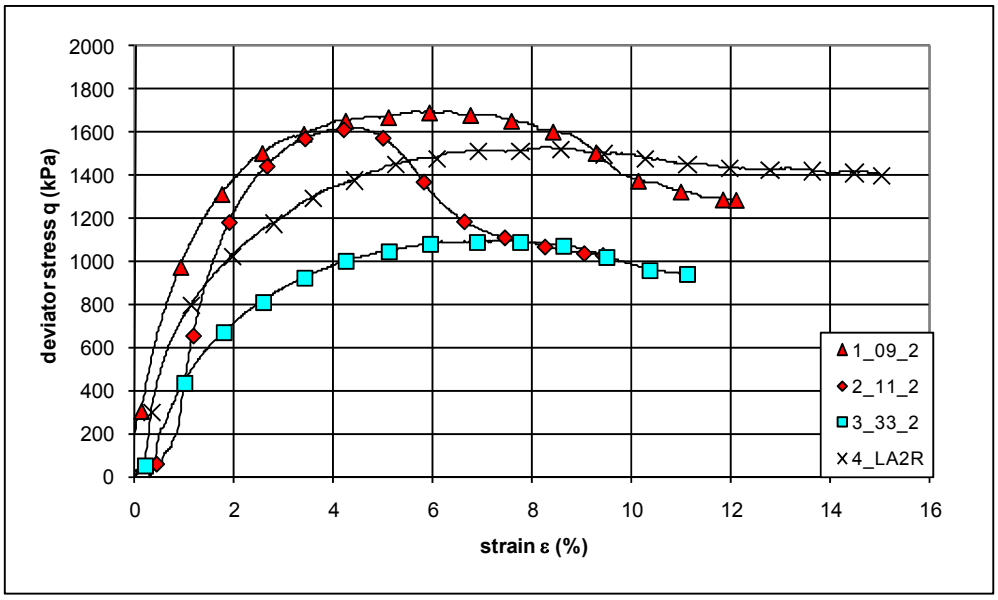

Figure 8-2 Deviator stress vs. strain resulting from the triaxial tests.

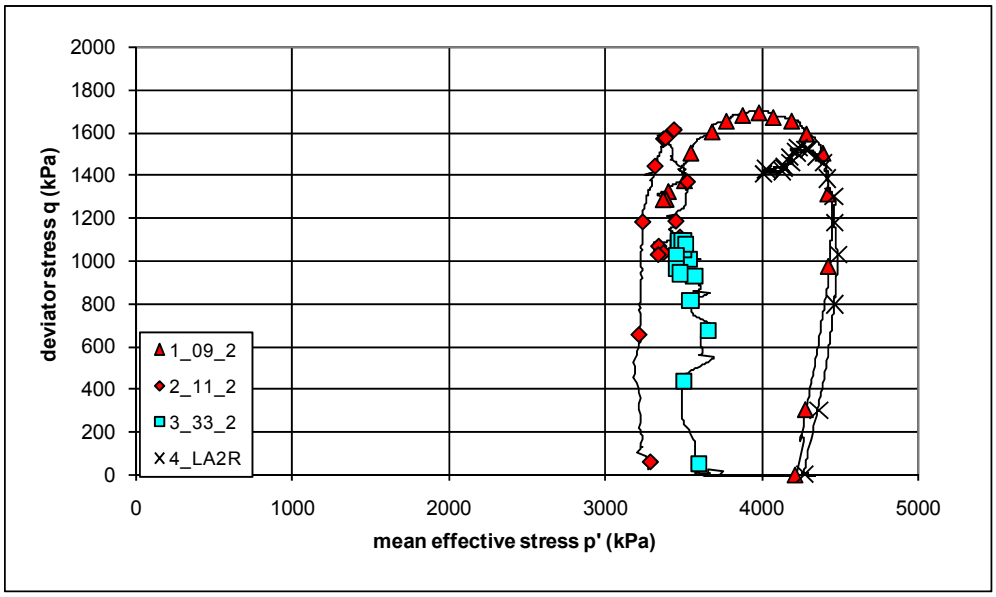

Figure 8-3 Stress paths plotted as deviatoric stress vs. mean effective stress.

Table 8-2 Results from the triaxial tests.

Test ID	Labels	Final average density g/cm^3	w %	swelling pressure kPa	shearing, at failure q_f kPa	p'_f kPa	ε_f %	σ_{3f} kPa	u_f kPa
LA2TL01	1_09_2	1,94	32,2	4400	1696	4043	6	4498	1020
LA2TL02	2_11_2	1,95	31,1	4000	1600	3458	5	4848	1924
LA2TL03	3_33_2	1,91	34,3	3400	1087	3497	6	4675	1540
LA2TL04	4_LA2R	1,94	32,0	3580	1531	4279	8	4515	746

8.1.7. Discussion

The result is presented in Figure 8-4 with values from the literature. No significant discrepancies are seen between the reference and parcel material with respect to shear strength and shear course. Since influence of salt seems to influence the resulting deviator stress (cf. MX-80 3.5% NaCl) the results were expected to fall on a line slightly above the results for MX-80 samples given in Figure 8-4. The sample deviating the most from this is 3_33_2, taken from a block representing low temperature conditions.

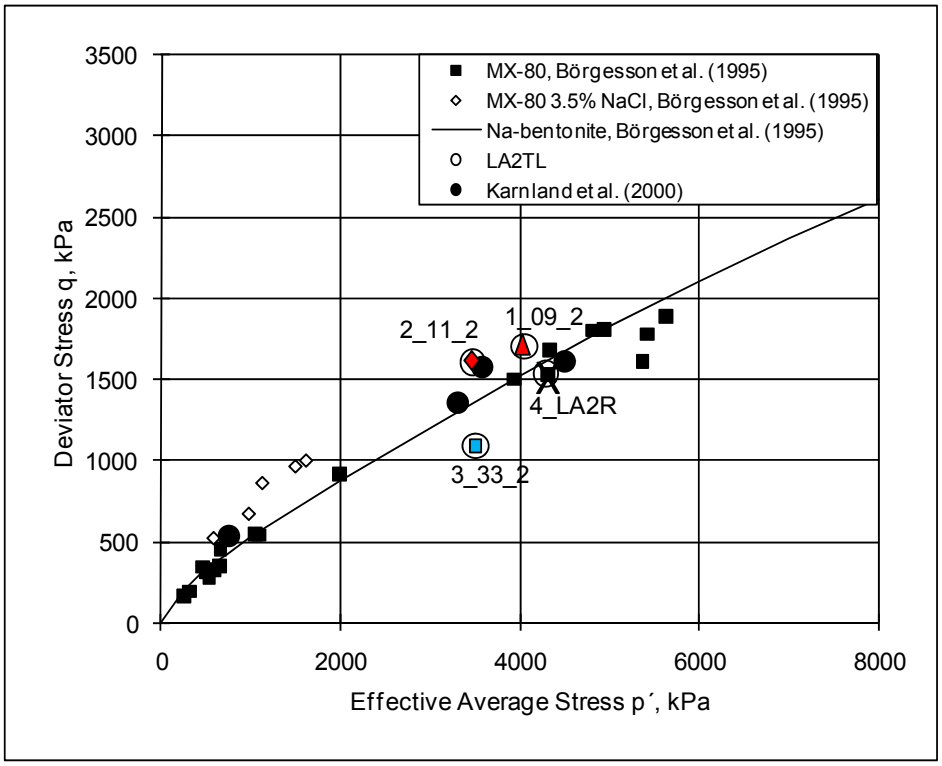

Figure 8-4 Maximum deviator stress versus effective average stress for different bentonites. Results from the present investigation are shown with circles around the symbols (triangle, rhomb, square, cross) denoting the block or reference (09, 11, 33, LA2R). The results are presented with results from /Karnland et al., 2000/ and /Börgesson et al., 1995/. The open rhombs represent MX-80 saturated with a 3.5% NaCl solution.

The deviation of the results from sample 3_33_2 might have been caused by a too high p' (Figure 8-4). In order to represent the conditions of the sample the effective average stress p' requires a representative pore pressure. The sample 3_33_2 suffered from leakage problems and the sample was dismantled and re-mounted in the triaxial cell. The slow response in pore water pressure was even slower after the re-mounting. This could

indicate that the effective average p' stress did not fully represent the conditions of this sample. In all tests the pore pressure was 200 kPa or higher at the start of the shearing.

8.1.8. Preliminary conclusions

From the limited series with only four tests the conclusion is that the results show no significant discrepancies from earlier reported results regarding shear strength. This is in agreement with the expected results.

8.2. Unconfined compression tests

8.2.1. Test principle

The stress-strain-strength properties are suitable indicator for evaluating relative rheological changes between different positions in the test parcel and the reference material. A simplified way to determine the stress-strain-strength properties is to perform unconfined compression tests, also called uniaxial compression test. In this type of test a sample is compressed axially with a constant rate of strain with no radial confinement or external radial stress. The test can be regarded as a consolidated unconfined compression test, since the fully water saturated samples are attained by a negative pore pressure, which is similar to the swelling pressure. Unconfined compression tests on saturated bentonite have been reported by /Börgesson and Johannesson, 2003/ and on unsaturated bentonite by /Börgesson and Johannesson, 1995/.

In the present test series the dimension of the test samples was minimized in order to get spatial resolution of the test parcel, and a rather small diameter (2 cm) was settled. It was important to ensure saturation of the samples and the height was therefore also minimized to 2 cm. The experience with respect to the absolute value of shear strength evaluated from samples with the height equal to the diameter is however limited since common practice is to use specimens with a height which is twice as long as the diameter. The results are therefore only used to evaluate relative changes, which was also the main purpose of the test type.

A relatively large number of specimens were tested in the series termed the LOT series (Table 8-3) representing high temperature parcel material (LA2UC01 to LA2UC12), low temperature parcel material (LA2UC13 to LA2UC18) and reference material (LA2UC19 to LA2UC30). Samples were sawn from the radial positions 1, 3, 5, 7, 9 cm in block no. 9, 11 and 33. The sixth sample in each block was a doublet sample taken from the radial position 1 cm. The maximum deviatoric stress resulting from the unconfined compression test will be influenced by for example sample density and reference tests were run in order to determine this relationship. Some of the reference tests were performed to improve the test technique.In addition, one series with parcel material (LA2UC101-106) including both high and low temperature material in the same series was run. Finally, one series with three specimens with air-dried, milled and compacted material from a warm section (LA2UC231-233) were run.

Table 8-3 The basic LOT test series with unconfined compression test series (LA2UC). The max temperatures are evaluated from Figure 4-4.

Test ID	Material	Preparation	Solution	Density	Max temperature
				kg/m^3	^{o}C
LA2UC01	LA209BS1b	drilled	LOT	parcel	125
LA2UC02	LA209BS3b	drilled	LOT	parcel	115

LA2UC03	LA209BS5b	drilled	LOT	parcel	100
LA2UC04	LA209BS7b	drilled	LOT	parcel	95
LA2UC05	LA209BS9b	drilled	LOT	parcel	80
LA2UC06	LA209BS1b	drilled	LOT	parcel	125
LA2UC07	LA211BS1b	drilled	LOT	parcel	125
LA2UC08	LA211BS3b	drilled	LOT	parcel	115
LA2UC09	LA211BS5b	drilled	LOT	parcel	100
LA2UC10	LA211BS7b	drilled	LOT	parcel	95
LA2UC11	LA211BS9b	drilled	LOT	parcel	80
LA2UC12	LA211BS1b	drilled	LOT	parcel	125
LA2UC13	LA233BS1b	drilled	LOT	parcel	35
LA2UC14	LA233BS3b	drilled	LOT	parcel	25
LA2UC15	LA233BS5b	drilled	LOT	parcel	25
LA2UC16	LA233BS7b	drilled	LOT	parcel	25
LA2UC17	LA233BS9b	drilled	LOT	parcel	25
LA2UC18	LA233BS1b	drilled	LOT	parcel	35
LA2UC19	MX-80 LA2R	compacted	de-ionized	1850	20
LA2UC20	MX-80 LA2R	compacted	LOT	1850	20
LA2UC21	MX-80 LA2R	compacted	de-ionized	1950	20
LA2UC22	MX-80 LA2R	compacted	LOT	1950	20
LA2UC23	MX-80 LA2R	compacted	de-ionized	2050	20
LA2UC24	MX-80 LA2R	compacted	LOT	2050	20
LA2UC25	MX-80 LA2R	compacted	LOT	1850	20
LA2UC26	MX-80 LA2R	compacted	LOT	1850	20
LA2UC27	MX-80 LA2R	compacted	LOT	1950	20
LA2UC28	MX-80 LA2R	compacted	LOT	1950	20
LA2UC29	MX-80 LA2R	compacted	LOT	2050	20
LA2UC30	MX-80 LA2R	compacted	LOT	2050	20
LA2UC101	LA211BN5b	drilled	LOT	parcel	100
LA2UC102	LA233BSE5b	drilled	LOT	parcel	25
LA2UC103	LA211BN5b	drilled	LOT	parcel	100
LA2UC104	LA233BN5b	drilled	LOT	parcel	25
LA2UC105	LA211BN5b	drilled	LOT	parcel	100
LA2UC106	LA233BN5b	drilled	LOT	parcel	25

LA2UC231	LA211BSE1b	milled and compacted	LOT	1970	125
LA2UC232	LA211BSE1b	milled and compacted	LOT	1970	125
LA2UC233	LA211BSE1b	milled and compacted	LOT	1970	125

It was decided to further investigate the influence of increased temperature also on material not exposed to the LOT field conditions. The series termed the LAB series (Table 8-4) was therefore performed. The objectives of this series was to illustrate the stress-strain behaviour after

- exposure to 20°C, 90°C, 120°C and 150°C after water saturation (LAUC201-218).
- cyclic change in temperature between 20°C and 120°C (LAUC219-225).
- exposure to 120°C before water saturation (LAUC234-236).
- influence of high water pressure (LAUC237-242).

The specimens were exposed to increased temperature in an oven in the laboratory. The material used was a reference material R1 with the same quality symbol MX-80 as LA2R. Tests were also made to show the influence of density (LAUC225-230).

Table 8-4 The LAB test series, in which influence of increased temperature was investigated on material not exposed to the LOT field conditions.

Test ID	Material	Preparation	Solution	Density	Temperature in oven
				kg/m^3	°C
LA2UC201	MX-80 R1	compacted	de-ionized	1970	20
LA2UC202	MX-80 R1	compacted	de-ionized	1970	20
LA2UC203	MX-80 R1	compacted	de-ionized	1970	20
LA2UC204	MX-80 R1	compacted	de-ionized	1970	120
LA2UC205	MX-80 R1	compacted	de-ionized	1970	120
LA2UC206	MX-80 R1	compacted	de-ionized	1970	120
LA2UC207	MX-80 R1	compacted	de-ionized	1970	20
LA2UC208	MX-80 R1	compacted	de-ionized	1970	20
LA2UC209	MX-80 R1	compacted	de-ionized	1970	20
LA2UC210	MX-80 R1	compacted	de-ionized	1970	150
LA2UC211	MX-80 R1	compacted	de-ionized	1970	150
LA2UC212	MX-80 R1	compacted	de-ionized	1970	150
LA2UC213	MX-80 R1	compacted	de-ionized	1970	90
LA2UC214	MX-80 R1	compacted	de-ionized	1970	90
LA2UC215	MX-80 R1	compacted	de-ionized	1970	90
LA2UC216	MX-80 R1	compacted	de-ionized	1970	120
LA2UC217	MX-80 R1	compacted	de-ionized	1970	120

LA2UC218	MX-80 R1	compacted	de-ionized	1970	120
LA2UC219	MX-80 R1	compacted	de-ionized	1970	120
LA2UC220	MX-80 R1	compacted	de-ionized	1970	120
LA2UC221	MX-80 R1	compacted	de-ionized	1970	120
LA2UC222	MX-80 R1	compacted	de-ionized	1970	120
LA2UC223	MX-80 R1	compacted	de-ionized	1970	120
LA2UC224	MX-80 R1	compacted	de-ionized	1970	120
LA2UC225	MX-80 R1	compacted	de-ionized	1850	20
LA2UC226	MX-80 R1	compacted	de-ionized	1950	20
LA2UC227	MX-80 R1	compacted	de-ionized	2050	20
LA2UC228	MX-80 R1	compacted	de-ionized	1850	20
LA2UC229	MX-80 R1	compacted	de-ionized	1950	20
LA2UC230	MX-80 R1	compacted	de-ionized	2050	20
LA2UC234	MX-80 R1	compacted	de-ionized	1970	120
LA2UC235	MX-80 R1	compacted	de-ionized	1970	120
LA2UC236	MX-80 R1	compacted	de-ionized	1970	120
LA2UC237	MX-80 R1	compacted	de-ionized	1970	20
LA2UC238	MX-80 R1	compacted	de-ionized	1970	20
LA2UC239	MX-80 R1	compacted	de-ionized	1970	20
LA2UC240	MX-80 R1	compacted	de-ionized	1970	20
LA2UC241	MX-80 R1	compacted	de-ionized	1970	20
LA2UC42	MX-80 R1	compacted	de-ionized	1970	20

8.2.2. Equipment

The test specimens were put in a saturation device prior to the shear tests in order to ensure full saturation. Two different devices were used for the saturation. The first one was divisible and made of steel (LA2UC01-06, LA2UC19-30) the second one was not divisible and made of peek (LA2UC07-18, LA2UC101-106, LA2UC201-242). No measurement of swelling pressure was done during the saturation.

After saturation each sample was taken out of the saturation device and placed in a mechanical press (Figure 8-5). During the test the deformation and the applied force were measured by means of standard laboratory force and strain transducers.

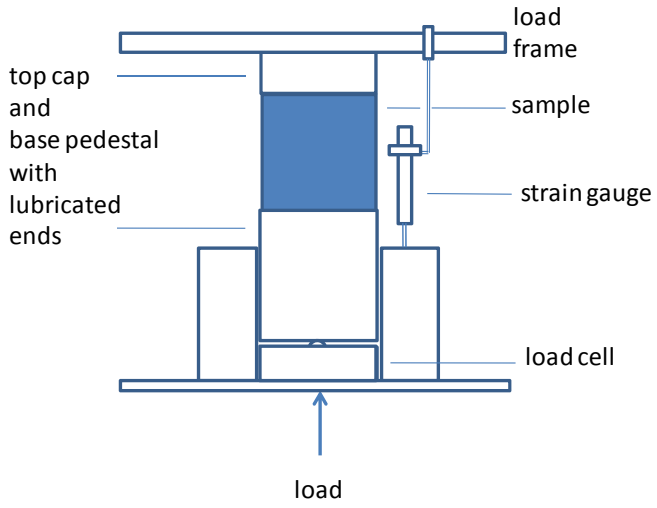

Figure 8-5 Set-up used for the unconfined compression tests, see also photos in Figure 8-13.

8.2.3. Sample preparation

Cylindrical specimens were prepared from the parcel material by core drilling cylindrical samples with 20 mm in diameter which were cut to the height 20 mm. The compacted samples were prepared in a compaction device to the same size from air-dry MX-80 powder and then saturated. All samples were placed in a saturation device for at least 2 weeks.

During the preparation and still in the saturation device some of the samples in the LAB series (Table 8-4) were exposed to increased temperature in an oven during 24h or more. Increases and decreases in temperature were made in steps of 30°C and each temperature was kept for a minimum of 5h. The saturation and dismounting used in the LAB series (Table 8-4) deviated slightly from the LOT series (Table 8-4) mainly due to the increasing temperature involved in the LAB series.

8.2.4. Test procedure

The samples were placed in a mechanical press after the saturation. The top cap and base pedestal had lubricated ends towards the specimen. The compression started and continued at a constant rate of 0.16 mm/min. After failure of the sample the water ratio was determined according to Section 6.1. The density was determined from the mass of the samples and the volume of specimen in the saturation device.

8.2.5. Data flow and evaluation

The samples were considered as undrained during shearing and no volume change was taken into account. The deviator stress is evaluated from:

$$q = \frac{F}{A_0} \cdot \left(\frac{l_0 - \Delta l}{l_0}\right) \qquad \text{Equation 15}$$

where q denote deviatoric stress, F applied vertical load, A_0 original cross section area, l_0 original length, and finally Δl denotes change in length

The axial force and deformation versus time were stored together with the calculated stress, strain, water ratio and density data in Excel files. The test series was termed

LA2UC (UC for unconfined compression test) and individual specimens were denominated according to general scheme e.g. A211BS2b. In the result section this individual specimen is denoted x_11_2 which means test number_block number_distance in cm from the canister.

8.2.6. Results

The test results from the parcel material are shown as deviatoric stress vs. strain in Figure 8-6 to Figure 8-6. The colours refer to the temperature coupled to the position of the specimen in the LOT parcel and given in Section 4.3.2. From the warmest to the coldest the colours (red, orange, yellow, green, blue and purple) represent the average temperatures (125˚C, 115˚C, 100˚C, 90˚C, 40˚C, 20˚C). The black lines are the reference tests for an applicable density. The density of each specimen is shown to the right in the Figures.

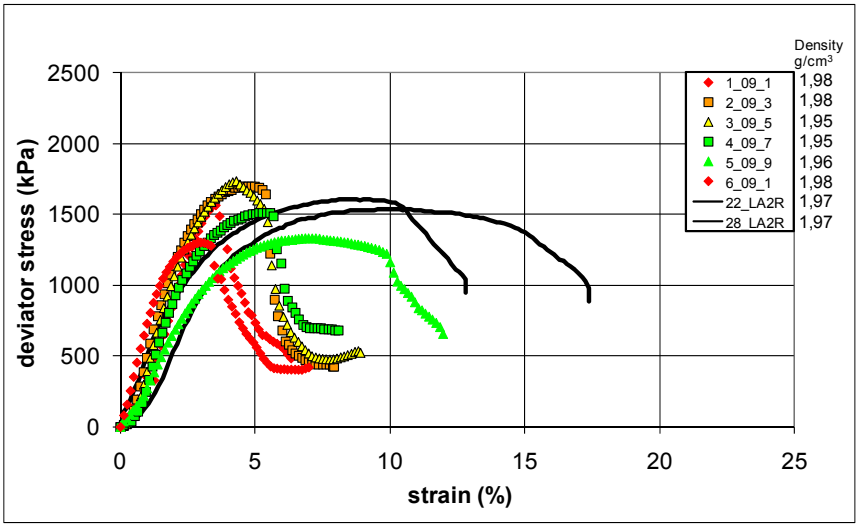

Figure 8-6 Test results from specimens from block 09. The labels denote the test number_ block_distance from the canister. Two reference tests are also shown.

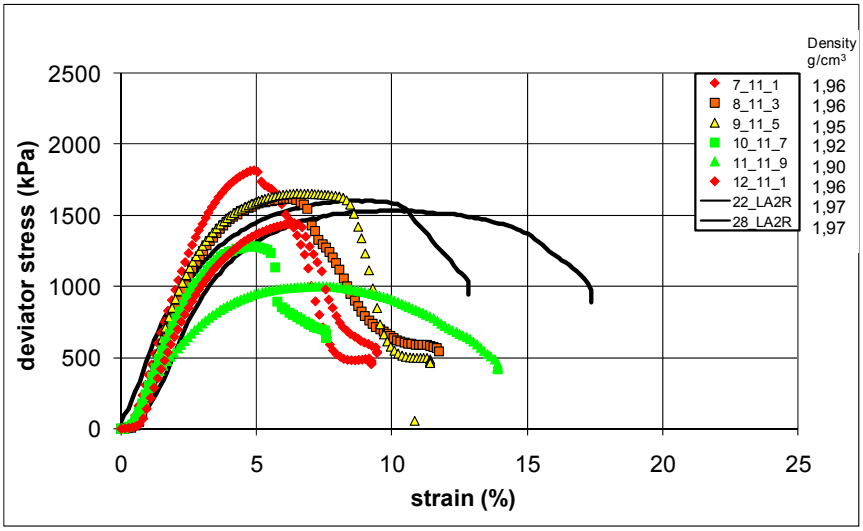

Figure 8-7 Test results from specimens from block 11. The labels denote the number of the test_the block_distance from the canister in cm. Two reference tests are also shown.

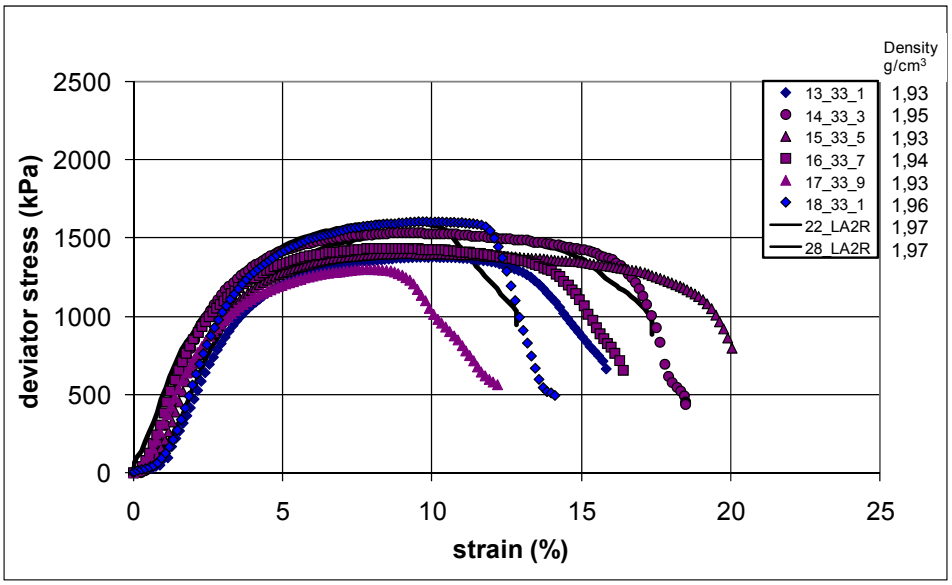

Figure 8-8 Test results from specimens from block 33. The labels denote the number of the test_the block_distance from the canister in cm. Two reference tests are also shown.

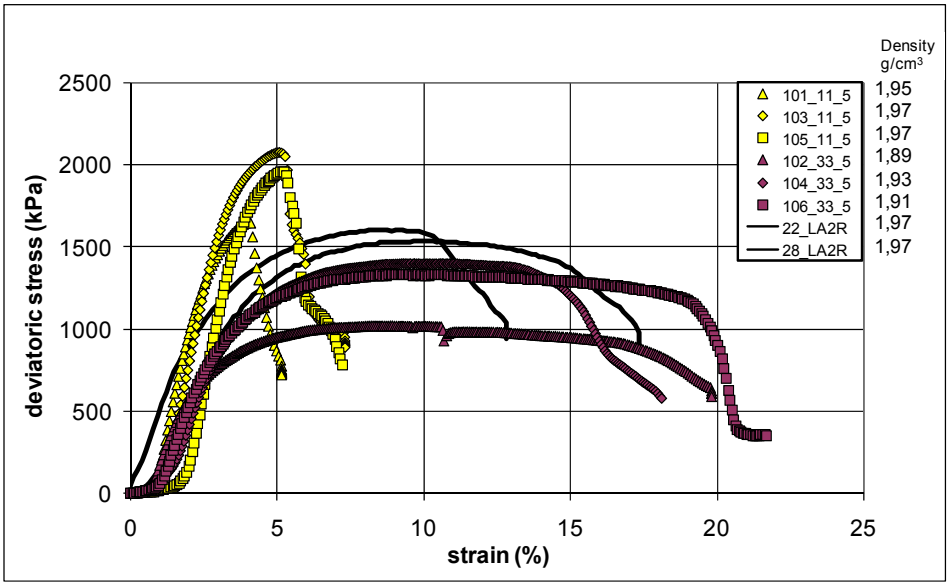

Figure 8-9 Test results from specimens from block 11 and 33. The labels denote the number of the test_the block_distance from the canister in cm. Two reference tests are also shown.

In Figure 8-6 and Figure 8-611 the maximum deviatoric stress, q_{max}, and the corresponding strain, ε, are plotted versus density. The colours refer to the position and the temperature in the same way as Figure 8-6 to Figure 8-6. The different shapes (rhombes, triangles, square) denote the block number (09, 11, 33). In Figure 8-6 and Figure 8-6 results from reference tests are shown with open circles linked with a best fit exponential line and linear solid line, respectively. The lines are based on six reference samples. The maximum deviatoric stress and the strain of each test are shown in Table 8-5 together with the final density and final water content.

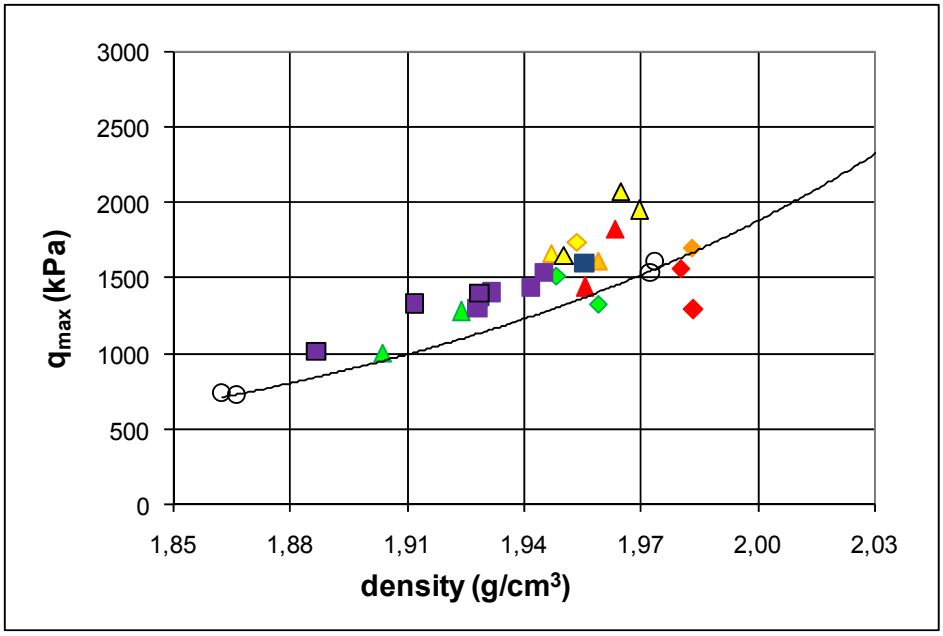

Figure 8-10 Maximum deviatoric stress vs.density for the drilled specimens in the LOT series. The colours refer to the exposed temperature in the LOT parcel from the warmest to the coldest (red, orange, yellow, green, blue and purple). Open circles are reference tests linked with a solid best fit line.

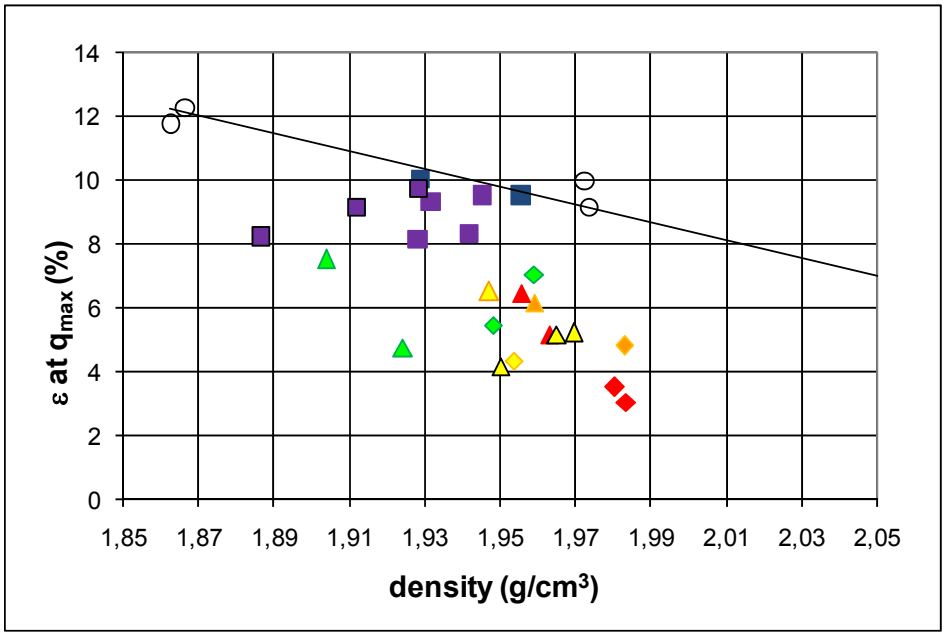

Figure 8-11 Strain at maximum deviatoric stress vs.density for the drilled specimens in the LOT series. The colours refer to the exposed temperature in the LOT parcel from the warmest to the coldest (red, orange, yellow, green, blue and purple). Open circles are reference tests linked with a best fit solid line.

There is an obvious scatter in the results from the specimens taken from the LOT parcel. However, there is also a clear trend in the strain at maximum deviator stress q_{max} in e.g. Figure 8-11. The strain at q_{max} resulting from the high temperature parcel material is for

all tests lower than the strain resulting from other tests. However, no significant difference was measured in q_{max}.

The LOT series also involved tests on air-dried, milled and compacted specimens. Results from these specimens are shown in Figure 8-12 with the same references as in Figure 8-12 to Figure 8-12. From the results measured on the milled specimen in the LOT series (Figure 8-12) the maximum deviatoric stress q_{max} is larger than the reference but similar to q_{max} resulting from the samples LOT samples 101_11_5,103_11_5 and 105_11_5. The strain at q_{max} is in the same range as for the reference samples.

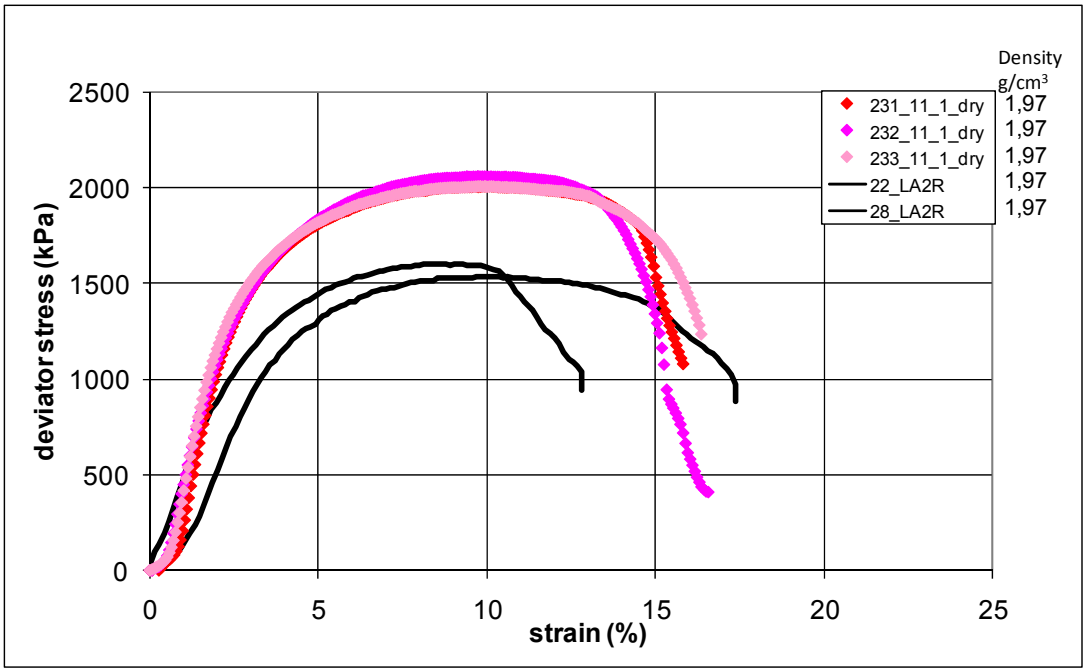

Figure 8-12 Test results from specimens taken from block 11, air dried, milled and compacted. The labels denote the number of the test_the block_distance from the canister in cm. Two reference tests are also shown.

In Table 8-5 the results from all tests are presented. Some of the reference tests (written in italic in Table 8-5) were used for improvement of the test technique and these samples were sheared with a deviating set-up compared to all other tests. In addition two of these samples were broken and no results at all were achieved. From the reference samples (20, 22, 24, 26, 28, 30) the influence of density is clearly seen i.e. the higher density the higher maximum deviatoric stress q_{max} and the smaller corresponding strain. The solid lines in Figure 8-12 and Figure 8-12 are based on the results from these reference specimens.

The shape of the failure surfaces differed between the individual specimens. Some of the specimens taken from block 09 and 11 showed a nearly vertical failure surface, exemplified in Figure 8-12 (upper left). This shape was not seen on specimens taken elsewhere or on any of the compacted specimens. The failure surfaces shown in Figure 8-12 (upper right and lower row) represent specimens from block 33, dried and milled material from block 11 and specimen exposed to high temperature in an oven in the laboratory, respectively. Other failure shapes and inclinations than the ones shown in Figure 8-12 were seen, in some cases more than one surface developed during failure.

Figure 8-13 Photos of selected specimens after failure. The specimens represent block 09 position 1 cm (upper left), block 33 position 1 cm (upper right), air dried, milled and compacted material from block 09 position 1 cm (lower left) and compacted specimen exposed to150^{o}C in an oven in the laboratory (lower right).

Table 8-5 Results from the basic LOT test series. Maximum deviatoric stress and strain with final water contents and densities. Densities are calculated from measured height and diameter of the saturation device.

Test ID	Label *Number_block_ _distance*	Density g/cm^3	w %	S_r %	At shearing q_{max} kPa	At shearing strain at q_{max} %
LA2UC01	1_09_1	1,98	29,4	101	1562	3,5
LA2UC02	2_09_3	1,98	29,5	102	1694	4,8
LA2UC03	3_09_5	1,95	29,9	99	1736	4,3
LA2UC04	4_09_7	1,95	31,7	101	1509	5,4
LA2UC05	5_09_9	1,96	32,5	104	1327	7
LA2UC06	6_09_1	1,98	31,4	105	1296	3
LA2UC07	7_11_1	1,96	29,8	100	1818	5,1
LA2UC08	8_11_3	1,96	30,4	101	1614	6,1
LA2UC09	9_11_5	1,95	30,6	100	1658	6,5
LA2UC10	10_11_7	1,92	32,8	101	1283	4,7
LA2UC11	11_11_9	1,90	34,8	101	1002	7,5
LA2UC12	12_11_1	1,96	31,0	101	1444	6,4
LA2UC13	13_33_1	1,93	31,8	100	1378	10
LA2UC14	14_33_3	1,95	31,4	101	1535	9,5
LA2UC15	15_33_5	1,93	31,8	100	1405	9,3
LA2UC16	16_33_7	1,94	31,7	101	1437	8,3
LA2UC17	17_33_9	1,93	32,5	100	1298	8,1
LA2UC18	18_33_1	1,96	30,8	101	1602	9,5
LA2UC19		*1,86*	*37,3*	99		
LA2UC20	20_LA2R	1,86	37,9	101	734	11,7
LA2UC21		*1,94*	*30,6*	99	*1136*	*10,2*
LA2UC22	22_LA2R	1,97	30,6	103	1603	9,1
LA2UC23			*25,8*			
LA2UC24	24_LA2R	2,09	22,8	102	2926	4,9
LA2UC25		*1,87*	*36,8*	100	*771*	*11,3*
LA2UC26	26_LA2R	1,87	37,9	101	726	12,2
LA2UC27		*1,99*	*31,3*	106	*1138*	*6,6*
LA2UC28	28_LA2R	1,97	30,7	103	1534	9,9
LA2UC29		*2,10*	*25,4*	108	*1973*	*4,1*
LA2UC30	30_LA2R	2,11	21,5	102	4968	5,8
LA2UC101	101_11_5	1,95	31,1	101	1649	4,1
LA2UC102	102_33_5	1,89	35,0	99	1018	8,2
LA2UC103	103_11_5	1,97	30,0	101	2074	5,1
LA2UC104	104_33_5	1,93	32,3	100	1401	9,7
LA2UC105	105_11_5	1,97	30,3	102	1954	5,2
LA2UC106	106_33_5	1,91	33,1	100	1332	9,1
LA2UC231	231_11_1_dry	1,97	30,0	101	2008	10
LA2UC232	232_11_1_dry	1,97	30,3	101	2060	10
LA2UC233	233_11_1_dry	1,97	30,0	101	2005	10

From the LAB series some selected results are shown in Figure 8-14 to illustrate the influence of temperature on the stress-strain behaviour. The colours (lilac, red, green, blue) denote the temperatures (150°C, 120°C, 90°C, 20°C). All specimens in the LAB series represent almost the same density.

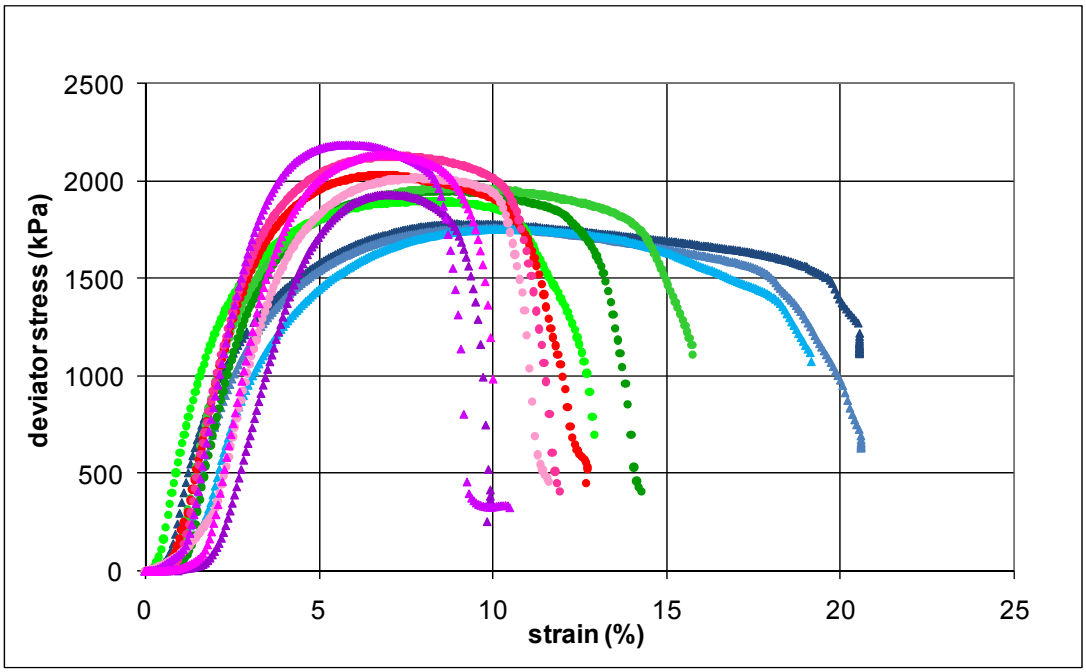

Figure 8-14 Selected test results from the LAB series with specimens stored in an oven at different temperature. The colours (lilac, red, green, blue) denote the temperatures (150°C, 120 °C, 90 °C, 20 °C). Specimens 07-18 also shown in Figure 8-12.

According to Figure 8-14 significant lower strain was measured at maximum deviatoric stress q_{max} on material exposed to high temperature in the laboratory. However, also a significant increase in q_{max} with increasing temperature was measured.

Results from all tests in the LAB series are shown in the Figure 8-12 to Figure 8-12 and in Table 8-6. In these Figures the labels denote *test number_maximum temperature*. The influences of the following factors are illustrated:

- exposure to 20°C, 90°C, 120°C and 150°C (Figure 8-145 and Figure 8-14).
- cyclic change in temperature between 20°C and 120°C (Figure 8-146 left).
- exposure to 120°C before the water saturation (Figure 8-14 right).
- influence of high water pressure (Figure 8-14).
- influence of density (Figure 8-149).

The water pressure used for the study of the influence of high water pressure was at least doubled the size of the water pressure used for the water saturation in the same series. The maximum water pressure used was 1900 kPa. Specimens with applied water pressure during saturation were kept at zero water pressure for 12h before the dismantling.

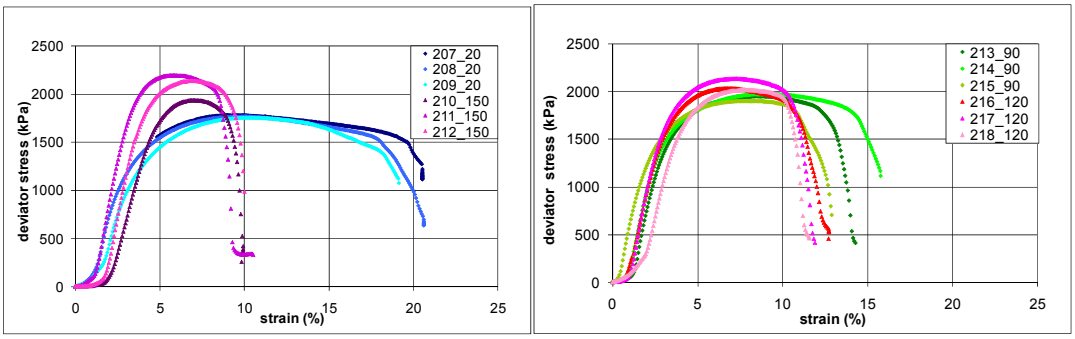

Figure 8-15 Illustration of influence of temperature. The colours (lilac, red, green, blue) denote the temperatures (150°C, 120°C, 90°C, 20°C). The labels show test number_temperature.

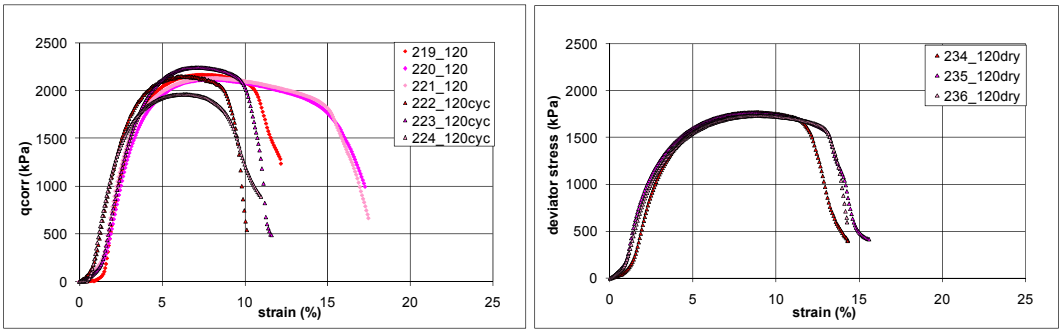

Figure 8-16 Illustration of influence of cyclic change of the temperature between 120°C/20°C (left) and drying before the water saturation (right). The labels show test number _temperature.

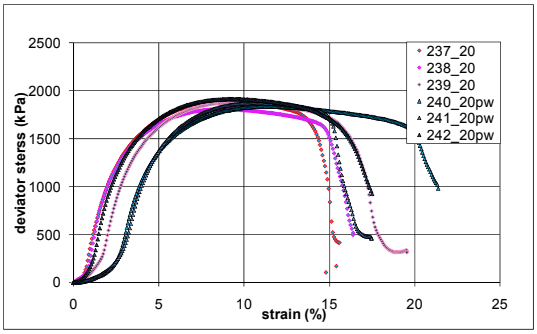

Figure 8-17 Illustration of influence of high water pressure at least doubled the size of the one used in the other tests in this series. The labels show test number _temperature.

Regarding cyclic change of temperature indications exist that this influences the stress-strain behaviour (Figure 8-14 left). However, drying the specimen before the saturation (Figure 8-146 right) or the use of high water pressure (Figure 8-14) seem not to have influenced the stress-strain behaviour.

When testing the specimens 225-230 and 201-206 the set-up was found to have been less rigid than during the other tests in the LAB series (Table 8-4). The stiffness of the set-ups were measured and at each measured stress during test 225-230 and 201-206 new values of the strain were calculated taking the stiffness into account. Only the corrected results are used in the following.

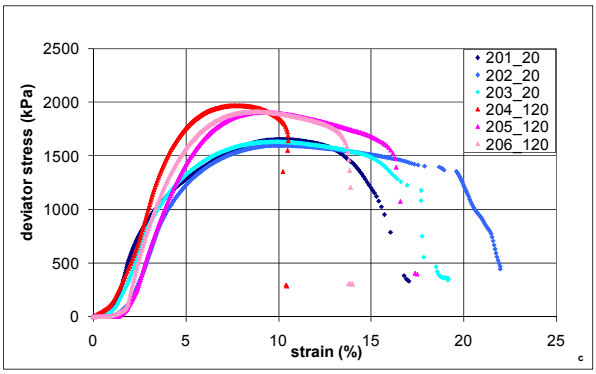

Figure 8-18 Illustration of influence of temperature. The colours (red, blue) denote the temperatures (120°C, 20°C). The labels show test number_temperature .Corrected results.

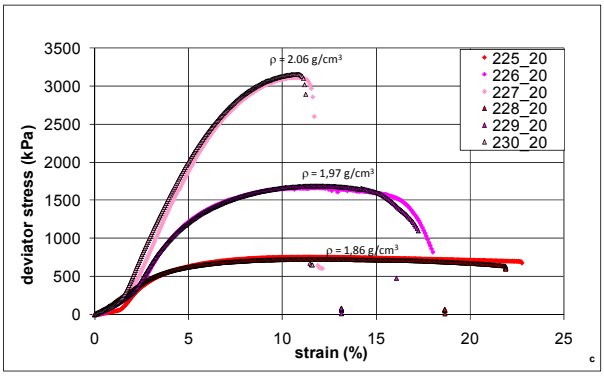

Figure 8-19 Illustration of influence of density. Observe that the maximum deviator stress is 3500 kPa. The labels show test number_temperature. Corrected results.

The results in Figure 8-12 agree with the results shown in Figure 8-12. Regarding the results presented in Figure 8-12 the shape of the curves differ according to the density. However, compared to the reference tests in the basic LOT series (20, 22, 24, 26, 28, 30) where the strain at failure decreased with increasing density this is not seen in Figure 8-12. Slightly different preparation was used in the two series and different time elapsed between the dismounting and shearing in the two series (0h in the basic LOT series and 12h in the LAB series). This difference might have caused this difference between the series.

In the comparison between results from different specimens a scatter was seen in the final part of the stress-strain curves which is found to be an effect of the dismantling of the specimen and accessibility of water during the dismantling, i.e. an artefact.

Table 8-6 Results from the LAB test series. Maximum deviatoric stress and strain with final water contents and densities. Densities are calculated from measured height and diameter of the saturation device. Remarks: 1 denotes that the strain is corrected for less stiffness in the set-up.

Test ID	Labels *Number_material_ _temperature*	Density g/cm^3	w %	S_r %	At shearing q_{max} kPa	strain at q_{max} %	Max T °C	Remark
LA2UC201	201_ 20	1,96	30,3	100	1650	10,1	20	[1]
LA2UC202	202_120	1,97	31,1	103	1600	10	20	[1]
LA2UC203	203_ 20	1,97	31,0	103	1650	9,8	20	[1]
LA2UC204	204_120	1,96	30,8	102	1970	7,5	120	[1]
LA2UC205	205_120	1,96	30,4	101	1900	9	120	[1]
LA2UC206	206_120	1,96	31,2	102	1910	8,6	120	[1]
LA2UC207	207_ 20	1,96	30,8	102	1800	9,5	20	
LA2UC208	208_ 20	1,97	30,7	102	1760	10	20	
LA2UC209	209_ 20	1,97	30,9	103	1760	10	20	
LA2UC210	210_150	1,96	31,7	103	1940	7	150	
LA2UC211	211_150	1,97	31,3	104	2200	5,8	150	
LA2UC212	212_150	1,97	31,5	104	2140	7	150	
LA2UC213	213_ 90	1,96	30,7	102	1950	8,5	90	
LA2UC214	214_ 90	1,97	31,3	103	1970	9	90	
LA2UC215	215_ 90	1,96	31,2	102	1900	8	90	
LA2UC216	216_120	1,96	31,1	102	2030	6,5	120	
LA2UC217	217_120	1,97	31,1	103	2130	7	120	
LA2UC218	218_120	1,96	31,2	102	2010	7,5	120	
LA2UC219	219_120	1,97	31,3	103	2185	7,5	120	
LA2UC220	220_120	1,97	30,7	102	2115	7,8	120	
LA2UC221	221_120	1,97	31,1	103	2130	8	120	
LA2UC222	222_120cyc	1,96	31,6	103	2150	6,1	120	cyclic
LA2UC223	223_120cyc	1,96	30,8	101	2240	7	120	change
LA2UC224	224_120cyc	1,95	32,1	103	1960	6,4	120	20°C/120°C
LA2UC225	225_20	1,86	38,5	101	750	10,3	20	[1]
LA2UC226	226_20	1,97	30,9	102	1670	11,5	20	[1]
LA2UC227	227_20	2,06	24,8	103	3110	10,5	20	[1]
LA2UC228	228_20	1,86	38,6	101	730	11	20	[1]
LA2UC229	229_20	1,96	30,9	101	1690	11,6	20	[1]
LA2UC230	230_20	2,06	25,1	103	3150	10,6	20	[1]
LA2UC234	234_120dry	1,97	30,1	101	1770	8,5	120	dried at
LA2UC235	235_120dry	1,97	30,1	101	1770	8,5	120	120°C then
LA2UC236	236_120dry	1,97	30,2	102	1730	8,7	120	saturated
LA2UC237	237_20	1,97	30,7	102	1883	8,8	20	
LA2UC238	238_20	1,97	30,7	102	1807	8,3	20	
LA2UC239	239_20	1,97	30,8	102	1880	9,3	20	
LA2UC240	240_20pw	1,97	30,4	102	1835	11	20	high
LA2UC241	241_20pw	1,97	30,5	102	1870	10,3	20	water
LA2UC242	242_20pw	1,97	30,3	101	1913	8,9	20	pressure

8.2.7. Additional analyses

The procedure used for the specimens exposed to increased temperature in the laboratory was further analysed by a hydro-mechanical model. The modelling of hydro-mechanical processes in the LAB test series was done in a similar way as reported by /Börgesson et al., 1999/. The focus of the analysis was mainly to study the occurrence of excess pore pressure in the specimens caused by the increase and decrease in temperature. It was found that enough time was given in the laboratory to avoid excess pore water pressure in the specimens. The calculation also showed that the 12 h elapsing from the removal of the applied pore water pressure to the dismantling of the specimens was enough to consider the pore water pressure as equalised before the dismantling. Thus, according to the model

enough time was given for the different steps in the procedure used in laboratory to be able consider the specimens as unaffected by excess pore water pressure during the preparation.

The THM modelling also showed that elastic displacements take place inside the specimen during the increase and the decrease in temperature, causing gradients in void ratio. Since reversible behaviour is assumed in the model void ratio returns to the initial value when the temperature, pore-water pressure and stresses return to their initial values. However, presence of non-reversible THM behaviour in the material after exposure to increased temperature cannot be excluded which then might explain the modified behaviour and further investigations of these effects should be done.

The specimens 207-224 in the LAB series were analysed regarding CEC, cation exchange capacity, according to Section 9.2.1.4. The results show values between 80 and 83 meq/100g clay but the difference between different specimens are not larger than can be explained by the variations in the method.

8.2.8. Preliminary conclusions

The results from the drilled specimens taken from the warm section of the LOT parcel compared to reference specimens with a comparable density gives that the strain at failure is less (increased brittleness) for all specimens from the warm section compared to the references, see e.g. Figure 8-6, Figure 8-6, Figure 8-6, and Figure 8-6.

From the LAB series where specimens were exposed to increased temperature in the laboratory (90^{o}C -150^{o}C) an increase in maximum deviator stress and a decrease in corresponding strain is seen already after a relatively short time of exposure (about 24 h), Figure 8-6. The results from the LAB series further confirm the coupling between the decrease in strain of the specimens from the warm section of the LOT parcel and the increased temperature. However, additional causes cannot be excluded.

The special behaviour of the specimens from the warm section of the LOT parcel is emphasised by the occurrence of a nearly vertical failure surface seen on some of these specimens after failure but not seen on other specimens for example from the LAB series, Figure 8-6.

The results from the milled specimens from the warm section of the LOT parcel show that both the maximum deviator stress and the corresponding strain are larger than the reference samples of the same density, Figure 8-6. The behaviour of the corresponding drilled specimens is thus not seen on milled specimens which indicate that the increased brittleness seen on these drilled specimens is destroyed when the specimens are dried, milled and compacted.

9 MINERALOGY AND CHEMICAL COMPOSITION

Siv Olsson, Ola Karnland, Martin Birgersson, Tania Hernan-Håkansson, Ulf Nilsson

9.1. Introduction

The chemical and mineralogical characteristics of bentonite from defined positions in the LOT A2 parcel have been compared with reference materials consisting of the specific batch of MX80 that was used for fabrication of the individual blocks of the A2 parcel. The aim of the study has been to elucidate how the bentonite has altered after the 5-year long exposure to the adverse conditions of the A2 test, which means both higher temperature and steeper temperature gradient compared to KBS-3 conditions. Two test series of bentonite blocks from the A2 parcel, in the following referred to as standard blocks and special blocks, have been analyzed. The standard block series comprises two blocks from the hottest section and one block from the cool section of the parcel. The special block series comprises five blocks in which cylindrical bentonite plugs containing either calcite, gypsum, K-feldspar or cement have been embedded in order to simulate various adverse chemical conditions that might accelerate the alteration processes.

9.2. Standard Blocks of the A2 parcel

9.2.1. Materials and methods

9.2.1.1.Sampling and sample nomenclature

The standard block series comprises blocks 09 and 11 from the hot section and block 33 from the cool section of the parcel. The entire volume of blocks 09 and 11 has been exposed to temperatures >80º C, and the innermost 4 centimeters to temperatures exceeding 100º C. Block no. 33 was never exposed to temperatures exceeding 30ºC, apart from the innermost centimeter. These blocks were sampled contiguously at five positions along the radius in the B-level (Figure 5-1 Schematic block partition. SE and NW denote the directions of compass in the test-hole, figures denote the centre of the specimens expressed in centimeters measured from the block inner mantel surface, and A, B and C denotes the analyzed three vertical position in the blocks.). A 1-2 mm thick layer of the contact surfaces bentonite/Cu-tube and bentonite/bedrock were removed before the sampling which was made by use of a band saw. The contact bentonite/Cu-tube (radial position 0) was sampled separately in one of the hot blocks (no. 12) by scraping off a 1-2 mm thick layer from the bentonite surface with a knife of stain-less steel. Bentonite used for and stored since the fabrication of the blocks has been used as reference material.

The analytical test protocol for the standard blocks is summarized in Table 1, where individual samples have been given an identity code according to the general nomenclature, e.g. A209BW1b means that the sample is from the LOT **A2** parcel, block no. **09**, level **B** of the **W**estern sector of the block, radial position **1.** The **b**ulk of the material has been analyzed (**c** is used if the material analyzed is the clay fraction). The identity code of the corresponding reference sample is A209Rb (or c for the clay fraction).

9.2.1.2.Sample preparation

Both the bulk material and the clay fraction of the bentonite samples have been analyzed when relevant (Table 9-1 Sample nomenclature and analytical test protocol for the

standard blocks 09, 11 and 33 of the LOT A2 parcel.). The bulk material was not subject to any pre-treatments prior to the analyses, apart from drying at 60º C and grinding.

The clay-sized fraction (<2μm) was separated by centrifuged sedimentation. In order to prepare a stable dispersion of the bentonite that allowed a separation of different size fractions, soluble salts were first dissolved by centrifuge-washing with water. After complete dispersion of the bentonite the suspension was left to rest for 10 minutes to allow sedimentation of the coarsest particles. The supernatant was thereafter collected in centrifuge bottles and centrifuged at 850 r/min for 5 minutes. The centrifugation time and speed required for sedimentation of particles >2 μm was calculated by use of the integrated form of Stokes´ Law.

After centrifugation the supernatants were collected in plastic containers and concentrated by evaporation at 60°C in a ventilated oven.

9.2.1.3. Chemical analysis of the bentonite

The chemical composition of the reference and the parcel bentonite was determined by ICP emission spectrometry (AES) and ICP mass spectrometry (MS) at an ISO 9001 certified laboratory (ACME Analytical Laboratories, Canada), using standard techniques for silicate analysis (fusion with $LiBO_2$ followed by nitric acid digestion). These analyses include major (Si, Al, Fe, Ca, Mg, K, Na, Mn, P, Ti), minor and trace elements (Ba, Co, Ce, Cr, Cu, Nb, Ni, Sc, Sr, Ta, Y, Zn, Zr). Loss on ignition (LOI) was determined as the difference in weight of the dried (105º C) and ignited (1000º C) sample.

Table 9-1 Sample nomenclature and analytical test protocol for the standard blocks 09, 11 and 33 of the LOT A2 parcel.

	Chemical analysis	**Cation exchange capacity**	**Exchangeable cations**	**X-ray diffraction analysis**		**Aqueous leaching**
SICADA test code b=bulk;c=clay fraction	**LA2EA** **b/c**	**LA2CE** **Cb/c**	**LA2EC** **b**	**LA2XRD** **b/c**		**LA2WA** **b**
Sample identity				random	oriented	
Reference bentonite samples						
A2(01-05)Rb	X	X	X	X		X
A2(01-05)Rc	X	X			X	
A211Rb	X	X	X	X		X
A211Rc	X	X			X	
A233Rb	X	X	X	X		X
A233Rc	X	X			X	
A224Rb	X	X	X	X		X
A224Rc		X			X	

	Chemical analysis	Cation exchange capacity	Exchangeable cations	X-ray diffraction analysis		Aqueous leaching
SICADA test code b=bulk;c=clay fraction	**LA2EA** **b/c**	**LA2CE** **Cb/c**	**LA2EC** **b**	**LA2XRD** **b/c**		**LA2WA** **b**
Sample identity				random	oriented	
A234Rb	X	X	X	X		X
A234Rc		X			X	
Standard block series						
A209BW1b	X	X	X	X		X
A209BW1c	X	X			X	
A209BW3b	X	X	X	X		X
A209BW3c	X	X			X	
A209BW5b	X	X	X	X		X
A209BW5c	X	X			X	
A209BW7b	X	X	X	X		X
A209BW7c	X	X			X	
A209BW9b	X	X	X	X		X
A209BW9c	X	X			X	
A211BW1b	X	X	X	X		X
A211BW1c	X	X			X	
A211BW3b	X	X	X	X		X
A211BW3c	X	X			X	
A211BW5b	X	X	X	X		X
A211BW5c	X	X			X	
A211BW7b	X	X	X	X		X
A211BW7c	X	X			X	
A211BW9b	X	X	X	X		X
A211BW9c	X	X			X	
A212(A-C)N0b	X	X	X	X		X
A212(A-C)N0c	X	X			X	
A233BW1b	X	X	X	X		X
A233BW1c	X	X			X	
A233BW3b	X	X	X	X		X
A233BW3c	X	X			X	

	Chemical analysis	Cation exchange capacity	Exchangeable cations	X-ray diffraction analysis		Aqueous leaching
SICADA test code b=bulk;c=clay fraction	**LA2EA b/c**	**LA2CE Cb/c**	**LA2EC b**	**LA2XRD b/c**		**LA2WA b**
Sample identity				random	oriented	
A233BW5b	X	X	X	X		X
A233BW5c	X	X			X	
A233BW7b	X	X	X	X		X
A233BW7c	X	X			X	
A233BW9b	X	X	X	X		X
A233BW9c	X	X			X	

Total carbon and sulfur were determined by evolved gas analysis (EGA) at the same laboratory by combustion of the samples in a Leco furnace, equipped with IR-detectors for CO_2 and SO_2. Carbonate carbon was determined as CO_2 evolved on treatment with hot 15% HCl.

Prior to the chemical analysis of the clay fractions, carbonates were removed by treatment with an acetic acid-sodium acetate buffer with pH 5 (e.g. Newman & Brown 1987). The purified clay was thereafter converted to homo-ionic Na-clay by repeated washings with 1 M NaCl solution (analytical grade reagent). Excess salts were removed by repeated centrifuge-washing with water followed by dialysis (Spectrapore 3, 3500 MWCO dialysis membrane) against deionized water until the electrical conductivity of the external solution remained <10 μS/cm for five days. The purpose of saturating the exchange sites with one single cation is to make the allocation of cations to exchange and structural sites, respectively, less ambiguous.

All samples were ground, dried at 105ºC and stored in desiccators prior to the analysis, i.e. all analytical results are expressed in wt% (major oxides) or ppm (trace elements) of the dry mass of the sample. The data have been stored in the SICADA database in a matrix in which concentration values are given for each parcel position using an identity code according to the general nomenclature.

9.2.1.4.Cation exchange capacity (CEC) and exchangeable cations (EC)

The cation exchange capacity (CEC) of bulk materials and of clay fractions was determined by exchange with copper(II)triethylenetetramine following the procedure of Meier & Kahr /1999/, modified according to Ammann et al. /2005/ to ensure complete exchange. The ground sample (400 mg) was dispersed in 50 ml deionised water by ultrasonic treatment. 20 ml of 15 mM Cu(II)-triethylene-tetramine solution was added to the suspension, which was left to react for 30 minutes on a vibrating table. After centrifugation the absorbance at 620 nm of the supernatant was measured using a spectrophotometer (Shimadzu). CEC was calculated on the basis of the uptake of Cu by the clay and is expressed in centimole of charge per kilogram clay (cmolc kg^{-1}), which is

numerically equivalent to milliequivalents per 100 g (meq/100 g). The water content of the clay was determined for a separate sample dried at 105º C to a constant weight. All CEC determinations were duplicated.

The exchangeable cations of the bulk bentonite were also extracted into alcoholic ammonium chloride solution (0,15 M NH_4Cl in 80% ethanol) according to a procedure originally recommended for CEC determinations of gypsiferous/calcareous soils, e.g. /Belyayeva, 1967/; /Jackson, 1975/. An alcoholic solution is used to minimize dissolution of gypsum and calcite, which are soluble or relatively soluble in aqueous solutions. Ideally, i.e. when the content of easily soluble salts, such as chlorides and carbonates of alkali metals, is low, the sum of cations extracted should be equivalent to the CEC of the sample.

0.8 g of the ground sample was shaken for 30 minutes in approximately one third of a total volume of 50 ml of the extractant. After centrifugation the supernatant was collected in a volumetric flask. The treatment was repeated twice. The concentration of Ca, Mg, Cu, Na and K in the extracts was determined by use of an ICP-AES equipment at the Department of Ecology, Lund University. The concentration of exchangeable cations is expressed in centimole of charge per kilogram (cmolc kg^{-1}), which is numerically equivalent to milliequivalents per 100 g (meq/100 g). The water content of the bentonite was determined for a separate sample.

The results have been delivered in Excel files from the laboratories involved and transferred to the SICADA database as a matrix in which calculated CEC values/exchangeable cation concentrations are given for each parcel position using an identity code according to the general scheme.

9.2.1.5.Aqueous leachates

Aqueous leaching of the bulk samples was used to obtain information about the pore water composition and the spatial distribution of soluble/sparingly soluble salts within the blocks. The dried and ground bentonite was dispersed in deionized water (solid : solution ratio 1:100) by ultrasonic treatment for 30 minutes and stirring overnight. The suspension was left for 7 days at room temperature to allow equilibration. The supernatant was collected in centrifuge bottles and centrifuged at 3000 rpm for half an hour, and thereafter ultra-filtered through 0,8 and 0,2 µm syringe filters (Acrodisc PF Syringe Filters) prior to analysis. Major cations were determined by ICP-AES and anions by use of ion chromatography (IC) at the Department of Ecology, Lund University.

The results have been delivered from the laboratory in Excel files in which concentration values are given for each parcel position. The code for the sample positions follows the general nomenclature.

9.2.1.6. X-ray diffraction analysis (XRD)

The mineralogical composition was determined by X-ray diffraction analysis of two different types of preparations, one type consisting of unsorted and randomly oriented powders of the bulk materials, the other type consisting of aggregates with maximized preferred orientation of the clay minerals.

The random powder of the bulk sample produces ”three-dimensional fingerprints” of all minerals and are needed for a general characterization of the materials. Also the distinction between di- and trioctahedral types of clay minerals by measurements of d(060) requires an X-ray diffraction profile of a randomly oriented sample.

The bulk material was ground in an agate mortar to a grain-size <10 μm. The montmorillonite of the parent bentonite is predominantly Na-saturated, giving a basal spacing around 12,5 Å under normal laboratory conditions. In order to improve the resolution of the 10 Å region to allow for a better detection of micaceous minerals, the samples were equilibrated in desiccators at a relative humidity of 75% (over saturated NaCl-solution) during a minimum of 5 days. X-ray scans were made as soon as possible after removal of the samples from the desiccators, but there was no RH control of the goniometer chamber during the scanning. The random powders were scanned with a step size of 0,02º 2θ in the 2θ interval 2-66°.

The oriented specimen of the clay fraction gives strongly enhanced basal (*00l*) reflections, and little or no evidence of the hk reflections of clay minerals. This type of preparation is useful for identification of the clay minerals and of interstratified structures and is also used for tests of the swelling properties of the clay after the clay has been solvated with a polyalcohol, such as ethylene glycol. However, the diffraction characteristics of smectites both in the air-dried and the ethylene glycol solvated state depend on the type of cation that is held in the exchange sites. Therefore, in order to give unambiguous diffraction characteristics, all clay samples were saturated with one single cation (Mg) prior to the X-ray scanning.

The clay fractions were deflocculated in deionized water, saturated with Mg and thereafter washed free of excess salt by centrifuge-washing with water just until incipient dispersion. Oriented aggregates were prepared of the clay slurry according to the "smear-on-glass" method" (Moore & Reynolds 1989) and dried at room temperature. The oriented mounts were X-ray scanned with a step size of 0,02º 2θ in the 2θ interval 2-36°. In order to test the swelling properties the samples were re-scanned after solvation with ethylene glycol (EG) at 60ºC for 48 hours.

A Seifert 3000 TT X-ray diffractometer with CuKα radiation and automatic slits was used for the X-ray diffraction analyses.

The results have been stored in the SICADA database in Excel files in which the intensity values and the corresponding 2θ values are listed. No interpretation is given in the SICADA database. The code for the sample positions follows the general scheme.

9.2.2. Results

9.2.2.1. Color

A visual inspection of the bentonite revealed a difference in color between samples from different positions in the parcel. Powders of the bentonite located proximal to the Cu-tube (sample 0 and 1) in the hottest parts had a dull reddish grey color which contrasted with the light grey color of the powdered bentonite from other positions. The color was imparted by minute, brick red, soft "grains" which occurred only in the innermost two centimeters of the blocks (Fig. 2). Efforts to characterize the soft "grains" by XRD-analysis of a concentrate picked by hand under a microscope were negative – the red "grains" appear to be X-ray amorphous.

9.2.2.2. Aqueous leachates (SICADA test code LA2WA)

The chemical data on non-reactive solutes and "water-soluble salts" are given in Table 2 together with the concentration of major anions and cations of the groundwater at Äspö, sampled in January 2006. Focus is laid on the major anions (chloride and sulfate) since the concentration of the cations is strongly affected by the exchange reactions that take

place when divalent cations are released from dissolving minerals during the contact with water. Moreover, the source of some of the cations included in the analysis, such as Al and Fe (and some Si and Mg), are most likely ultra-fine clay particles which the filtering method failed to remove from the solution. Evidence for this is a strong correlation (R^2=0,98) between Al and Fe and also the fact that their concentrations are at a minimum in samples with maximum sulfate concentrations, because dissolution of salts during the extraction promoted flocculation and sedimentation of clay particles.

Figure 9-1 The section 0-3 cm of block 11 from the LOT A2 parcel. Note the brick-red "grains" occurring in the innermost 2 cm of the block. Fissures formed during storage.

The radial concentration profiles of chloride and sulfate, expressed as mg/g dry bentonite and as the molar concentration of the pore water, are presented in Figure 7-2. The pore water concentration of chloride is more or less constant in all three blocks but has increased compared with the chloride concentration of the reference bentonite. Thus, the groundwater must be the essential source of chloride (cf. Table 9-2). However, the pore water concentration is still only half of that of the Äspö groundwater, which conforms to ion equilibrium theory /Birgersson & Karnland/.

The sulfate concentration of the pore water in all blocks is significantly higher than that of the Äspö groundwater (cf. Table 9-2 and Figure 9-1 The section 0-3 cm of block 11 from the LOT A2 parcel. Note the brick-red "grains" occurring in the innermost 2 cm of the block. Fissures formed during storage.). Accordingly, the essential source must be the inventory of soluble sulfates initially present in the parent bentonite MX80 as gypsum. The concentration in the cool block no. 33 is constant and more or less the same as that of the reference bentonite. In contrast, both hot blocks display an irregular distribution pattern with maxima 2-6 cm from the central heater and minima in the peripheral parts of the blocks, where the concentration is lower than that of the reference samples. Thus, it is evident that calcium sulfate has been redistributed along the thermal gradient in the blocks. The spatial distribution pattern is confirmed by other chemical data (chapter 9.2.2.5) and by the XRD analysis (chapter 9.2.2.5), which shows that the re-precipitated calcium sulfate in the hot zone is anhydrite ($CaSO_4$).

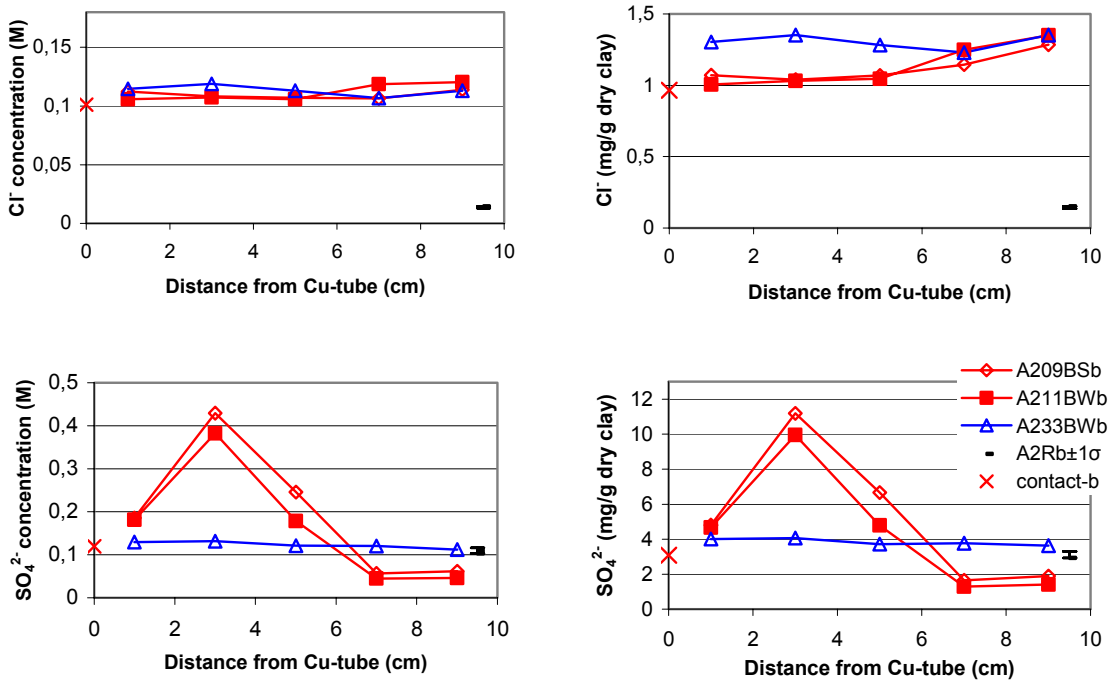

Figure 9-2 The radial distribution of Cl^- and SO_4^{2-} in water extracts of bulk samples from blocks 09, 11 and 33 of the LOT A2 parcel. The concentration of the reference samples (A2Rb) is shown at position 9.5 cm as the mean ±1 standard deviation of five samples.

Table 9-2 Major anions and cations (mg/g dry clay) extracted by dispersion of bentonite in deionised water in a solid:liquid ratio of 1:100. Data for blocks 09, 11 and 33 together with one contact sample and five reference samples for the LOT A2 parcel. Included is also the concentration of major anions and cations in Äspö groundwater sampled in January 2006. n.d.=not determined. SICADA test code LA2WA.

Sample id.	Al	B	Ca	Cl^-	CO_3^{2-}-C	Cu	Fe	K	Li	Mg	Mn	Na	P	S	Si	SO_4^{2-}-S	Sr
	mg/g dry clay																
A212(A-C)N0b	0.129	0.016	0.068	0.965	0.109	0.0089	0.034	0.094	0.0009	0.033	0.0003	4.14	0.004	1.030	1.183	0.973	0.00041
A209BS1b	0.031	0.027	0.080	1.070	0.100	0.0026	0.008	0.128	0.0010	0.002	0.0001	5.28	0.005	1.599	0.975	1.430	0.00034
A209BS3b	0.020	0.007	0.155	1.039	0.091	0.0004	0.008	0.262	0.0019	0.032	0.0038	8.55	0.008	3.732	1.120	4.018	0.00316
A209BS5b	0.045	0.008	0.082	1.068	0.104	0.0006	0.011	0.176	0.0017	0.030	0.0001	7.13	0.012	2.222	1.095	2.164	0.00123
A209BS7b	0.025	0.008	0.074	1.145	0.104	0.0008	0.006	0.105	0.0007	0.013	0.0000	5.23	0.007	0.553	1.056	0.579	0.00034
A209BS9b	0.047	0.012	0.079	1.284	0.095	0.0007	0.012	0.100	0.0010	0.008	0.0000	5.22	0.004	0.631	1.145	0.509	0.00039
A211BW1b	0.094	0.007	0.068	1.005	0.107	0.0035	0.025	0.112	0.0011	0.030	0.0002	5.11	0.000	1.556	1.134	1.565	0.00041
A211BW3b	0.015	0.018	0.108	1.031	0.123	0.0003	0.004	0.234	0.0020	0.016	0.0001	8.15	0.002	3.320	1.264	2.876	0.00247
A211BW5b	0.015	0.034	0.074	1.045	0.113	0.0005	0.004	0.167	0.0015	0.012	0.0002	6.68	0.005	1.598	1.031	1.586	0.00106
A211BW7b	0.120	0.021	0.078	1.248	0.111	0.0003	0.032	0.105	0.0010	0.020	0.0003	5.23	0.013	0.430	1.303	0.529	0.00043
A211BW9b	0.041	0.025	0.076	1.349	0.108	0.0010	0.011	0.095	0.0009	0.004	0.0001	3.25	0.004	0.468	1.156	0.371	0.00043
A233BW1b	0.057	0.018	0.107	1.303	0.090	0.0016	0.014	0.137	0.0007	0.014	0.0002	6.60	0.015	1.336	1.413	1.300	0.00088
A233BW3b	0.057	0.011	0.132	1.353	0.121	0.0011	0.014	0.129	0.0010	0.023	0.0001	6.32	0.005	1.353	1.431	1.288	0.00081
A233BW5b	0.072	0.027	0.103	1.282	0.108	0.0009	0.018	0.144	0.0007	0.012	0.0002	6.09	0.012	1.241	1.457	1.235	0.00079
A233BW7b	0.023	0.007	0.098	1.230	0.104	0.0006	0.005	0.123	0.0006	0.002	0.0000	5.70	0.000	1.255	1.168	1.229	0.00055
A233BW9b	0.074	0.002	0.083	1.351	0.083	0.0008	0.018	0.120	0.0010	0.020	0.0001	5.97	0.000	1.209	1.328	1.213	0.00062
A2(1-5)Rb	0.070	0.014	0.087	0.134	0.103	0.0008	0.016	0.106	0.0006	0.022	0.0000	5.32	0.000	1.102	1.259	1.093	0.00063
A211Rb	0.173	0.016	0.124	0.148	0.158	0.0010	0.039	0.132	0.0002	0.044	-0.0001	5.47	0.000	1.038	1.863	1.089	0.00077
A224Rb	0.112	n.d.	0.026	0.124	0.019	0.0004	0.026	0.089	n.d.	0.023	0.0001	3.87	n.d.	1.008	0.864	1.128	0.0002
A233Rb	0.039	0.019	0.064	0.149	0.094	0.0003	0.009	0.101	0.0010	0.011	0.0000	4.72	0.013	0.975	1.038	0.945	0.00054
A234Rb	0.115	n.d.	0.024	0.122	0.019	0.0005	0.026	0.084	n.d.	0.021	0.0001	3.99	n.d.	1.050	0.878	1.142	0.0002
	mg/L (mM)																
Äspö groundwater			2250 (56)	6301 (178)		0.002		10.3 (0.26)		40.0 (1.6)		2210 (96)		191 (6)	4.58 (0.16)		39.9 (0.46)

Trace amounts of Cu were extracted into water from all samples, but the maximum concentration is found in the central samples of the hot blocks (Table 2). The chemical data on the solid bentonite (Table 9-5 and Table 9-6) show that quite significant amounts of Cu has been incorporated in these samples but less than 0,3% of the total available Cu content is extractable into water.

9.2.2.3.Exchangeable cations (SICADA test code LA2EC)

The data on the cations extracted by exchange with ammonium in alcoholic solutions are summarized in Table 6-3. The sum of cations is generally somewhat lower than the CEC of the sample (cf. Table 9-4) and varies quite randomly within the blocks. This fact probably reflects the problems inherent with the extraction method: the requirement of minimal dissolution of Ca sulfates and carbonates, the dissolution of which would inevitably lead to erroneous results for the exchangeable cations, may, on the other hand, lead to incomplete extraction.

Table 9-3 Exchangeable cations of the samples of blocks 03, 11 and 33 from the LOT A2 parcel. Included are also five reference samples and one sample (0) from the Cu-tube/bentonite contact. Cations extracted by exchange with NH_4^+ in alcoholic solution. SICADA test code LA2EC

Sample id	Ca		Cu		K		Mg		Na		Sum
	$cmol^+kg^{-1}$	%	$cmol^+kg^{-1}$	%	$cmol^+kg^{-1}$	%	$cmol^+kg^{-1}$	%	$cmol^+kg^{-1}$	%	$cmol^+kg^{-1}$
A209BW1b	17.2	24	0.2	0.3	1.1	1.6	8.5	12	45.6	63	73
A209BW3b	17.5	23	0.0	0.0	1.3	1.7	8.5	11	48.6	64	76
A209BW5b	17.4	22	0.0	0.0	1.4	1.7	8.2	10	51.5	66	79
A209BW7b	17.1	21	0.0	0.0	1.3	1.6	8.0	10	54.8	68	81
A209BW9b	15.8	21	0.0	0.0	1.2	1.5	7.5	10	51.7	68	76
A211BW1b	18.2	25	0.3	0.3	1.2	1.7	8.3	11	46.3	62	74
A211BW3b	17.6	24	0.0	0.0	1.2	1.7	7.6	10	47.6	64	74
A211BW5b	16.5	23	0.0	0.0	1.2	1.6	7.3	10	48.1	66	73
A211BW7b	15.8	21	0.0	0.0	1.2	1.5	7.0	9	51.3	68	75
A211BW9b	15.3	21	0.0	0.0	1.1	1.5	6.6	9	49.0	68	72
A233BW1b	16.3	23	0.0	0.0	1.2	1.7	5.5	8	49.2	68	72
A233BW3b	17.6	23	0.0	0.0	1.3	1.7	5.3	7	52.8	69	77
A233BW5b	16.6	22	0.0	0.0	1.4	1.8	5.2	7	50.8	69	74
A233BW7b	16.4	23	0.0	0.0	1.2	1.7	5.1	7	49.1	68	72
A233BW9b	16.0	22	0.0	0.0	1.1	1.5	5.0	7	50.4	69	73
A212(A-C)N0b	18.5	24	1.4	1.8	1.1	1.5	9.7	12	47.4	61	78
A2(5-1)Rb	16.5	23	0.0	0.0	1.2	1.7	4.4	6	49.9	69	72
A211Rb	15.9	22	0.0	0.0	1.2	1.7	4.7	7	49.7	70	72
A224Rb	16.8	21	n.d.	-	1.3	1.6	6.1	7	56.6	70	81
A233Rb	16.2	22	0.0	0.0	1.3	1.8	4.9	7	50.5	69	73
A234Rb	17.1	21	n.d.	-	1.3	1.6	6.5	8	56.3	69	81

The concentrations of the major exchangeable cations, K, Na, Mg and Ca, have been plotted against the distance from the Cu-tube in Figure 9-3.

Block 33 from the cool part of the parcel has essentially the same pool of exchangeable cations as the reference samples, i.e. almost 70 % of the exchange sites are occupied by sodium, 22-23 % by calcium and 7% by Mg. In contrast, sodium has been replaced by Ca and Mg in the hot blocks, where divalent cations constitute a gradually increasing proportion of the cation pool towards the heater. This is clearly demonstrated by the plot of the ratios Na/Ca and Na/Mg in Fig. 5. It is also notable that the overall proportion of Mg has increased in the hot blocks, particularly in their hottest parts. As shown by the chemical analysis of the clay fraction (Chapter 9.2.2.5), the increase in exchangeable Mg is paralleled by increasing content of non-exchangeable Mg in the clay.

Cu concentrations in excess of the analytical detection limit were found only in extracts of the innermost samples (samples no. 0 and 1) of the hot blocks (cf. Table 9-3). The extractable amount is, however, generally less than 1% of the total exchangeable cation pool and make up 9 % at most of the maximum available amount of Cu (4951 ppm Cu in the contact surface of block 12 (cf. Table 9-5) is equivalent to 16 $cmol^{+}kg^{-1}$, but the extracted amount is less than 1.5 $cmol^{+}kg^{-1}$). This fact suggests that Cu has been incorporated in the bentonite matrix mainly in a form that is not readily soluble or accessible for cation exchange.

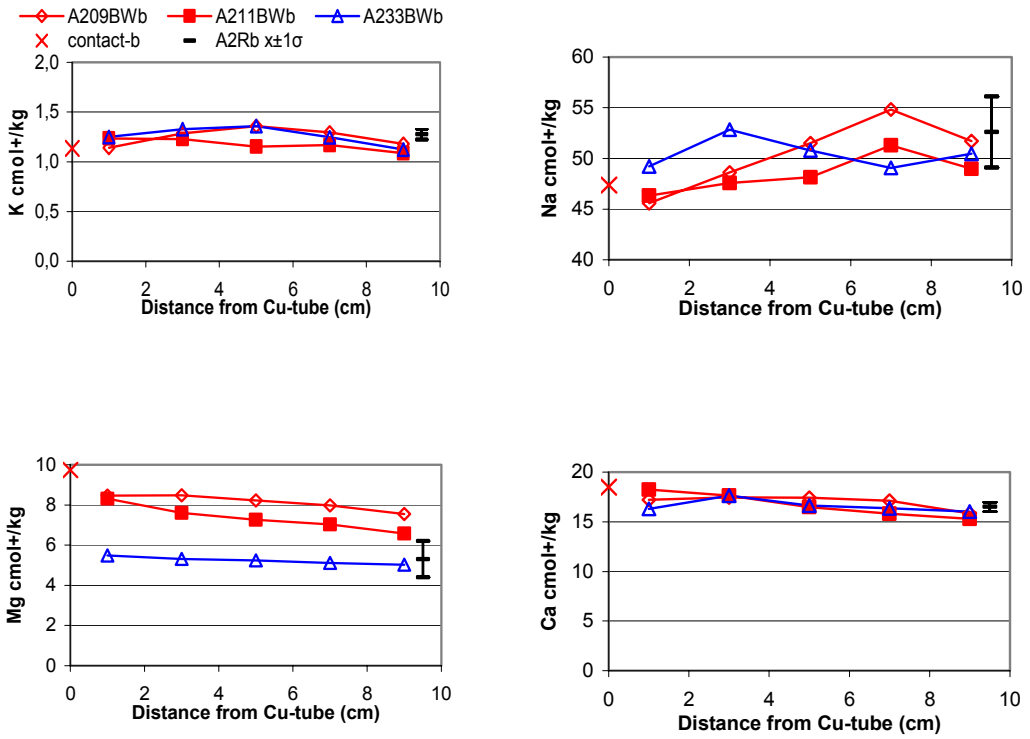

Figure 9-3 Plots of exchangeable K, Na, Mg and Ca, respectively, versus the distance from the Cu-tube for blocks 09, 11 and 33 of the LOT A2 parcel. Values of the reference samples (A2Rb) are shown at position 9.5 cm as the mean ±1 standard deviation of five samples

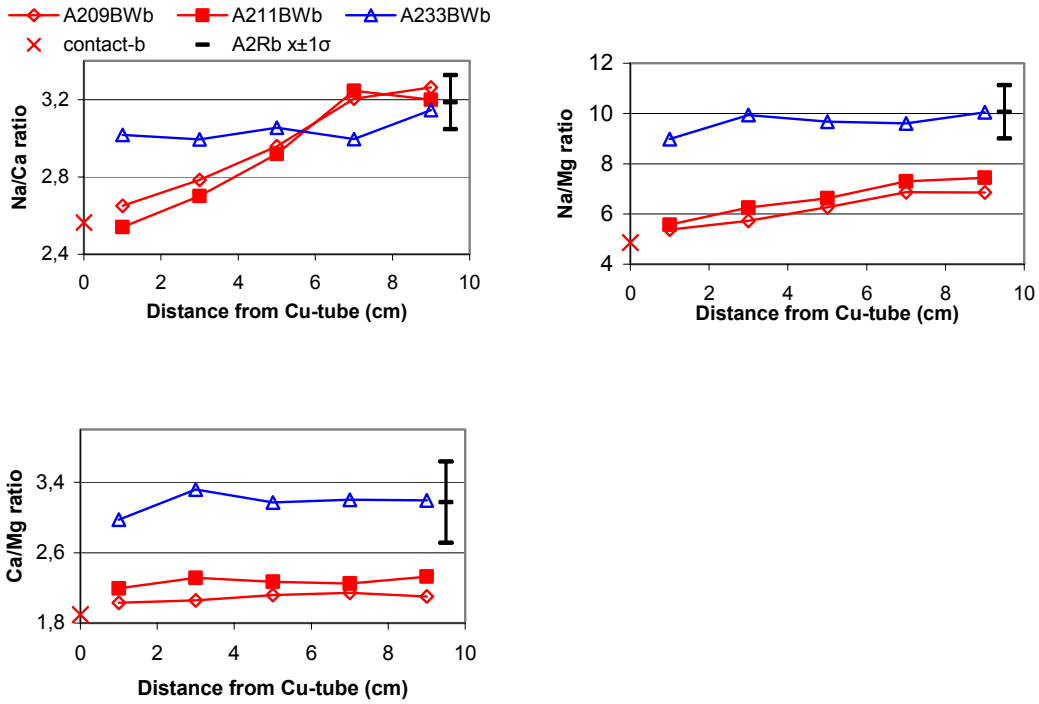

Figure 9-4 Plot of the ratios of exchangeable Na/Ca, Na/Mg, and Ca/Mg, respectively, versus the distance from the Cu-tube. Samples of blocks 09, 11 and 33 of the LOT A2 parcel. Values for the reference samples (A2R) are shown at position 9,5 cm as the mean ±1 standard deviation of five samples.

9.2.2.4. Cation exchange capacity (SICADA test code LA2CEC)

The data on the cation exchange capacity (Cu-CEC) of bulk samples and of clay fractions are compiled in Table 9-4.

The mean CEC value of five LOT A2 reference bentonites, 81 $cmol^{+}kg^{-1}$ (std. dev. 0.64) matches the Cu-CEC value previously reported for the bentonite MX80, that was used for the LOT parcels /Karnland et al. 2000/. The samples from the cool part of parcel A2, block 33, have essentially the same CEC (mean CEC 80 $cmol^{+}kg^{-1}$, std. dev. 0.34) as the reference samples, whereas CEC values of the samples from the two hot blocks are more variable and have higher means (mean CEC 82 $cmol^{+}kg^{-1}$, std. dev. 0.96 for block 09; mean CEC 83 $cmol^{+}kg^{-1}$, std. dev. 0.94 for block 11).

These rather subtle differences in CEC may simply reflect the range of variation in CEC measurements of fairly inhomogeneous materials like bentonites. Moreover, differential mineral dissolution/precipitation along the thermal gradient has increased the inhomogeneity of the hot blocks.

It is notable, however, that the CEC of both bulk samples and of clay fractions of the hot blocks display similar and quite systematic trends, with peak values for the two innermost samples (1 and 0), as shown by the plot of CEC against the radial distance in Fig. 6. Interestingly enough, these samples are distinguished also by higher contents of non-exchangeable Mg in the clay (cf. Table 9-5 and Table 9-6; and Section 9.2.2.5) and higher Mg-concentrations in the pore water. It is tempting to assume an interconnection between these alterations, but it remains to establish whether artifacts in the CEC measurements may arise - directly or indirectly –due to other changes of the bentonite close to the Cu-tube.

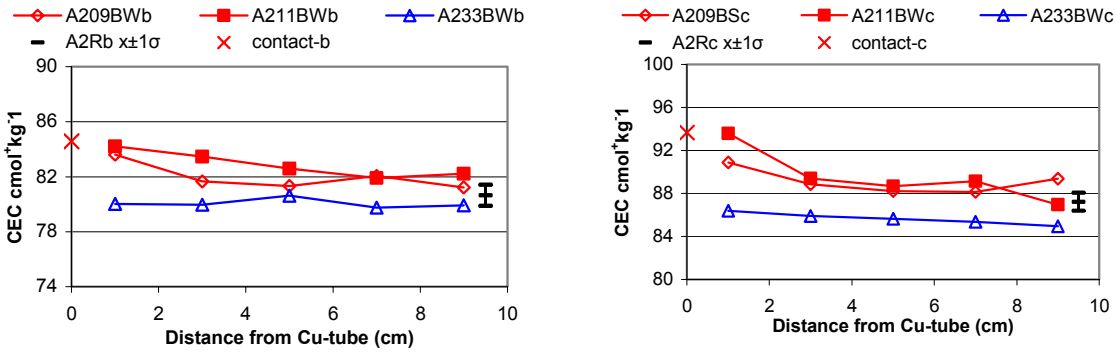

Figure 9-5 Plot of the CEC of bulk samples (left) and of clay fractions (right) versus radial distance for blocks 09, 11 and 33 of the LOT A2 parcel. Values for the reference samples (A2R) are shown at position 9.5 cm as the mean ±1 standard deviation of five samples.

Table 9-4 Cation exchange capacity (CEC) in $cmol^{+}kg^{-1}$ of bulk samples (left) and of clay fractions (right) from blocks 09, 11and 33 together with one sample of the contact surface (sample 0) and five reference samples for the LOT A2 parcel. CEC determined by exchange with the Cu-triethylene tetramine complex. SICADA test code LA2CEC

Bulk sample							<2µm
Sample id.	CEC_1	CEC_2	CEC_{mean}	Sample id.	CEC_1	CEC_2	CEC_{mean}
A209BW1b	84	83	84	A209BS1c	92	90	91
A209BW3b	81	82	82	A209BS3c	88	90	89
A209BW5b	81	82	81	A209BS5c	89	88	88
A209BW7b	82	82	82	A209BS7c	89	87	88
A209BW9b	81	81	81	A209BS9c	89	88	89
block mean ± 1σ			82±0.96				89±1.14
A211BW1b	84	84	84	A211BW1c	94	93	94
A211BW3b	83	84	83	A211BW3c	89	89	89
A211BW5b	83	82	83	A211BW5c	88	89	89
A211BW7b	82	82	82	A211BW7c	89	90	89
A211BW9b	82	82	82	A211BW9c	88	86	87
block mean ± 1σ			83±0.94				90±2.45
A212(A-C)N0b	85	84	85	A212(A-C)N0c	94	94	94
A233BW1b	80	80	80	A233BW1c	86	87	86
A233BW3b	80	80	80	A233BW3c	86	86	86
A233BW5b	80	81	81	A233BW5c	85	86	86
A233BW7b	79	80	80	A233BW7c	85	86	85
A233BW9b	79	81	80	A233BW9c	85	85	85
block mean ± 1σ			80±0.34				86±0.55
A2(1-5)Rb	80	81	81	A2R(1-5)c	87	86	87
A211Rb	81	80	80	A211Rc	86	87	87
A224Rb	82	81	81	A233Rc	87	86	87

A233Rb	80	79	80	A224Rc	88	88	88
A2R34b	81	81	81	A234Rc	88	87	88
reference mean ± 1σ			81±0.64				87±0.68

9.2.2.5.Bentonite composition (SICADA test code LA2EA)

The chemical composition of the bentonite samples is given in Table 9-5 (bulk samples) and Table 9-6 (clay fractions).

One of the questions of interest was to what extent copper had been mobilized from the Cu-tube under the adverse conditions of the LOT A2 test. The radial Cu-distribution within the blocks (Figure 9-6) clearly shows that copper has been incorporated into the bentonite matrix proximal to the Cu-tube at all temperatures, although the concentration in the hot blocks is 10 to 20 times higher than that of the cool block. The increase in Cu is seen only in the contact samples, i.e. sample 0 and 1, (sample 1 with a 1-2 mm thick layer of the contact surface removed). All samples beyond 2 cm from the Cu tube have concentrations equal to that of the references.

The Cu concentrations of the A2 blocks, i.e. after a test period of 5 years, are, however, not significantly higher (15 % at a maximum) than those of the equivalent blocks of the 1-year LOT test /Karnland et al. 2000/. This fact suggests that mobilization of Cu was most intense during an early stage of the test period, possibly before the bentonite had been completely saturated with water.

A small increase in Cu, which is paralleled by an increase in Ni (cf. Table 9-5) in the peripheral sample of block 33 suggests that the source of Cu in this case is the gauges that were aligned on the outer mantle surface of the block during the A2 test.

The Cu concentration of the clay fraction of the contact samples is 20-30 % of that of the corresponding bulk samples. Provided that the clay fraction extracted is representative of the entire sample volume, this fact indicates that the major fraction of Cu is not incorporated in the structure of the montmorillonite. The form in which copper has been incorporated has not been identified but, as previously described, less than 0,3 % of the total available Cu content is extractable into water and 9 % at most into the alcoholic ammonium chloride solution used for the extraction of the exchangeable cations (cf. 9.2.2.2 and 9.2.2.3)

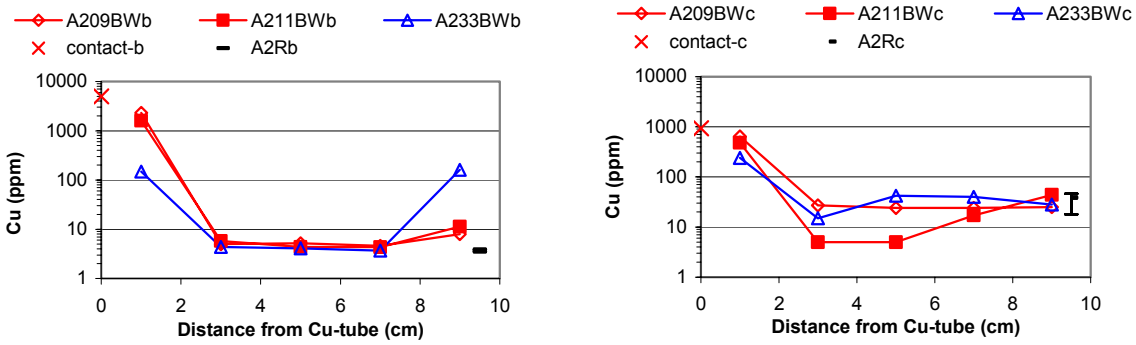

Figure 9-6 Plot of the Cu concentration in bulk samples (left) and clay fractions (right) versus the distance from the Cu-tube for blocks 09, 11 and 33 of the LOT A2 parcel. Values for the reference samples (A2R) are shown at position 9.5 cm as the mean ±1 standard deviation of five samples

The sulfate and carbonate minerals are trace constituents (<1,5%) in the parent bentonite MX80 but attention is paid to these minerals because of their temperature-dependant solubility - that is, the solubility decreases with increasing temperature. Under non-isothermal conditions with steep temperature gradients these salts may consequently accumulate in the warmer parts of the buffer, which would affect both the rheology of the bentonite and the composition of the pore water.

The mean concentration of total sulfur in the reference bentonite samples is 0.21% (std.dev. 0.07; N=5). According to the data on water-soluble salts (Table 9-2) approximately 40% of the total sulphur content is derived from water-soluble minerals (mainly gypsum, $CaSO_4*2H_2O$). The source of the remaining fraction, 0.10-0.15% S, is sulfides and, possibly, also sulfates of low solubility (e.g. $BaSO_4$). The distribution of total sulfur plotted in Fig. 8 matches the results of the analysis of aqueous leachates (cf. Fig 3), and shows that the sulfur distribution in the cool block has remained more or less unaffected during the LOT test. In the hot blocks the total sulfur content has increased by 40-90 % in the interval 3-6 cm from the heater where $CaSO_4$ has accumulated, whereas the peripheral parts appear to be depleted in sulfur.

No separate analysis of sulfide was made, but the insoluble fraction of S (i.e. the differences between total and water-soluble S) is most likely dominated by iron sulfide (pyrite FeS_2) although no precautions were taken to prevent oxidation during the leaching with water. The distribution pattern of this fraction of sulfur (Figure 9-7) suggests that a supplementary sulfide analysis might provide useful information about differences in iron sulfide stability between hot and cool blocks and should therefore be considered in future investigations of the LOT parcels.

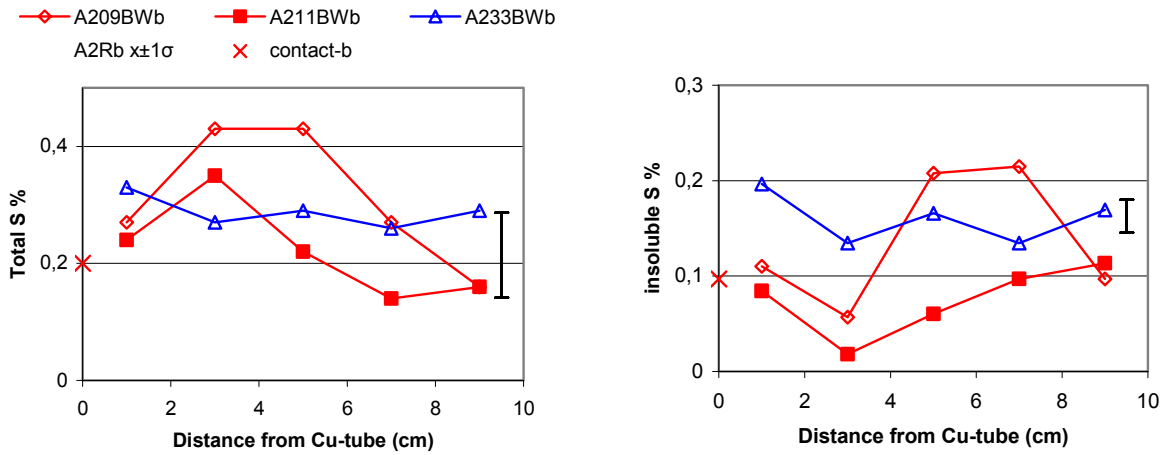

Figure 9-7 The content of total (left) and water-insoluble sulphur (right) in bulk samples of block 09, 11 and 33 of the LOT A2 parcel. Values for the reference samples (A2Rb) are shown at position 9,5 cm as the mean ±1 standard deviation of five samples

Table 9-5 Chemical composition of the bulk bentonite samples of blocks 09, 11 and 33 together with one sample of the contact surface (sample 0) and five reference samples of the LOT A2 parcel. Major elements by ICP-AES, trace elements by ICP-MS except for samples A224Rb and A234Rb (different detection limits for AES and MS), S and C by evolved gas analysis. n.d.=not determined. SICADA test code LA2EAb.

Sample id.	SiO_2	Al_2O_3	Fe_2O_3	MgO	CaO	Na_2O	K_2O	TiO_2	P_2O_5	MnO	Cr_2O_3	LOI	TOT/C	CO_2-C	TOT/S	SUM	Ni	Sc	Cu	Zn	Ba	Co	Nb	Sr	Ta	Zr	Y	Ce
	%	%	%	%	%	%	%	%	%	%	%	%	%	%	%	%	ppm	ppm	ppm	ppm	ppm	ppm	ppm	ppm	ppm	ppm	ppm	ppm
A209BW1b	62.48	19.00	3.68	2.47	1.12	1.99	0.51	0.14	0.05	0.01	0.003	8.1	0.28	0.068	0.27	99.94	5	5	2325	88	257	5	29	234	5	177	44	102
A209BW3b	63.01	18.96	3.60	2.20	1.55	2.07	0.53	0.14	0.05	0.01	0.001	7.8	0.29	0.085	0.48	100.06	5	5	5	112	356	5	29	313	7	171	44	108
A209BW3b-2.	62.91	19.03	3.66	2.26	1.44	2.06	0.53	0.14	0.05	0.01	0.001	7.7	0.33	n.d.	0.43	99.94	5	5	5	99	411	5	32	303	7	176	46	104
A209BW5b	63.01	18.86	3.74	2.34	1.59	2.07	0.55	0.15	0.05	0.01	0.005	7.7	0.35	0.155	0.43	100.07	5	5	5	93	261	1.2	27	325	3	177	46	123
A209BW7b	63.21	19.18	3.71	2.27	1.47	2.07	0.53	0.15	0.05	0.02	0.002	7.4	0.37	0.142	0.27	100.06	5	5	5	78	465	1	28	344	3	182	46	127
A209BW9b	63.51	19.06	3.78	2.25	1.22	2.12	0.54	0.15	0.05	0.01	0.004	7.4	0.35	0.153	0.16	100.09	9	5	8	96	279	1	28	273	3	197	48	130
Block mean	*63.02*	*19.02*	*3.70*	*2.30*	*1.40*	*2.06*	*0.53*	*0.15*	*0.05*	*0.01*	*0.003*	*7.68*	*0.33*	*0.121*	*0.34*	*100.03*	*5.7*	*5*	*392*	*94*	*338*	*3*	*29*	*299*	*5*	*180*	*46*	*116*
A211BW1b	62.96	18.91	3.70	2.55	1.11	2.03	0.50	0.15	0.05	0.01	0.001	7.9	0.27	0.057	0.24	99.87	5	5	1600	72	196	0.9	28	237	3	187	47	128
A211BW3b	62.93	18.97	3.75	2.39	1.38	2.04	0.52	0.15	0.05	0.01	0.003	7.9	0.29	0.085	0.35	100.09	5	5	6	91	258	0.8	27	274	3	198	45	124
A211BW5b	63.50	18.77	3.77	2.25	1.30	2.04	0.51	0.14	0.05	0.02	0.001	7.7	0.38	0.136	0.22	100.05	5	5	4	94	589	1	27	330	3	185	47	124
A211BW7b	63.59	18.88	3.75	2.29	1.25	2.11	0.51	0.14	0.05	0.01	0.011	7.5	0.35	0.139	0.14	100.1	5	6	4	68	174	1	28	229	3	197	47	125
A211BW9b	62.84	19.09	3.66	2.24	1.32	2.12	0.50	0.15	0.06	0.01	0.001	8.1	0.39	0.139	0.16	100.09	5	5	11	68	204	1	28	271	3	183	50	131
Block mean	*63.16*	*18.92*	*3.73*	*2.34*	*1.27*	*2.07*	*0.51*	*0.15*	*0.05*	*0.01*	*0.003*	*7.82*	*0.34*	*0.111*	*0.22*	*100.04*	*5.0*	*5.2*	*325*	*79*	*284*	*0.94*	*28*	*268*	*3.2*	*190*	*47*	*126*
A212(A-C)N0b	62.51	18.84	3.64	2.65	1.05	2.03	0.50	0.14	0.05	0.01	0.003	8.0	0.31	0.063	0.2	99.43	5	5	4951	52	188	0.8	28	238	3	189	47	126
A233BW1b	63.38	19.11	3.82	2.36	1.40	2.15	0.52	0.15	0.06	0.01	0.001	7.1	0.37	n.d	0.33	100.06	5	5	149	82	295	0.9	28	291	3	184	47	129
A233BW3b	62.94	19.44	3.83	2.41	1.39	2.12	0.54	0.15	0.05	0.01	0.005	7.2	0.37	n.d	0.27	100.09	6	5	4	85	373	1.6	28	298	3	197	46	130
A233BW5b	63.90	18.86	3.80	2.32	1.34	2.12	0.52	0.15	0.05	0.01	0.009	7.0	0.36	n.d	0.29	100.08	7	5	4	91	323	1.1	28	301	3	188	48	133
A233BW7b	63.61	18.81	3.84	2.35	1.35	2.08	0.53	0.15	0.05	0.01	0.001	7.3	0.37	n.d	0.26	100.08	5	5	4	96	283	1	28	291	3	185	46	129
A233BW9b	62.99	19.10	3.68	2.31	1.33	2.14	0.50	0.15	0.05	0.01	0.006	7.8	0.37	n.d	0.29	100.07	63	5	162	88	273	0.9	27	273	3	192	45	126
Block mean	*63.36*	*19.06*	*3.79*	*2.35*	*1.36*	*2.12*	*0.52*	*0.15*	*0.05*	*0.01*	*0.004*	*7.28*	*0.37*	n.d	*0.29*	*100.08*	*17*	*5*	*65*	*88*	*309*	*1.10*	*28*	*291*	*3.26*	*189*	*46*	*129*
A2(1-5)Rb	63.46	19.03	3.81	2.38	1.35	2.08	0.55	0.15	0.06	0.01	0.005	7.2	0.38	0.145	0.26	100.08	7	5	4	76	442	1	28	289	3	206	46	130
A211Rb	62.84	19.01	3.70	2.30	1.27	2.06	0.51	0.14	0.05	0.01	0.002	8.2	0.36	0.131	0.26	100.1	5	5	4	69	240	0.9	27	270	3	185	47	129
A224Rb	63.42	19.68	3.70	2.39	1.17	2.14	0.51	0.14	0.05	0.01	0.001	6.6	0.37	0.145	0.13	99.93	<5	6	<10	74	258	<5	32	275	<20	192	45	94
A233Rb	63.65	19.13	3.74	2.35	1.30	2.09	0.53	0.15	0.05	0.01	0.001	7.1	0.34	0.134	0.28	100.1	5	5	4	82	257	0.9	29	276	3	200	47	135
A234Rb	64.12	19.28	3.64	2.33	1.21	2.09	0.53	0.14	0.04	0.01	0.002	6.4	0.37	0.145	0.14	99.93	<5	5	<10	103	395	<5	33	287	<20	187	44	90
Reference mean	*63.50*	*19.23*	*3.72*	*2.35*	*1.26*	*2.09*	*0.53*	*0.14*	*0.05*	*0.01*	*0.002*	*7.10*	*0.36*	*0.140*	*0.21*	*100.03*		*5.2*		*81*	*318*		*30*	*279*		*194*	*46*	*115*

Table 9-6 Chemical composition of the Na-saturated clay fractions of samples from blocks 09, 11 and 33 together with one sample of the contact surface Cu-tube/bentonite (sample 0) and three reference samples of the LOT A2 parcel. Analysis by ICP-AES. SICADA test code LA2EAc.

Sample id.	SiO_2	Al_2O_3	Fe_2O_3	MgO	CaO	Na_2O	K_2O	TiO_2	P_2O_5	MnO	Cr_2O_3	LOI	TOT/C	TOT/S	SUM	Ba	Cu	Zn	Ni	Co	Sr	Zr	Ce	Y	Nb	Sc	Ta
	%	%	%	%	%	%	%	%	%	%	%	%	%	%	%	ppm	ppm	ppm	ppm	ppm	ppm	ppm	ppm	ppm	ppm	ppm	ppm
A209BS1c	63.20	21.25	3.81	2.63	0.06	2.33	0.07	0.13	0.03	0.01	0.001	6.3	0.24	0.01	99.94	11	642	89	5	5	13	149	83	35	32	6	5
A209BS3c	64.05	20.32	3.83	2.44	0.06	2.31	0.12	0.13	0.03	0.01	0.002	6.7	0.27	0.01	100.06	35	27	57	10	25	18	151	104	38	36	6	9
A209BS5c	63.68	20.64	3.86	2.42	0.04	2.30	0.10	0.13	0.03	0.01	0.001	6.8	0.36	0.01	100.07	32	24	39	8	5	17	151	91	37	29	6	5
A209BS7c	64.19	20.39	3.82	2.34	0.12	2.20	0.13	0.14	0.03	0.01	0.001	6.5	0.25	0.01	99.93	37	24	56	5	5	18	155	99	40	32	6	7
A209BS9c	63.86	20.40	3.85	2.40	0.10	2.24	0.08	0.13	0.03	0.01	0.001	6.9	0.27	0.01	100.05	19	25	42	5	6	17	150	88	34	34	6	5
Block mean	*63.80*	*20.60*	*3.83*	*2.45*	*0.08*	*2.28*	*0.10*	*0.13*	*0.03*	*0.01*	*0.00*	*6.64*	*0.28*	*0.01*	*100.01*	*27*	*148*	*57*	*7*	*9*	*17*	*151*	*93*	*37*	*33*	*6*	*6*
A211BW1c	63.28	21.19	3.81	2.58	0.03	2.21	0.07	0.12	0.02	0.01	0.001	6.5	0.19	0.01	99.93	18	479	77	5	5	12	148	79	35	34	6	8
A211BW3c	64.27	20.17	3.54	2.37	0.05	2.33	0.09	0.12	0.02	0.01	0.002	6.9	0.26	0.01	99.93	26	5	52	5	8	18	156	135	37	33	6	5
A211BW5c	64.50	20.20	3.59	2.28	0.04	2.32	0.10	0.13	0.02	0.01	0.001	6.7	0.27	0.01	99.94	52	5	37	5	8	19	156	114	37	37	5	5
A211BW7c	65.17	19.98	3.51	2.22	0.04	2.28	0.11	0.13	0.02	0.01	0.002	6.4	0.27	0.01	99.93	30	17	36	22	5	16	157	124	38	39	6	5
A211BW9c	64.94	20.09	3.64	2.26	0.14	2.24	0.11	0.13	0.01	0.01	0.001	6.3	0.27	0.01	99.93	26	44	54	43	5	18	157	111	38	36	6	5
Block mean	*64.43*	*20.33*	*3.62*	*2.34*	*0.06*	*2.28*	*0.10*	*0.13*	*0.02*	*0.01*	*0.0015*	*6.56*	*0.25*	*0.01*	*99.93*	*30*	*110*	*51*	*16*	*6*	*17*	*155*	*113*	*37*	*36*	*6*	*6*
A212(A-C)N0c	63.00	21.29	3.82	2.71	0.04	2.38	0.07	0.13	0.02	0.01	0.001	6.3	0.37	0.01	99.93	12	932	67	5	5	15	148	95	37	33	6	5
A233BS1c	63.96	20.53	3.70	2.37	0.06	2.25	0.13	0.13	0.04	0.01	0.001	6.8	0.30	0.01	100.06	40	241	38	5	5	19	155	100	40	34	6	10
A233BS3c	64.00	20.73	3.73	2.41	0.06	2.27	0.14	0.13	0.03	0.01	0.001	6.5	0.26	0.01	100.07	39	15	38	5	6	19	153	92	41	32	6	5
A233BS5c	64.22	20.40	3.75	2.39	0.09	2.33	0.15	0.14	0.03	0.01	0.001	6.5	0.26	0.01	100.07	46	42	44	5	5	21	155	100	40	27	6	5
A233BS7c	64.27	20.44	3.70	2.37	0.06	2.26	0.13	0.13	0.03	0.01	0.001	6.6	0.26	0.01	100.06	39	40	37	5	7	19	152	91	39	36	6	5
A233BS9c	63.71	20.25	3.71	2.41	0.12	2.12	0.12	0.13	0.03	0.01	0.001	7.4	0.29	0.01	100.07	34	28	53	5	5	18	153	96	38	28	6	5
Block mean	*64.03*	*20.47*	*3.718*	*2.39*	*0.078*	*2.246*	*0.134*	*0.132*	*0.032*	*0.01*	*0.001*	*6.76*	*0.274*	*0.01*	*100.066*	*40*	*73*	*42*	*5*	*6*	*19*	*154*	*96*	*40*	*31*	*6*	*6*
A2(1-5)Rc	64.06	21.06	3.56	2.36	0.03	2.18	0.08	0.12	0.03	0.01	0.001	6.4	0.39	0.01	99.93	14	11	27	5	5	13	146	91	35	32	6	5
A211Rc	64.17	20.85	3.62	2.34	0.04	2.21	0.11	0.13	0.03	0.01	0.001	6.5	0.27	0.01	100.06	29	39	32	5	5	15	151	110	38	34	6	6
A233Rc	63.78	21.40	3.67	2.34	0.04	2.21	0.10	0.13	0.03	0.01	0.001	6.3	0.28	0.01	100.07	36	38	35	5	5	13	153	105	38	30	6	5
A233Rc-2	63.88	21.23	3.64	2.35	0.04	2.26	0.11	0.13	0.03	0.01	0.001	6.2	0.27	0.01	99.93	37	41	34	5	5	13	154	89	39	33	6	5
Reference mean	*63.97*	*21.14*	*3.62*	*2.35*	*0.04*	*2.22*	*0.10*	*0.13*	*0.03*	*0.01*	*0.001*	*6.35*	*0.30*	*0.01*	*100.00*	*29*	*32*	*32*	*5*	*5*	*13.5*	*151*	*99*	*38*	*32*	*6*	*5*

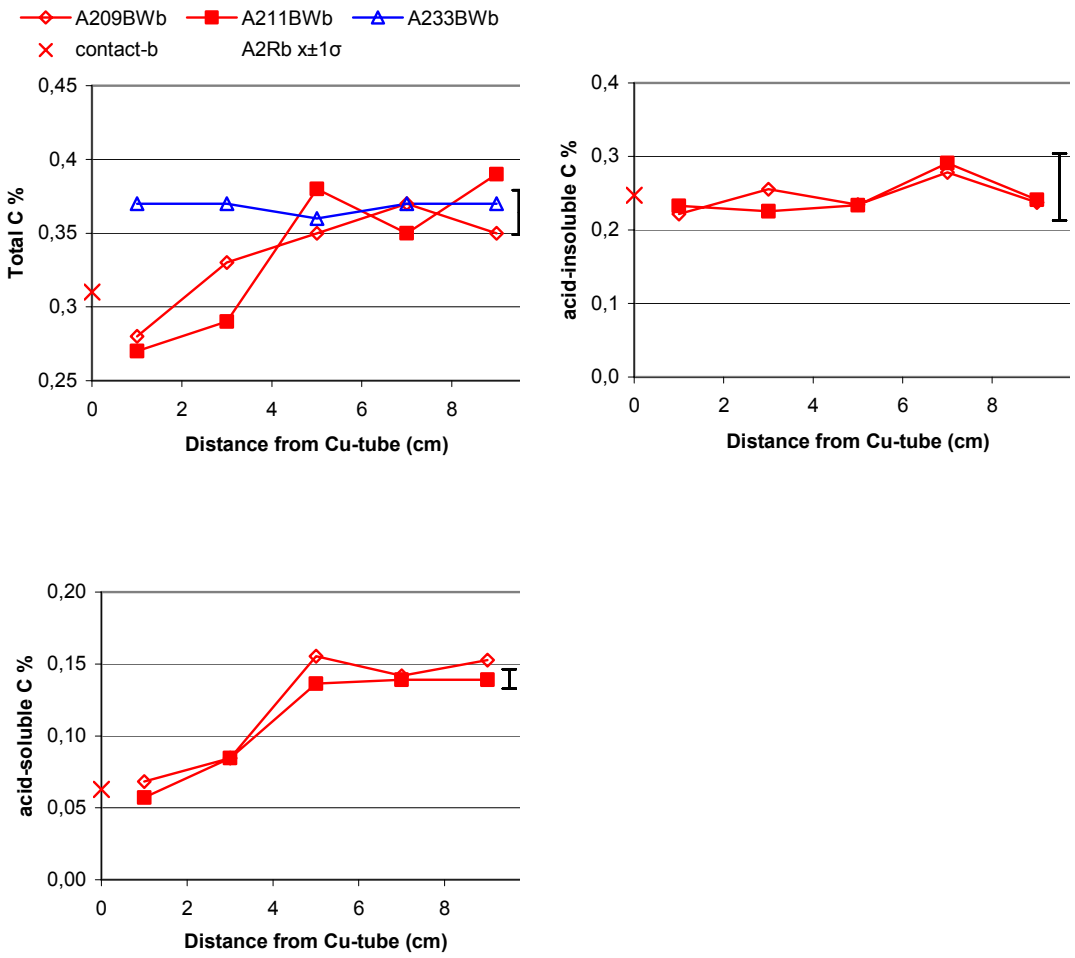

Figure 9-8 Total, acid-insoluble and acid-soluble carbon in bulk samples of block 09, 11 and 33 of the LOT A2 parcel (for block 33 only total carbon). Values for the reference samples (A2Rb) are shown at position 9.5 cm as the mean ±1 standard deviation of five samples.

The average total carbon content of the reference samples is 0.36% (std.dev. 0.02; N=5). The content of acid-soluble carbon, which is derived mainly from carbonate phases, is 0.14 % C. The source of the remaining, acid-insoluble fraction is most likely organic matter.

The plots of the distribution of the different fractions of carbon (9.2.2.3) show that the acid-insoluble fraction of carbon is more or less constant in all blocks irrespective of the block temperature. The content of carbonate carbon, on the other hand, decreases in the interval 0-5 cm from the Cu-tube in the hot blocks, suggesting that carbonate dissolution has increased with increasing temperature.

The exact composition of the carbonate phase is not known but a normative calculation based on the CaO content remaining after allocating Ca to sulfate and to exchangeable Ca, suggests that Ca-carbonate is predominant. Dissolution/precipitation reactions involving both sulfates and carbonates of calcium have necessarily influenced the composition of the pore water in the hot blocks and, consequently, explain some of the changes in the pool of the exchangeable cations indicated in Figure 9-3 and Figure 9-4.

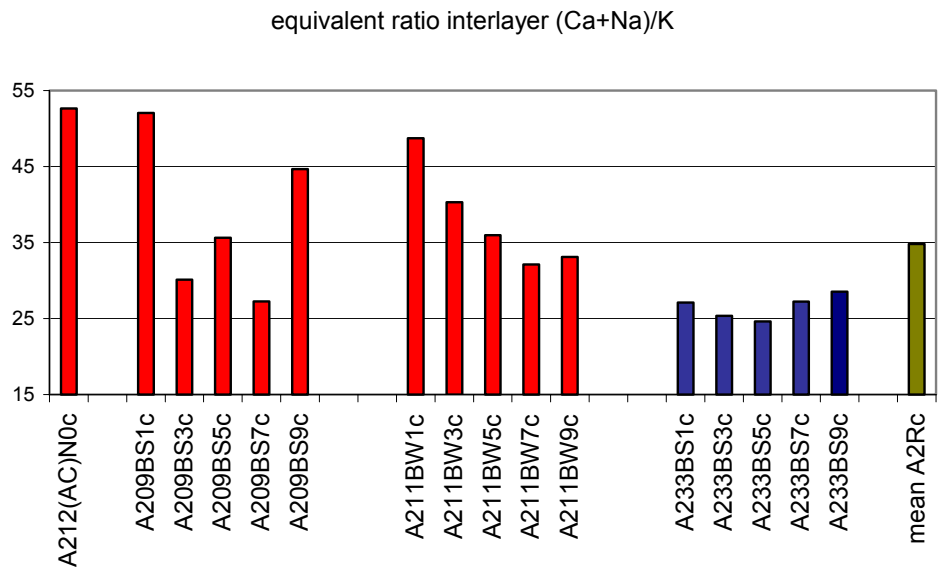

Figure 9-9 The equivalent ratio of interlayer (Ca+Na)/K of the Na-saturated <2 μm fractions of sample 1-9 from the hot blocks 9 and 11 and from the cool block 33 of the LOT A2 parcel. One sample from the contact with the Cu-tube (sample 0) and the mean of three reference samples are also included.

Calculations of the structural formulas of the smectite based on the available chemical data was considered too uncertain, since it is obvious from the XRD-analysis that the SiO_2 content of the clay fraction is derived not only from smectite but also from fine-grained quartz and cristobalite. Nevertheless, some clear trends can be seen in the composition of the silicate fraction, which are demonstrated in Figure 9-9 to Figure 9-11 by some selected parameters extracted from the chemical data on the clay fraction (Table 9-6). Prior to the chemical analysis, carbonates and sulfates were removed from the clay, which thereafter was saturated with sodium (and dialyzed) in order to make the allocation of cations to exchange and structural sites, respectively, less ambiguous. Therefore, exchangeable sodium is the predominant interlayer cation but any calcium carbonate/sulfate that survived the pre-treatments will dissolve during the dialysis, supplying calcium for exchange. The same would be true for magnesium but no soluble Mg-bearing phase has been identified (cf. below). Potassium in the clay is, on the other hand, derived predominantly from illitic layers (cf. Section 9.2.2.6) and thus fixed in the interlayers. Accordingly, the equivalent ratio (Ca+Na)/K reflect the proportion between the exchangeable and non-exchangeable interlayer cations. As shown in Figure 9-9, this ratio has changed during the long term test in samples proximal to the heater, apparently due to loss of some potassium.

Also the MgO content of the clay fractions (Figure 9-10) displays a clear gradient towards the Cu-tube in the hot blocks and has increased from 2.35% (mean of references) to ca. 2.6% in the innermost samples, whereas the peripheral parts of the blocks appear to be depleted in magnesium. The MgO-values plotted in Fig. 10 have been re-calculated on an ignited basis to avoid the artifacts that may arise due to variable amounts of volatiles among the samples. Mg in exchange positions can be assumed to contribute insignificantly to the total MgO content in the Na-saturated clay, since no other Mg-

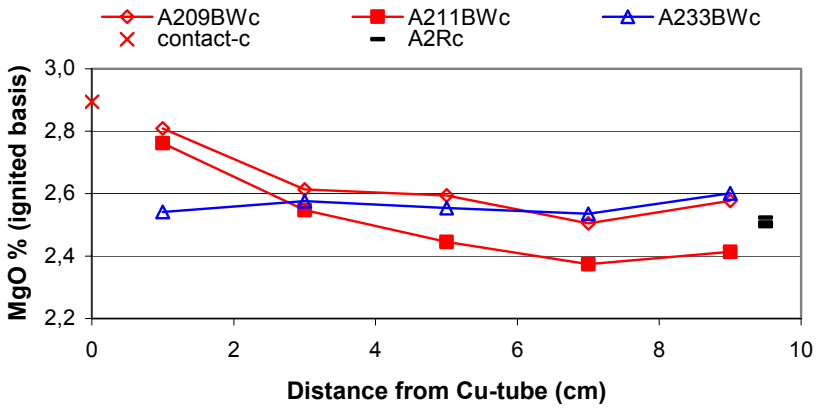

Figure 9-10 Plot of the MgO content of the Na-saturated <2 µm fractions (ignited basis) versus the distance from the Cu-tube for block 09, 11 and 33 of the LOT A2 parcel. Values for three reference samples are indicated at the position 9.5 cm

bearing mineral phase than montmorillonite has been identified in the XRD-analysis (cf. Section 9.2.2.6). The detection limit of this method may, however, be too poor to detect trace minerals, and depends, among other things, on the "crystallinity" of the phase.

Magnesium in the montmorillonite structure is located in the octahedral sheet together with Al and Fe (strictly, Al is normally a minor constituent also of the tetrahedral sheet of montmorillonite). As illustrated by the plots of the oxide ratios Al_2O_3/MgO and Fe_2O_3/MgO (Fig. 12), the concentration gradient is manifested more or less distinctly also in the relation between MgO and the other major "octahedral" elements.

It is notable that the Mg-rich samples proximal to the heater are distinguished also by higher CEC values (cf. Section 9.2.2.4). However, it remains to establish whether the increase in CEC is interconnected to redistribution of Mg and/or losses in fixed interlayer K - or simply, an experimental artifact, since the changes in CEC are close to the analytical resolution.

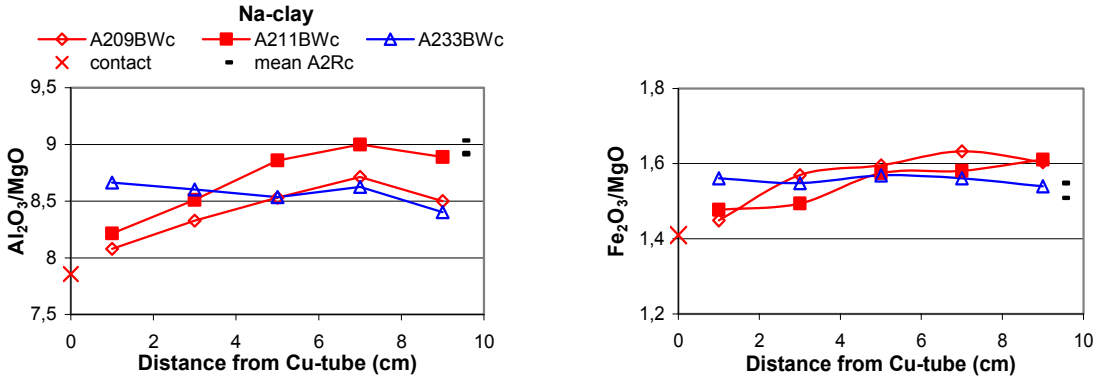

Figure 9-11 Plots of the ratios of the "octahedral" elements of the Na-saturated <2 µm fraction versus the distance from the Cu-tube. Samples from block 9, 11 and 33 of the LOT A2 parcel. Values for three reference samples are plotted at the position 9.5 cm.

9.2.2.6. Bentonite mineralogy (SICADA test code LA2XRD)

9.2.2.6.1. The reference bentonite

The XRD-profiles of random powders of the bulk material of five LOT A2 reference samples are shown in Figure 9-12 and the mean XRD-profile of the references in Figure 9-13. The strongest peaks of the major non-phyllosilicates, i.e. quartz, cristobalite and feldspars (K-feldspar and Na-plagioclase), are indicated in Figure 9-13. Traces of gypsum are generally found in MX80 bentonite, used for the LOT A2 parcel, and peak positions for gypsum are also indicated in Fig. 14, but according to the chemical data the maximum amount of gypsum that can exist (i.e. if all sulfur is allocated to $CaSO_4*2H_2O$) in the reference bentonite is below 2 % and close to the detection limit of the XRD analysis. Also calcite has been found in MX80 /eg. Karnland et al. 2000/, and is indicated in the chemical data but, again, the quantity (ca. 1.5 % if all acid-soluble carbon is allocated to $CaCO_3$) is close to the detection limit of the XRD method.

In the XRD-profile of Figure 9-13 also the strongest basal reflections (00l) and the two-dimensional hk-bands of montmorillonite are indicated. The positions of the basal reflections (ca. 12.5 Å for (001)) are typical of the monolayer hydrate of Na-montmorillonite, which is stable at relative humidities below 60-70% /Brindley & Brown 1980/. The shoulder on the low-angle side of the first order peak suggests, however, that mixed hydration states occur, probably due to the lack of RH control during the X-ray scanning and/or due to the mixed interlayer cation pool of the reference bentonite – approximately 20% of the interlayer sites are occupied by Ca which forms a two-layer hydrate at the relative humidity of normal laboratory conditions (RH 50±10%).

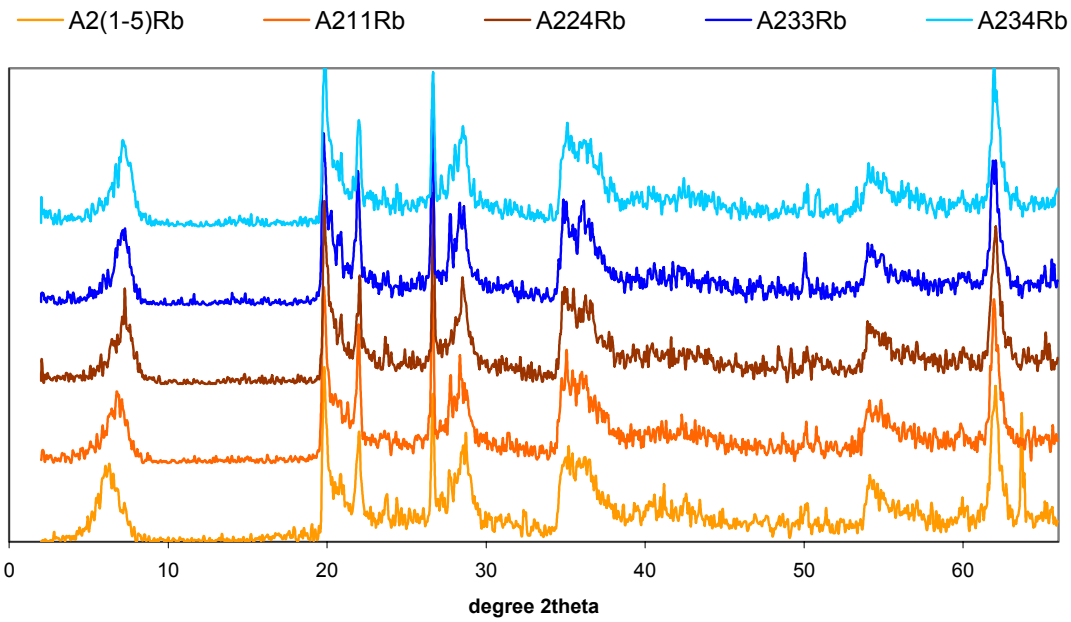

Figure 9-12 XRD-profiles of random powders of the bulk of five reference samples for the LOT A2 parcel. Peak positions are given in Figure 9-13. CuKα radiation.

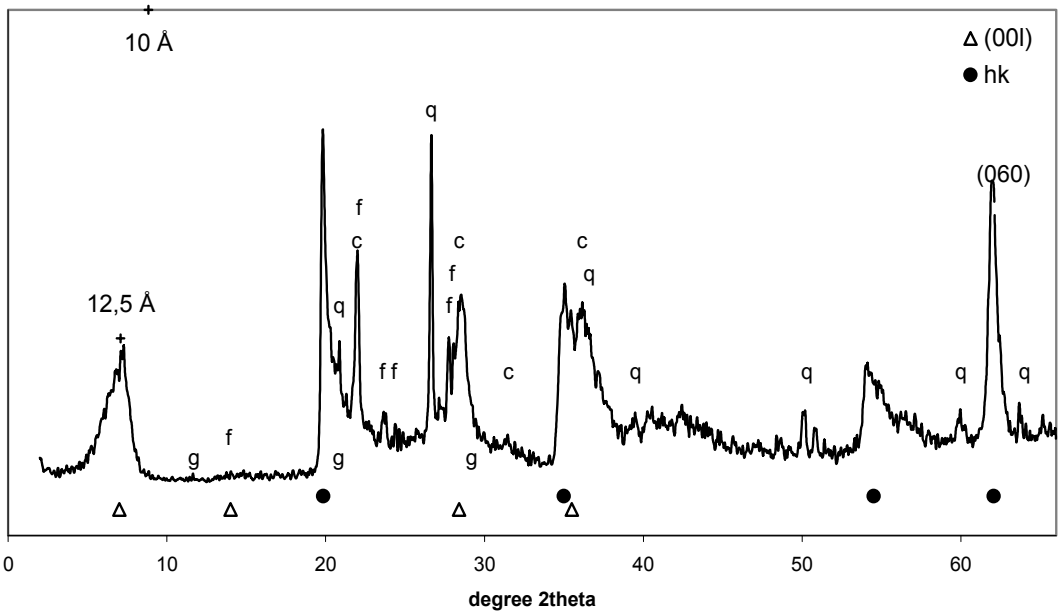

Figure 9-13 Mean XRD-profile of random powders of bulk material of five reference samples for the LOT A2 parcel (individual samples shown in Figure 9-12). The position of the strongest peaks of the major non-clay minerals is indicated; q=quartz, c=cristobalite, f=feldspars, g=gypsum. The position of the strongest 00l- and hk-peaks/bands of montmorillonite and the (001) mica/illlite peak (10Å) is also indicated. CuKα radiation.

In Figure 9-13 also the position of the so called (060)-peak is indicated. This reflection is useful for recognizing di- and trioctahedral sub-groups of clay minerals since it includes the *b* cell dimension which is more sensitive to the size of the cations and to site occupancy in the octahedral sheet than are the *a* or *c* cell dimensions. For smectites this peak is distinct enough to allow an estimate of the b parameter to an accuracy of perhaps ±0.5% (cf. Brindley & Brown 1980). An indicated d(060) value of 1.49-1.50 Å (62º 2θ) is typical of the dioctahedral sub-group of smectites, to which montmorillonite belongs.

Micaceous minerals, which have their (001) reflection at 10 Å, occur in such small quantities that basal peaks would barely be detectable in the XRD-trace of a randomly oriented preparation of good quality. No peaks can be detected in the mean XRD-profile of the references in Figure 9-13 but, depending on the degree of accidental orientation, individual samples display a peak of low intensity in the 10 Å-region, which indicates that trace amounts of mica/illite occur (cf Fig 13).

XRD-profiles of oriented aggregates of the Mg-saturated <2 μm fraction of the reference samples are shown in Figure 9-13 (air-dried clay) and 16 (EG-solvated clay). The clay fractions are almost pure montmorillonite, but traces of cristobalite (4.05 Å) and quartz (3.34 Å) can be seen in the XRD-profiles of all clay samples, showing that a small fraction of these minerals are extremely fine-grained. In contrast, feldspars cannot be detected in the XRD-traces of the clay fraction, suggesting that the grain size of the feldpars is generally >2 μm.

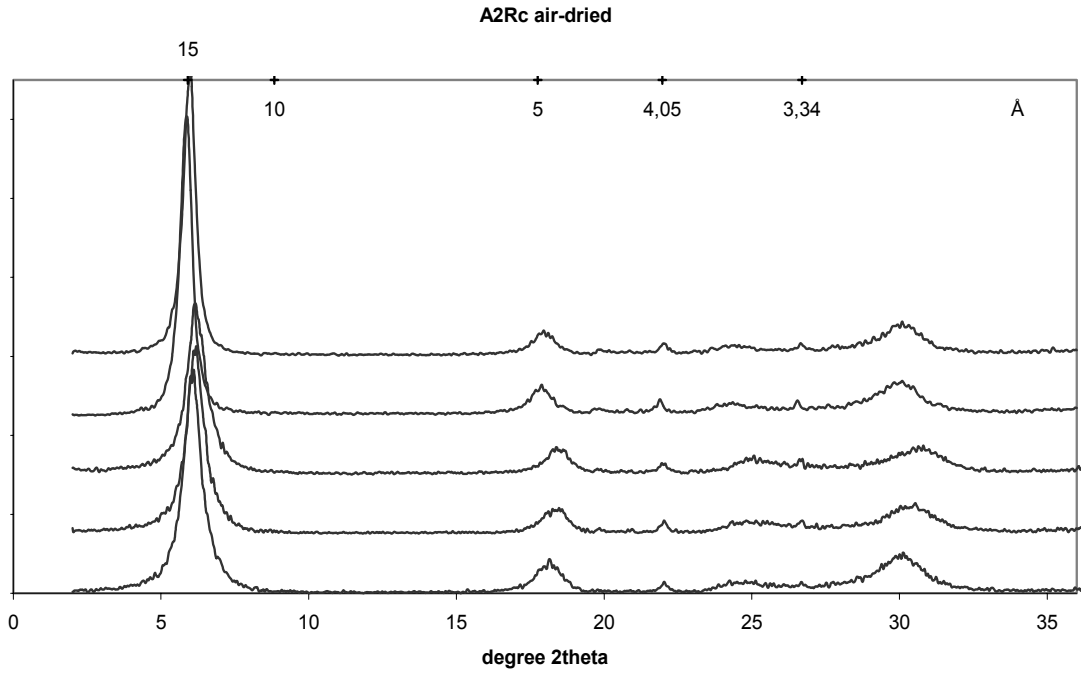

Figure 9-14 XRD-profiles of oriented aggregates of the air-dried, Mg-saturated clay fraction of five reference samples for LOT A2. The positions of the strongest basal reflections of montmorillonite are indicated in the upper scale together with the strongest peaks of cristobalite (4.05Å), quartz (3.34Å) and mica/illlite (10Å). CuKα radiation.

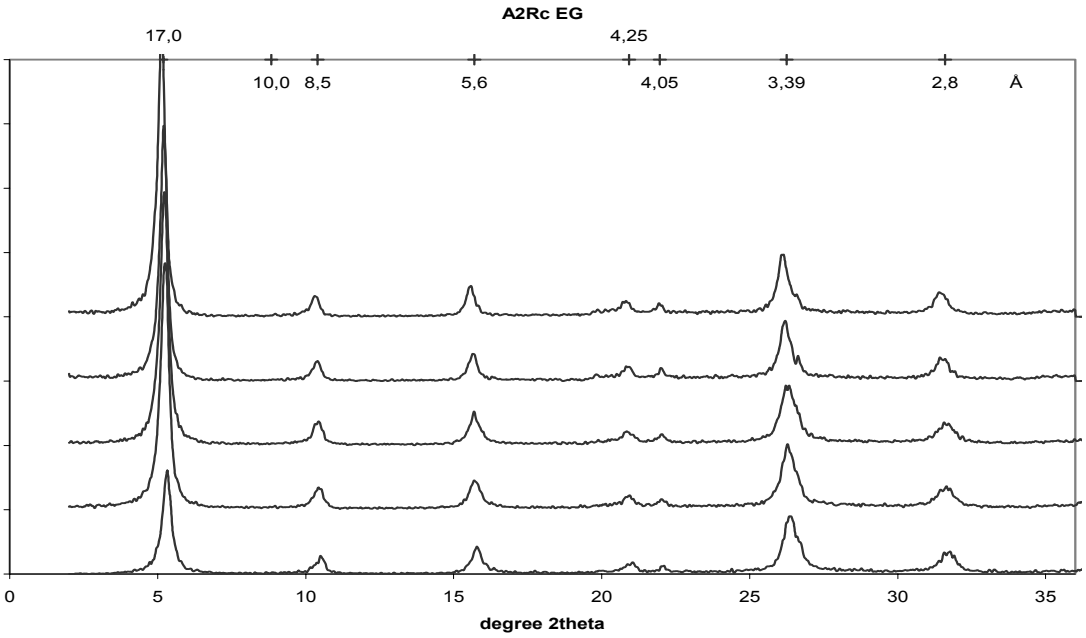

Figure 9-15 XRD-profiles of oriented aggregates of the clay fraction of five reference samples for LOT A2. Mg-saturated, ethylene glycol solvated samples. The positions of the basal reflections of montmorillonite are indicated in the upper scale together with the strongest peaks of cristobalite (4.05Å), and mica/illlite (10Å). CuKα radiation.

The homo-ionic Mg-clay has a basal spacing of 14-15 Å when air-dried (RH 50±10%) and expands to 16.9-17 Å upon ethylene glycol treatment (EG). As can be seen in the diffractograms of EG-solvated clays (Figure 9-15), the series of basal reflections deviates little from a complete, periodic diffraction pattern, which is indicative of well-ordered stacking sequences with virtually no interstratification (in interstratified clay minerals individual crystals are composed of basic unit layers of two or more types).Similarly, the $\Delta 2\theta_{002/003}$ value (the difference between the (002) and (003) peaks in degrees 2θ) is 5.27-5.30 which is typical of a well-defined montmorillonite phase, cf. /Moore & Reynolds 1989/. However, judged by the chemical data on the clay fraction, some illitic layers may exist - the amount of non-exchangeable potassium (0.1% K_2O, Table 9-6) would correspond to 1-1.5 % illite. No discrete 10-Å phase can be detected and such small amount of illitic layers in the smectite structure cannot be detected by routine XRD analysis (for comparison, ~10% illitic layers in the montmorillonite structure would give a $\Delta 2\theta_{002/003}$ value of 5.5).

In summary, the XRD analysis of the reference bentonite shows that:

The bulk bentonite contains montmorillonite, quartz, cristobalite, feldspars and traces of gypsum and mica/illite. No carbonate phases have been detected but are indicated in the chemistry of the solid phase. The amount is, however, close to or below the detection limit of the XRD-method.

The clay fraction is almost pure montmorillonite but traces of quartz and cristobalite still occur. No discrete 10 Å phase, i.e. mica/illite, can be detected.

Montmorillonite in the “as-received state” has a basal spacing of 12.5 Å at an RH of around 60% but the 001-peak tends to be broad and asymmetrical. The air-dried, homoionic Mg-exchanged clay has a basal spacing of 14-15 Å, and expands to 16.9-17 Å on EG-solvation, giving a complete, periodic diffraction pattern, typical of well-defined montmorillonite.

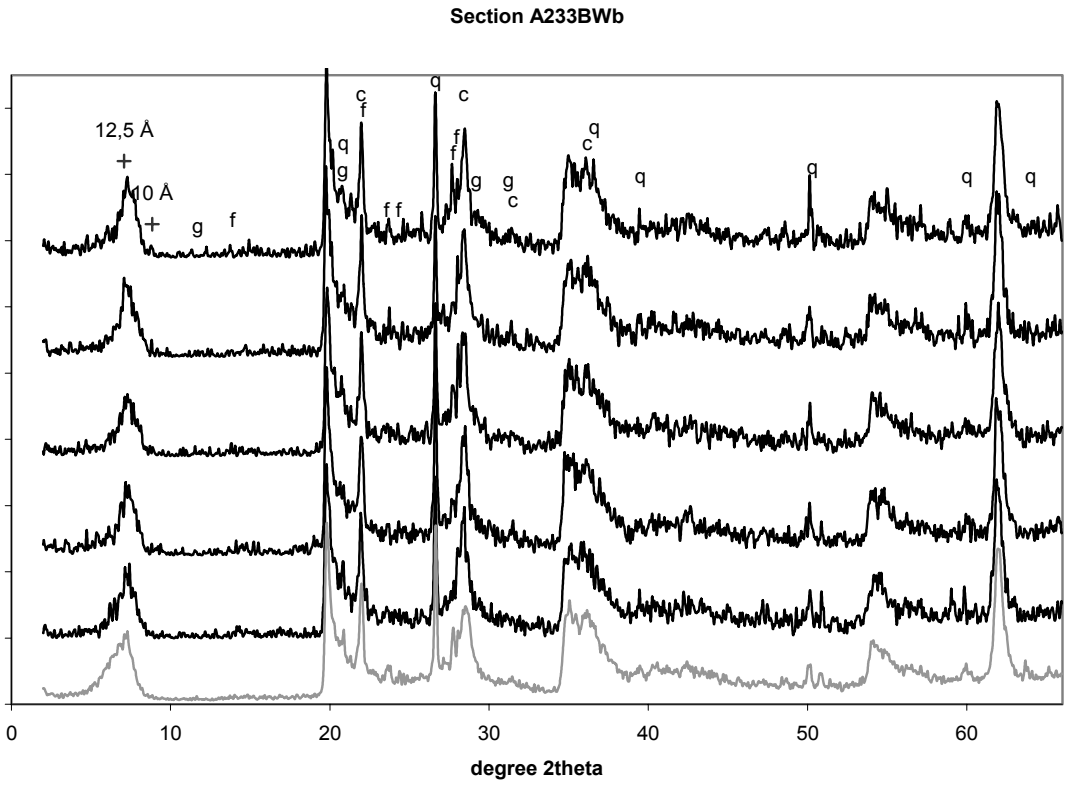

Figure 9-16 Black curves: XRD-profiles of sample 1 (bottom) to 9 (top) from block 33 of the LOT A2 parcel. Grey curve: mean XRD-profile of five reference samples. The position of the strongest peaks of the major non-clay minerals is indicated; q=quartz, c=cristobalite, f=feldspars, g=gypsum. The (001) peaks of mica/illite at 10Å and of Na-smectite at 12.5Å are also indicated. Random powder of bulk samples; CuKα radiation.

9.2.2.6.2. Bentonite of the LOT A2 parcel

The XRD-profiles of the bulk samples from block 33, 09, 11 and from the contact bentonite/Cu-tube are presented in Figure 9-16 to Figure 9-163. The cool block 33 (Figure 9-16) displays no significant changes compared with the reference samples, neither with respect to the type nor to the peak intensities of accessory minerals. A variation of the intensity of the feldspar peaks can be seen among the samples, but both the excellent {010} and {001} cleavage of feldspars, which promotes preferred orientation, and the coarse grain size of feldspars, may give a random variation in the peak intensities. Similarly, depending on the degree of random orientation of the preparation, some but not all samples display a 10Å peak of low intensity produced by mica.

The shape and width of the (001) basal reflection of montmorillonite varies somewhat among the samples, most likely due to the lack of humidity control during the X-ray scanning. However, like the references, all samples have the peak centred around 12.5 Å, which is typical of the monolayer hydrate of a Na-montmorillonite and consistent with the data on the composition of the exchangeable cation pool, showing that the proportion between divalent and monovalent cations in block 33 has changed very little compared with the reference bentonite (cf. Table 9-3).

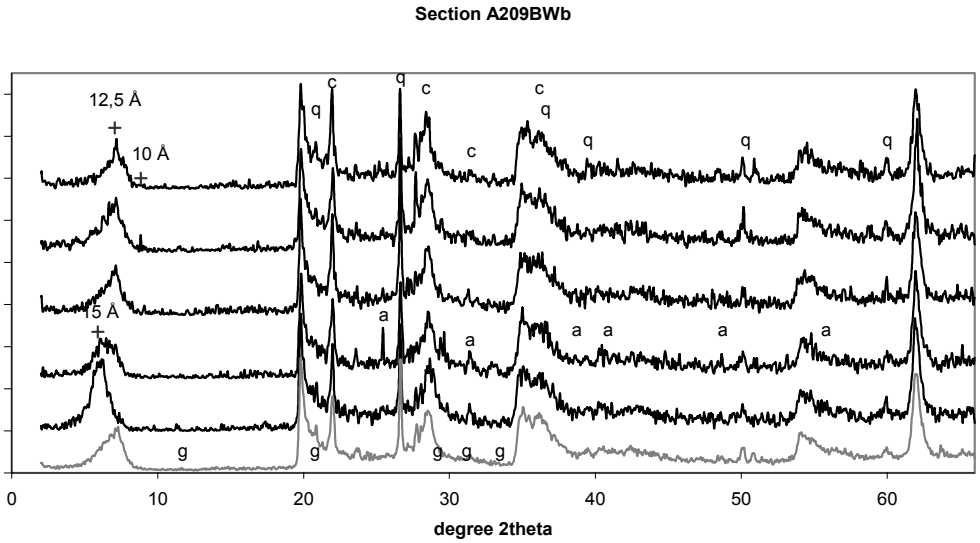

Figure 9-17 Black curves: XRD-profiles of sample 1 (bottom) to 9 (top) from block 9 of the LOT A2 parcel. Grey curve: mean XRD-profile of five reference samples. The position of the strongest peaks of the major non-clay minerals are indicated; q=quartz, c=cristobalite, g=gypsum, a=anhydrite ($CaSO_4$). The (001) peaks of mica/illite at 10Å and of Na-smectite at 12.5Å are also indicated (cf. text). Random powder of bulk material;CuKα.radiation

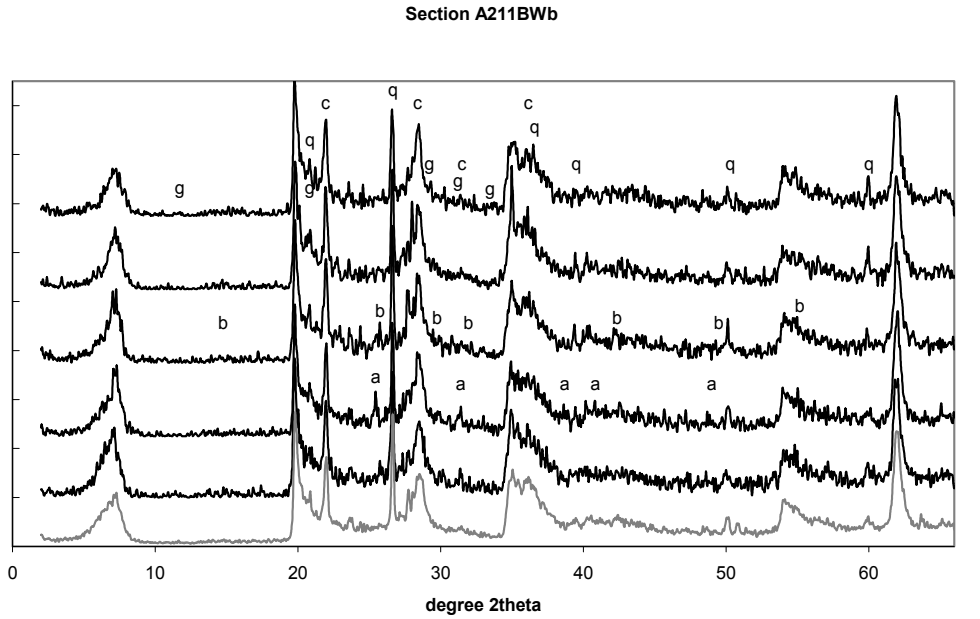

Figure 9-18 Black curves: XRD-profiles of sample 1 (bottom) to 9 (top) from block 11 of the LOT A2 parcel. Grey curve: mean XRD-profile of five reference samples. The position of the strongest peaks of the major non-clay minerals are indicated; q=quartz, c=cristobalite, f=feldspars, g=gypsum, b=bassanite ($CaSO_4*½H_2O$), a=anhydrite ($CaSO_4$). Random powder of bulk material; CuKα radiation.

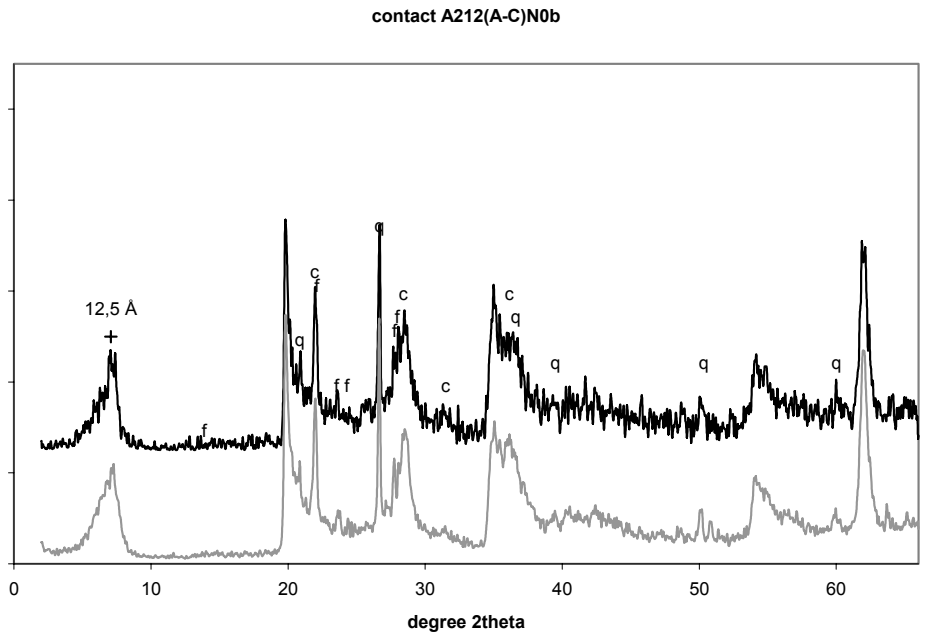

Figure 9-19 Black curve: XRD-profile of the contact sample Cu-tube/bentonite from block 12 of the LOT A2 parcel. Grey curve: mean XRD-profile of five reference samples. The position of the strongest peaks of the major non-clay minerals are indicated; q=quartz, c=cristobalite, f=feldspars. Random powder of bulk material; CuKα radiation

The most conspicuous mineralogical change in the hot blocks is the appearance of moderately intense peaks of anhydrite in the interval 2-6 cm from the central heater (Figure 9-17 and Figure 9-17). Accordingly, the mineralogical data match the chemical data, which clearly show that Ca-sulfate has been redistributed along the thermal gradient in the hot blocks. In some of the samples from the "anhydrite interval" the re-precipitated sulfate phase may include the hemi-hydrate bassanite ($CaSO_4*½H_2O$).

It is also evident, in particular for block 9, that the basal spacing of montmorillonite has shifted from 12.5 to 15 Å in the innermost samples. This increase in the basal distance is consistent with a replacement of interlayer Na by divalent cations, as indicated in the data on the composition of the interlayer cation pool (Figure 9-4) but the XRD-results are inconclusive due to the lack of humidity control during the X-ray scanning.

A close-up of the region 60-64º 2θ (i.e. scan resolution is not changed) of the XRD-profiles of the parcel and reference samples (Figure 9-20) shows that the d-value of the (060) peak is more or less identical in all samples (ca. 1.50 Å). Those variations that may exist appear to be random and independent of the position of the sample in the parcel. Thus, the available XRD-data provide no evidence of any significant change of the *b* cell dimension of the clay mineral, which would be an expected effect of, for instance, a change of the cations or the site occupancy in the octahedral sheet, or of a change of the amount of Al in tetrahedral coordination.

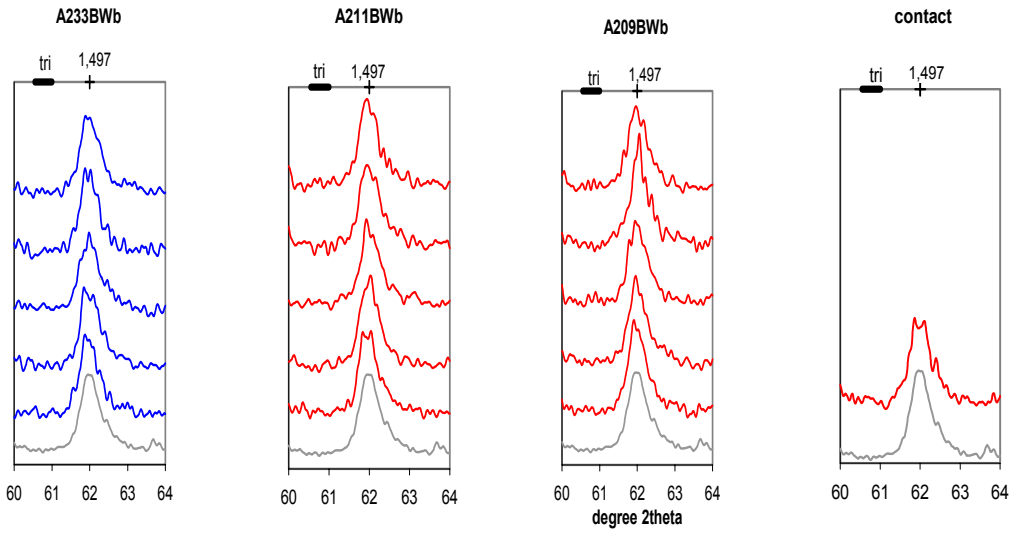

Figure 9-20 Close-up of the (060)-peak position. Blue curves: XRD-profiles of sample 1 (bottom) to 9 (top) from block 33; red curves: XRD-profiles of sample 1 (bottom) to 9 (top) from block 11 and 09 and from the contact bentonite/Cu-tube of the LOT A2 parcel. Grey curve: Mean XRD-profile of five reference samples. The indicated d-value (1.497 Å) of the (060)-peak is typical of dioctahedral smectites. The position of the (060)-peak of trioctahedral smectites is also indicated. Cu Kα radiation.

XRD-profiles of oriented mounts of the Mg-exchanged clay fraction of the individual samples from the A2 parcel are shown in Figure 9-22 to Figure 9-229 (air-dried clay) and Figure 9-22 to Figure 9-22 (EG-solvated clay) together with the corresponding average XRD profiles of the reference samples.

Traces of quartz and cristobalite occur in all clay fractions, but apart from these minerals, the clay fraction appears to be pure montmorillonite. With no exception the basal spacing of the air-dried, homo-ionic Mg-clay is 15 Å (relative humidity 50±10%). The clay expands to 16.9 Å upon EG-solvation. A close-up of the 17 Å region of the XRD-profiles of the parcel and reference samples (Figure 9-21) shows that the d-value of the (001) peak of the expanded clay is more or less identical in all samples. Those variations that may exist appear to be random and independent of the position of the sample in the parcel. The expansion behavior is typical of Mg-saturated montmorillonite and identical to that of the reference clay. As can also be seen in the diffractograms of the EG-solvated clays (Figure 9-22 to Figure 9-22), the series of basal reflections forms a complete, periodic diffraction pattern, which is indicative of well-ordered stacking sequences with virtually no interstratification. Similarly, the value of $\Delta 2\theta_{002/003}$ is the same (5.25-5.3) as that of the references and typical of a well-defined montmorillonite phase /Moore & Reynolds 1989/.

In summary, the available XRD-data provide no evidence of any structural change in the montmorillonite of the LOT A2 parcel. Changes that may exist in chemical composition and in the cation exchange properties of the clay mineral do not manifest themselves in the X-ray characteristics of the clay mineral. The question is, on the other hand, whether the resolution of XRD-technique is adequate for detecting small-scaled structural changes.

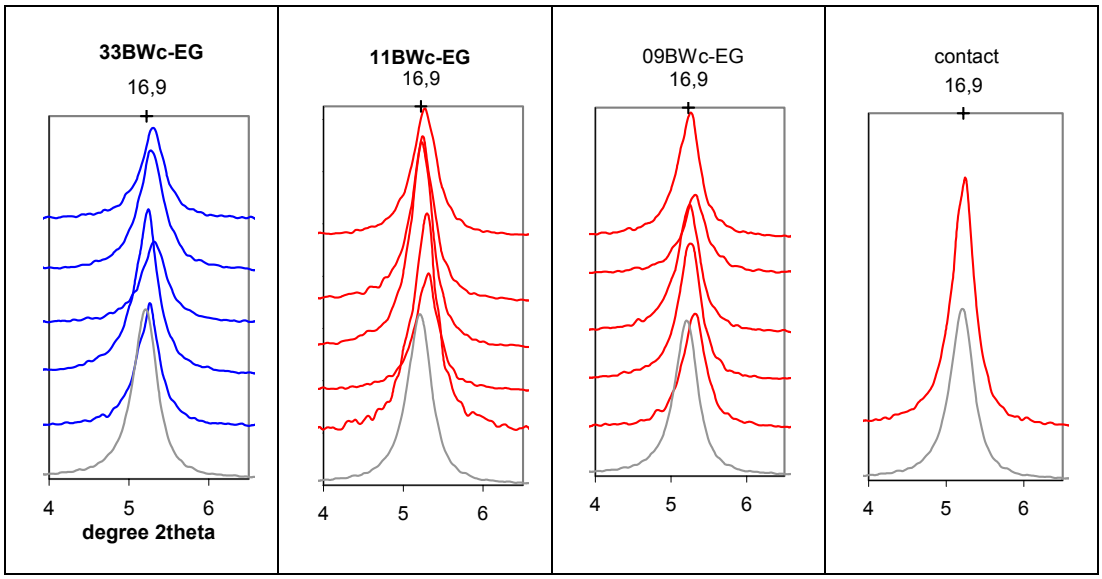

Figure 9-21 Close-up of the 17 Å region of EG-solvated, Mg-saturated clay fractions from the LOT A2 parcel. Blue curves: XRD-profiles of sample 1 (bottom) to 9 (top) from block 33; red curves: XRD-profiles of sample 1 (bottom) to 9 (top) from block 11 and 09 and from the contact bentonite/Cu-tube. Grey curve: Mean XRD-profile of five reference samples. The indicated d-value (16.9 Å) of the (001)-peak is typical of Mg-saturated, EG-solvated smectites. Cu Kα radiation.

9.2.3. Summary and conclusions

The chemical and mineralogical investigation of the bentonite of the standard blocks 09, 11 and 33 from the LOT A2 parcel indicates that

Cu has been incorporated in the bentonite matrix proximal (0-2 cm) to the Cu-tube in *all* blocks. The hot blocks have higher concentrations with a maximum of ~0,5% Cu in the mm-thick contact zone. However, the Cu concentrations of the A2 blocks are not significantly higher than those of equivalent blocks of the 1-year LOT test, cf. /Karnland et al. 2000/.

The Cu concentration of the clay fractions is 20-30 % of that of the corresponding bulk samples, which suggests that the major fraction of Cu is *not* incorporated in the structure of the montmorillonite. The form in which copper has been incorporated has not been identified, but the major fraction is not readily soluble or accessible for cation exchange.

Sulfates have been redistributed along the thermal gradient in hot blocks. Anhydrite has accumulated ~3-5 cm from the heater, whereas the peripheral parts of the blocks are depleted in sulfates.

The carbonate content decreases with increasing temperature in hot blocks.

Dissolution/precipitation reactions involving sulfates and carbonates of calcium have influenced the pore water composition and, consequently, the pool of exchangeable cations. Accordingly, *some exchangeable sodium has been replaced by calcium* in the inner parts of the hot blocks.

Exchangeable Mg increases with increasing temperature in hot blocks. The trend is paralleled by an *increase in the content of non-exchangeable Mg of the clay* (Na-

saturated fraction <2µm;) towards the heater whereas the peripheral parts of the blocks appear to be depleted in Mg. The source of Mg has not been identified and remains to be established but the most significant source of Mg available is the octahedral sheet of the montmorillonite.

The proportion between exchangeable and non-exchangeable interlayer cations (the equivalent ratio (Ca+Na)/K) has increased in samples adjacent to the Cu-tube in hot blocks.

CEC of the bulk samples and of the clay fractions tends to increase towards the Cu-tube in the hot blocks. However, it remains to establish whether the increase in CEC is interconnected to redistribution of Mg and/or losses in fixed interlayer K - or simply, an experimental artifact, since the differences in CEC are close to the analytical resolution.

The available XRD-data provide *no evidence of a structural change of the montmorillonite*. Both the expansion behavior, a complete, periodic diffraction pattern of the basal reflections and the *b* cell dimension of the clay mineral are typical of montmorillonite and identical to that of the reference material. Thus, those changes that exist in the chemical composition and/or in the cation exchange properties of the clay mineral do not manifest themselves in the X-ray diffraction characteristics of the clay mineral. However, the resolution of the XRD-technique may be inadequate for detecting very small-scaled structural changes.

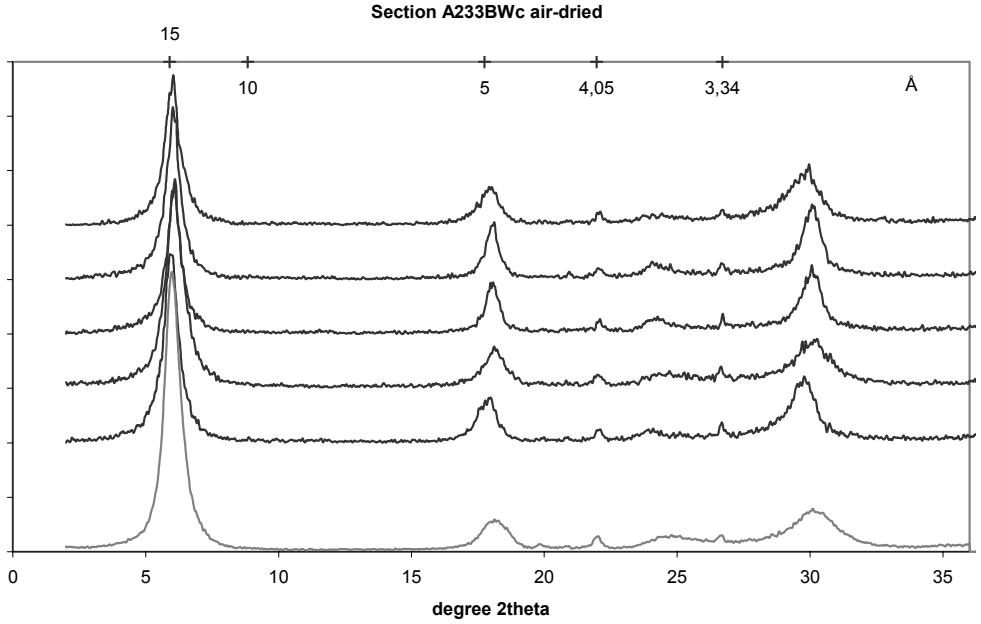

Figure 9-22 Black curves: XRD-profiles of oriented aggregates of the clay fraction of sample 1 (bottom) to 9 (top) of block 33 from the LOT A2 parcel. Grey curve: mean XRD-profile of the clay fraction of five reference samples. The strongest peaks of cristobalite (4.05Å), quartz (3.34Å) and mica/illlite (10Å) are indicated in the upper scale. Mg-saturated air-dried samples; CuKα radiation.

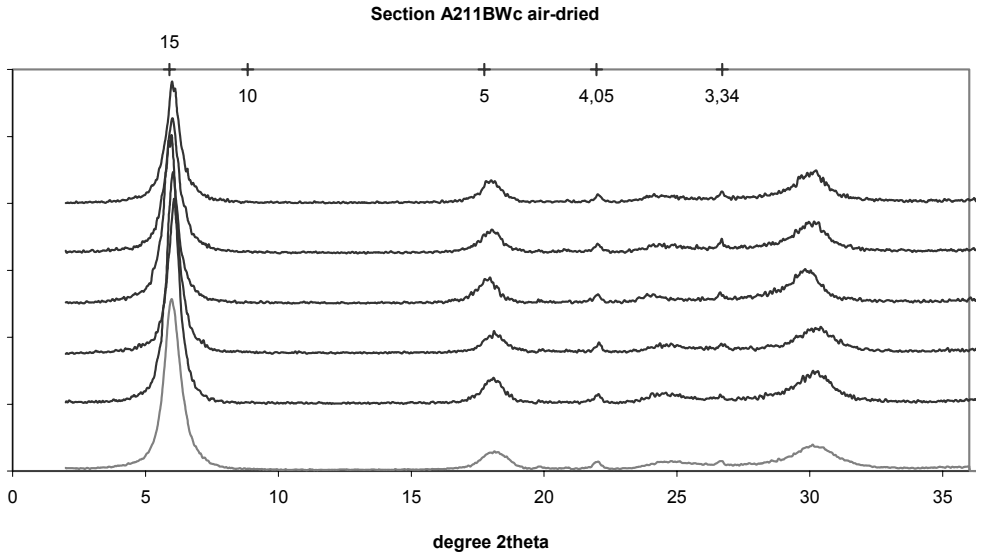

Figure 9-23 Black curves: XRD-profiles of oriented aggregates of the clay fraction of sample 1 (bottom) to 9 (top) of block 11 from the LOT A2 parcel. Grey curve: mean XRD-profile of the clay fraction of five reference samples. The strongest peaks of cristobalite (4.05Å), quartz (3.34Å) and mica/illlite (10Å) are indicated in the upper scale. Mg-saturated, air-dried samples; CuKα radiation.

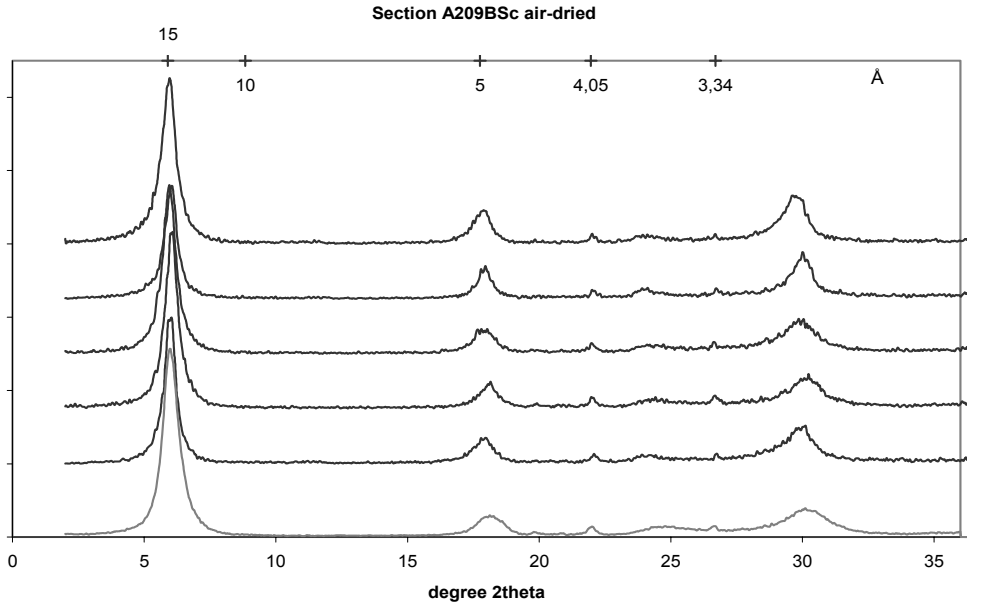

Figure 9-24 Black curves: XRD-profiles of oriented aggregates of the clay fraction of sample 1 (bottom) to 9 (top) of block 09 from the LOT A2 parcel. Grey curve: mean XRD-profile of the clay fraction of five reference samples. The strongest peaks of cristobalite (4.05Å), quartz (3.34Å) and mica/illlite (10Å) are indicated in the upper scale. Mg-saturated, air-dried samples; CuKα radiation.

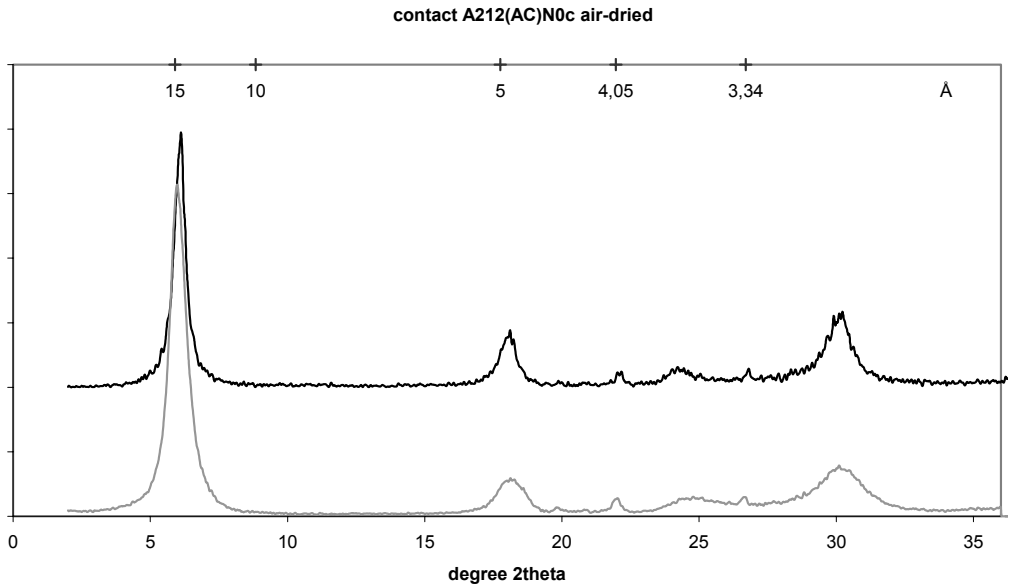

Figure 9-25 Black curve: XRD-profile of oriented aggregates of the clay fraction of the contact sample of block 12 from the LOT A2 parcel. Grey curve: mean XRD-profile of the clay fraction of five reference samples. The strongest peaks of cristobalite (4.05Å), quartz (3.34Å) and mica/illlite (10Å) are indicated in the upper scale. Mg-saturated, air-dried samples; CuKα radiation.

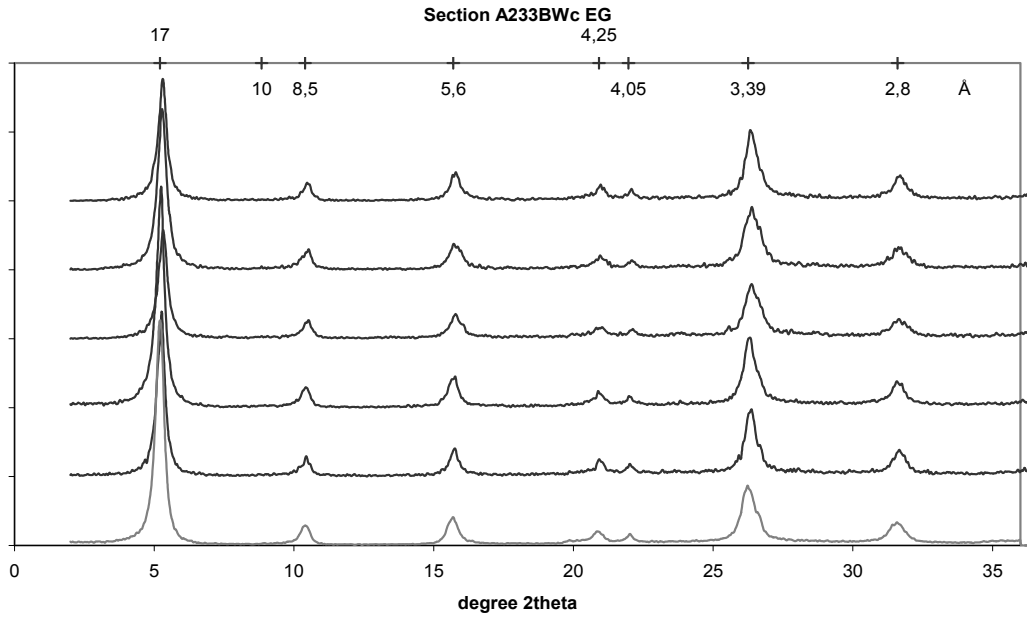

Figure 9-26 Black curves: XRD-profiles of oriented aggregates of the clay fraction of sample 1 (bottom) to 9 (top) of block 33 from the LOT A2 parcel. Grey curve: mean XRD-profile of the clay fraction of five reference samples. The positions of the basal reflections of montmorillonite are indicated in the upper scale together with the strongest peaks of cristobalite (4.05Å) and mica/illlite (10Å). Mg-saturated, ethylene glycol solvated samples; CuKα radiation.

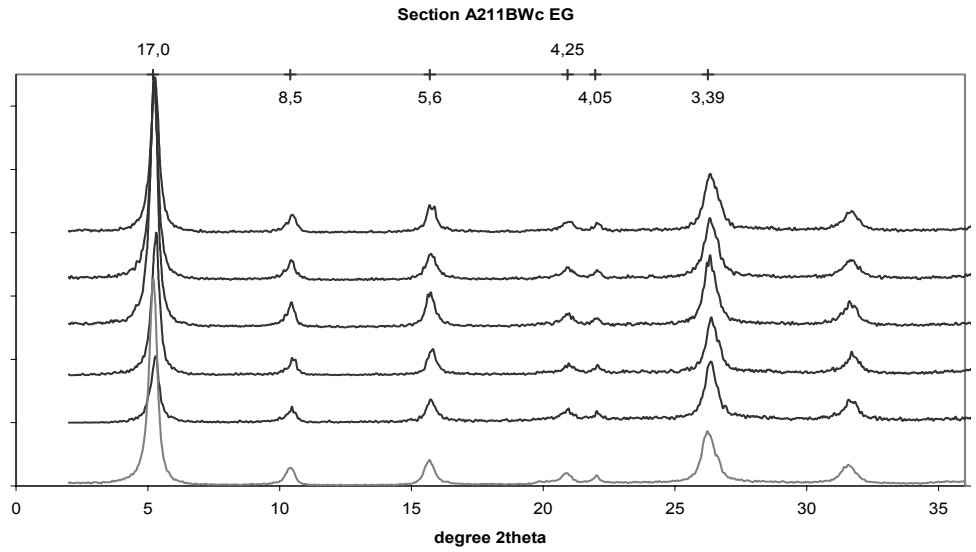

Figure 9-27 Black curves: XRD-profiles of oriented aggregates of the clay fraction of sample 1 (bottom) to 9 (top) of block 11 from the LOT A2 parcel. Grey curve: mean XRD-profile of the clay fraction of five reference samples. The positions of the basal reflections of montmorillonite are indicated in the upper scale together with the strongest peaks of cristobalite (4.05Å). Mg-saturated, ethylene glycol solvated samples; CuKα radiation.

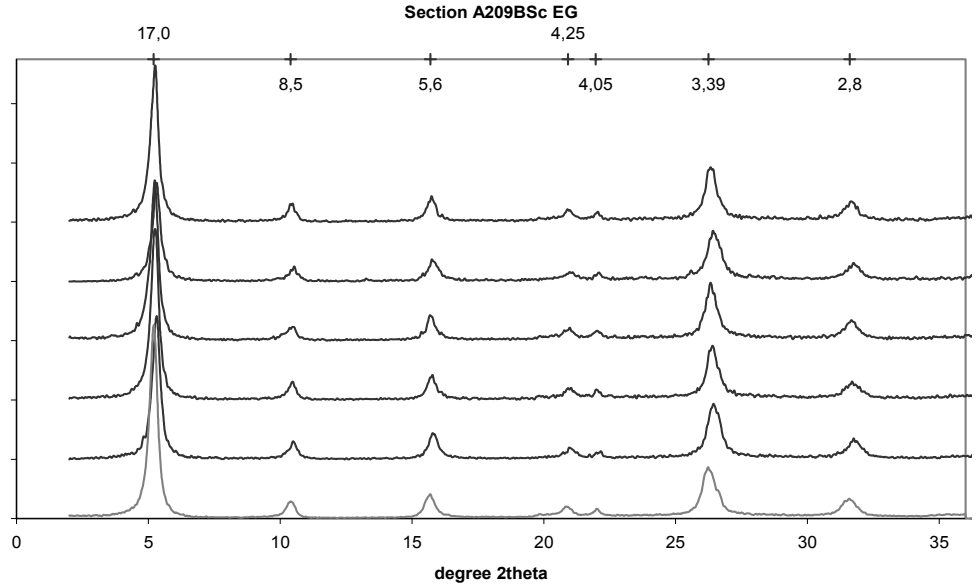

Figure 9-28 Black curves: XRD-profiles of oriented aggregates of the clay fraction of sample 1 (bottom) to 9 (top) of block 09 from the LOT A2 parcel. Grey curve: mean XRD-profile of the clay fraction of five reference samples. The positions of the basal reflections of montmorillonite are indicated in the upper scale together with the strongest peaks of cristobalite (4.05Å). Mg-saturated, ethylene glycol solvated samples; CuKα radiation.

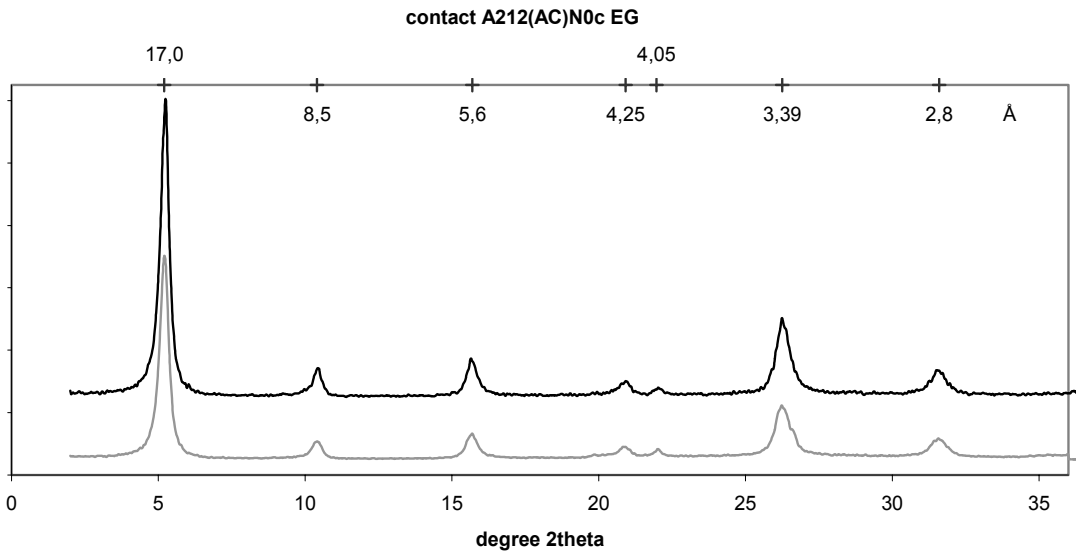

Figure 9-29 Black curve: XRD-profile of oriented aggregates of the clay fraction of the contact sample of block 12 from the LOT A2 parcel. Grey curve: mean XRD-profile of the clay fraction of five reference samples. The positions of the basal reflections of montmorillonite are indicated in the upper scale together with the strongest peaks of cristobalite (4.05Å). Mg-saturated, ethylene glycol solvated samples; CuKα radiation.

9.3. Blocks with additives

9.3.1. Materials and methods

9.3.1.1. Sampling and sample nomenclature

The special block series comprises five blocks (10, 12, 16, 24 and 34) in which cylindrical bentonite plugs with an admixture of calcite, gypsum, K-feldspar or cement, respectively, were embedded in order to simulate various adverse chemical conditions that may accelerate alteration processes in the bentonite. The plugs had been placed in cylindrical holes, drilled in the B-level from the mantle surface of the blocks in connection with the block fabrication.

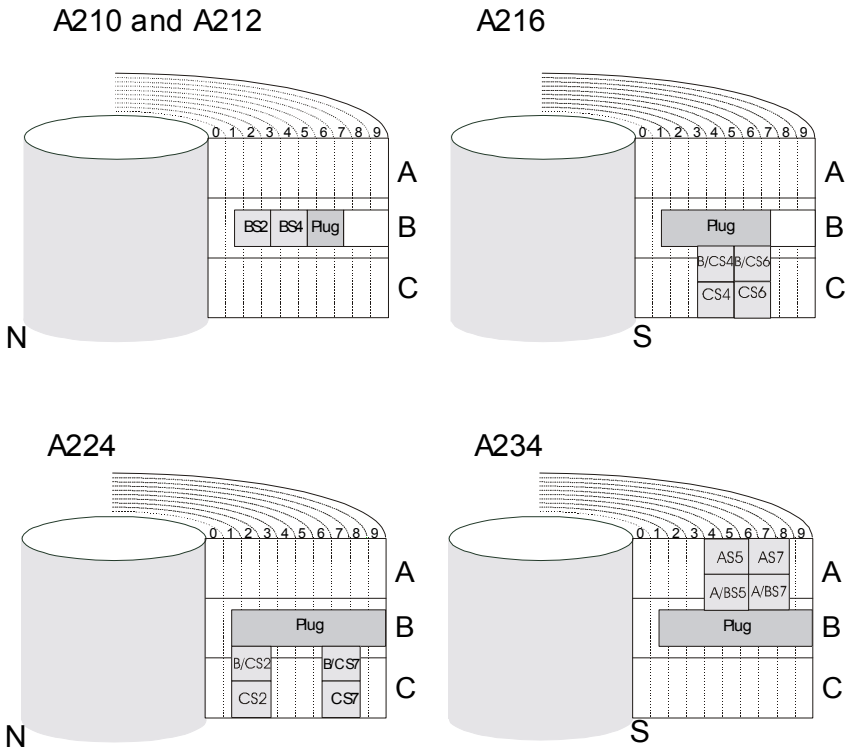

Figure 9-30 Sampled positions and sample nomenclature for the LOT A2 blocks 10, 12, 16, 24 and 34. Cylindrical bentonite plugs (Ø20 mm) with additives (10% calcite in 10, 10% gypsum in 12, 50% K-feldspar in 16 and cement in 24 and 34) were embedded in the B-level of the blocks.

Table 9-7 Chemical composition of potassium feldspar used as additive in block 16, LOT A2.

SiO_2	Al_2O_3	Fe_2O_3	MgO	CaO	Na_2O	K_2O	TiO_2	P_2O_5	MnO	Ba	Sr	Zr	LOI	Sum
%	%	%	%	%	%	%	%	%	%	ppm	ppm	ppm	%	%
64.23	18.72	0.42	0.01	0.37	2.74	12.65	<0.01	0.01	<0.01	124	39	7	0.9	100.1

Blocks 10 and 12 have 2-cm long plugs (Ø 20 mm) with an addition of 10% finely ground calcium carbonate and calcium sulfate, respectively, embedded in the B-level in each cardinal compass point. These blocks were sampled in the B-level between the

southern plug and the inner mantel surface of the block, at two distances (0-2 cm and 2-4 cm) from the plug (Figure 9-30). The sample size was 2x2x2 cm.

Block 16 has 6-cm long bentonite plugs (Ø 20 mm) containing 50% potassium feldspar in the B-level in each cardinal compass point. The chemical composition of the potassium feldspar used as additive is given in Table 9-7.

Blocks 24 and 34 have 8-cm long plugs (Ø 20 mm) of cement (Aalborg white Portland cement) in the B-level to the north and south. The blocks 16, 24 and 34 were sampled at two radial positions along the southern plug and at two distances (0-2 cm and 2-4 cm) from the plug, above or below the plug (i.e. in the A/B and A- alternatively in the B/C and C-level; cf. Figure 9-30). The sample size varies from 2x2x2 to 2x2x2,5 cm.

All sampling was made by use of a band saw. A 2 mm-thick layer of the contact surface was removed from the samples that were in direct contact with plugs.

Individual samples have been given an identity code according to the general nomenclature. The code for the horizontal position of samples taken across the boundary between the A and B level (or B and C) is A/B (B/C) (Figure 9-30).

When available, bentonite used for the fabrication of the blocks has been used as reference material, supplemented with the reference material used for the standard blocks.

9.3.1.2. Methods

The analytical test protocol for the special blocks is summarized in Table 8. The samples have been analyzed for the same parameters as the standard blocks, i.e.

- cation exchange capacity by exchange with Cu-triethylene tetramine
- exchangeable cations by exchange with NH_4^+ in alcoholic solution
- non-reactive solutes and soluble/sparingly soluble salts by aqueous leaching (s:l 1:100) followed by analysis with ICP-AES and IC. These analyses were applied for blocks 24 and 34 only
- chemical composition of the bentonite using standard digestion techniques for silicates and analysis by ICP-AES (MS)
- carbon and sulphur by evolved-gas analysis using a Leco-furnace
- mineralogy of the bentonite by X-ray diffraction analysis

The methods applied are described in paragraph 2.1. Apart from block 10 and 12, both the bulk material and the clay fraction of the bentonite samples have been analyzed when relevant (cf.

Table 9-8).

Table 9-8 Sample nomenclature and analytical test protocol for the special blocks with additives (10, 12, 16, 24 and 34) from the LOT A2 parcel

	Chemical analysis	Cation exchange capacity	Exchangeable cations	X-ray diffraction analysis		Aqueous leachates
SICADA test code	**LA2EA**	**LA2CEC**	**LA2EC**	**LA2XRD**		**LA2WA**
b=bulk;c=clay fraction	**b/c**	**b/c**	**b**	**b/c**		**b**
				random	oriented	
Sample identity						
Reference bentonite samples						
A2(1-5)Rb	X	X	X	X		X
A2(1-5)Rc	X	X			X	
A211Rb	X	X	X	X		X
A211Rc	X	X			X	
A233Rb	X	X	X	X		X
A233Rc	X	X			X	
A224Rb	X	X	X	X		X
A224Rc		X			X	
A234Rb	X	X	X	X		X
A234Rc		X			X	
Special block series						
A210BS2b	X	X	X	X		
A210BS4b	X	X	X	X		
A212BS2b	X	X	X	X		
A212BS4b	X	X	X	X		
A216B/CS4b	X	X	X	X		
A216B/CS4c	X	X			X	
A216B/CS6b	X	X	X	X		
A216B/CS6c	X	X			X	
A216CS4b	X	X	X	X		
A216CS4c	X	X			X	
A216CS6b	X	X	X	X		
A216CS6c	X	X			X	
A224B/CS2b	X	X	X	X		X
A224B/CS2c	X	X			X	
A224CS2b	X	X	X	X		X
A224CS2c	X	X			X	

	Chemical analysis	Cation exchange capacity	Exchangeable cations	X-ray diffraction analysis		Aqueous leachates
SICADA test code	**LA2EA**	**LA2CEC**	**LA2EC**	**LA2XRD**		**LA2WA**
b=bulk;c=clay fraction	**b/c**	**b/c**	**b**	**b/c**		**b**
				random	oriented	
Sample identity						
A224B/CS7b	X	X	X	X		X
A224B/CS7c	X	X			X	
A224CS7b	X	X	X	X		X
A224CS7c	X	X			X	
A234A/BS5b	X	X	X	X		X
A234A/BS5c	X	X			X	
A234AS5b	X	X	X	X		X
A234AS5c	X	X			X	
A234A/BS7b	X	X	X	X		X
A234A/BS7c	X	X			X	
A234AS7b	X	X	X	X		X
A234AS7c	X	X			X	

9.3.2. Results

9.3.2.1. Block 10 with additive of $CaCO_3$ and block 12 with additive of $CaSO_4$

The inventory of calcite and gypsum is small (<1.5%) in the parent bentonite MX80, but special attention is paid to these minerals because their solubility is temperature dependant. Under non-isothermal conditions with steep temperature gradient, dissolution and re-precipitation of these minerals can be expected to result in salt accumulations in the warmer parts of the buffer, which will affect the porosity and rheology of the bentonite. In the adverse-condition tests, the inventory of calcium carbonate and calcium sulfate had been increased by the addition of bentonite plugs containing 10% finely ground calcite and gypsum, respectively. The entire volume of block 10 and 12 has been exposed to temperatures exceeding 80º C and the sampled interval 1.5-5.5 cm from the heater to temperatures exceeding 100º C.

The chemical data on the bulk bentonite are listed in Table 10 (the samples have been analyzed in bulk only). Some selected parameters have been re-calculated on a molar, water-free basis (i.e. correction was made for LOI-(SO_2+CO_2)) to avoid artifacts that may arise due to variable water content among the samples. The bar graph presented in Fig. 32 shows the loss or gain in Ca, S and C relative to the average reference sample. Consistent with the trends displayed in the hot standard blocks, blocks 10 and 12 have gained sulfur at the two sampled positions. The increase in sulfur is paralleled by a more or less equivalent increase in calcium, whereas the carbon content is lower than the mean of the references. The maximum increase in S and Ca is found in sample 4

proximal to the gypsum plug in block 12. The S content of this sample is equivalent to 4 % anhydrite, if all S is allocated to $CaSO_4$

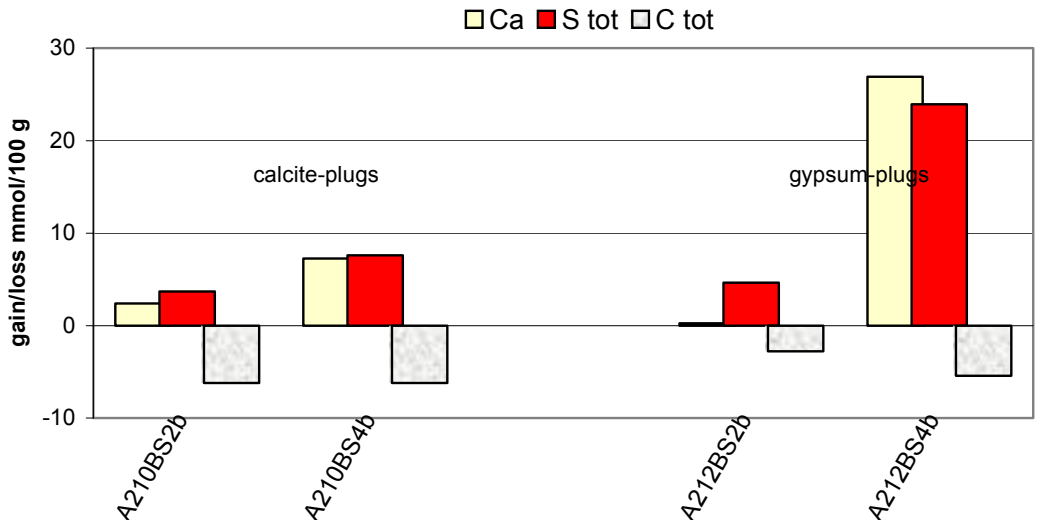

Figure 9-31 Bar graph showing the loss/gain (relative to the mean of the references) in total Ca, S and C in samples of blocks 10 and 12 from the LOT A2 parcel. Data are from Table 10 but have been re-calculated on a molar basis.

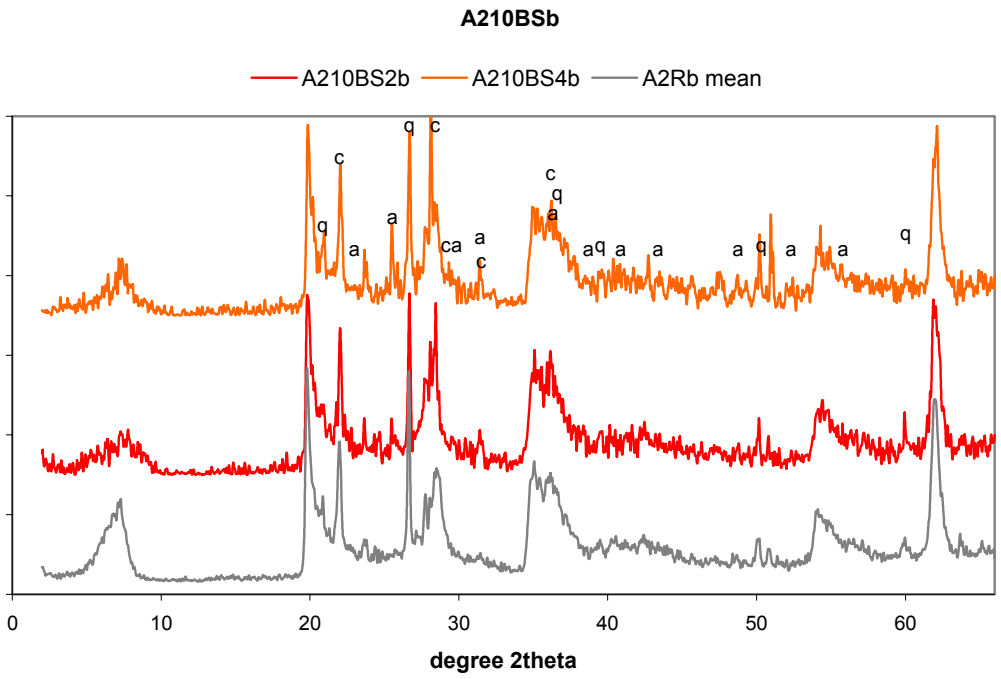

Figure 9-32 XRD-profiles of sample 2 and 4 (orange) from block 10, with additive of calcite, of the LOT A2 parcel. Grey curve: mean XRD-profile of five reference samples. The position of the strongest peaks of the major non-clay minerals is indicated; q=quartz, c=cristobalite, a=anhydrite ($CaSO_4$). The position of the strongest peak of calcite (ca) is also indicated. Random powder of bulk samples; CuKα radiation

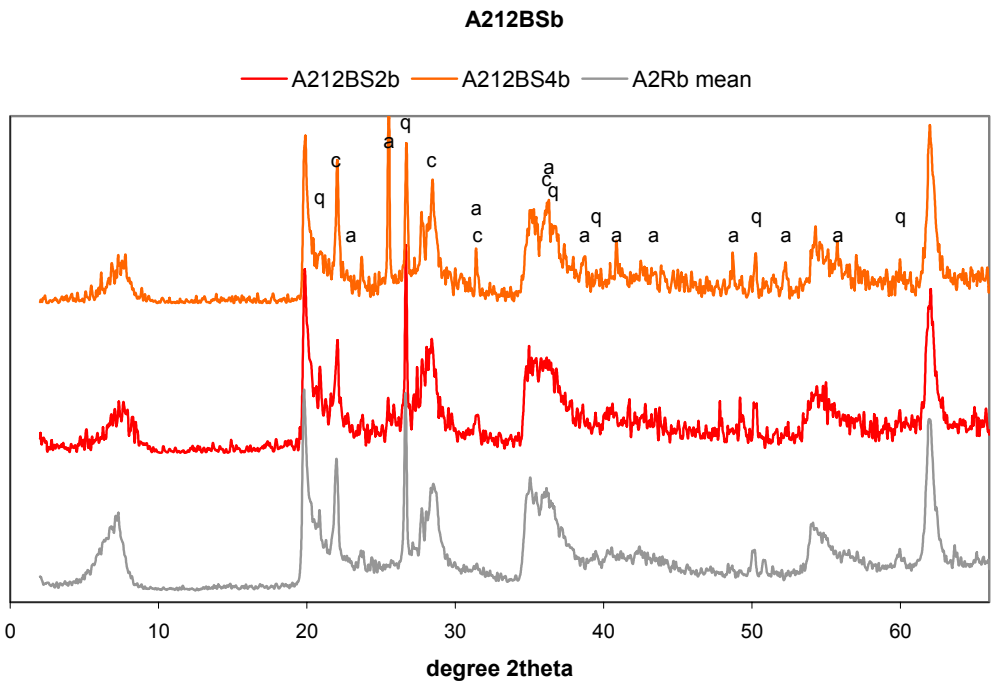

Figure 9-33 XRD-profiles of sample 2 (red) and 4 (orange) from block 12, with additive of gypsum, of the LOT A2 parcel. Grey curve: mean XRD-profile of five reference samples. The position of the strongest peaks of the major non-clay minerals is indicated; q=quartz, c=cristobalite, a=anhydrite ($CaSO_4$). Random powder of bulk samples; CuKα radiation

Table 9-9 Exchangeable cations and mean Cu-CEC (cmole of charge/kg dry matter) of blocks 10 and 12 of the LOT A2 parcel. Data for the mean of five reference samples are also included. Cations extracted by exchange with NH_4^+ in alcoholic solution.

Sample id	Additive	Ca		K		Mg		Na		Sum	mean Cu-CEC
		$cmol^+/kg$	%	$cmol^+/kg$	%	$cmol^+/kg$	%	$cmol^+/kg$	%	$cmol^+/kg$	$cmol^+/kg$
LA210BS2b	calcite	17	21	1.5	1.8	7.1	9	56	69	82	80
LA210BS4b	calcite	17	21	1.5	1.8	6.8	8	56	69	81	80
LA212BS2b	gypsum	15	20	1.4	1.9	6.0	8	54	71	76	83
LA212BS4b	gypsum	17	22	1.4	1.7	7.0	9	54	68	80	76
LA2Rb-mean	ref	16	22	1.3	1.7	5.30	7	53	69	76	81

The chemical data are supported by the XRD data which show that anhydrite has formed at all the sampled positions in block 10 and 12 (Figure 9-32 and Figure 9-32) but sample 4 proximal to the gypsum plug in block 12 is distinguished by very intense anhydrite peaks.

Calcite cannot be detected with certainty in any of the samples. In the XRD-profile of sample 4 proximal to the calcite plug in block 10, a peak of low intensity appears at the

position where calcite has its most intense peak but cannot unambiguously be attributed to calcite.

Data on the cation exchange capacity and the exchangeable cations are listed in Table 9 and have also been compiled in Figure 9-34. Sample 4, block 12 has the lowest CEC values, 76 meq/100 g, which can be explained by the "dilution" of the bentonite with ca. 4% anhydrite. The CEC values of the rest of the samples range from 80 to 83 meq/100 g, which is comparable to the mean CEC, 81 meq/100g, of the references.

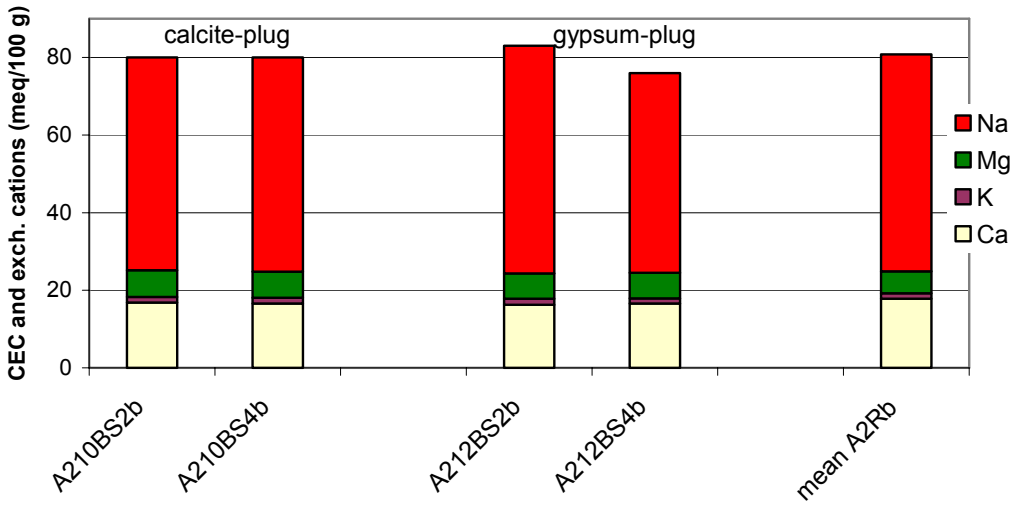

Figure 9-34 Bar graph showing the CEC and the relative distribution of exchangeable Na, K, Ca and Mg in samples from block 10 (additive of calcite) and 12 (additive of gypsum) of the LOT A2 parcel. The mean values of five reference samples shown to the right.

All samples have essentially the same pool of exchangeable cations as the references, i.e. approximately 70 % of the exchange sites are saturated with sodium and 20 % with calcium. Exchangeable Mg is somewhat higher in the samples from block 10 and 12 (i.e. ca. 1-5 cm from the heater) than in the references, which is in harmony with the trend displayed in the hot standard blocks, where exchangeable Mg increases with increasing temperature.

Although the available data for block 12 are for two samples only, it seems clear that calcium sulfate has been redistributed from the plug with gypsum towards the warmer, inner part of the block. Re-precipitation (as anhydrite) has increased the sulfur content of the bentonite volume (2x2x2 cm; contact surface removed) proximal to the plug by a factor 3-4 compared to the reference bentonite. A lowering of the CEC value at this position can be explained by the "dilution" of the bentonite with anhydrite.

Based on the data for the two samples from the block with calcite plugs, it cannot be proved that calcium carbonate has been redistributed in a similar way as calcium sulfate. However, a sampling strategy that allows higher resolution may be necessary to verify the results.

9.3.2.2. Block 16 with additive of K-feldspar

One of the buffer alteration processes that has been considered in the long term test program is the smectite-to-illite transformation, which is believed to be accelerated by factors such as high potassium activity and elevated temperature.

The entire volume of block 16 has been exposed to temperatures exceeding 80º C and the sampled interval to temperatures between 90 and 100º C.

The potassium content in the parent bentonite MX 80 is 0.53±0.02 % K_2O, the major sources being feldspars and mica/illite. In the adverse-condition test, the inventory of potassium was increased significantly by the addition of bentonite plugs containing 50% finely ground potassium feldspar with a K_2O content of 12.65 % (Table 9-7).

The chemical data on the bulk bentonite samples from block 16 (Table 9-10) indicate no significant change in the composition and the potassium content of the block samples is in the same range, 0,52 to 0,55 % K_2O, as that of the references. Those changes in the compositions that exist (in S and CaO) are consistent with the pattern of calcium sulfate redistribution observed in other hot blocks.

The chemical data are supported by the XRD profiles of the bulk samples (Figure 9-35). Thus, anhydrite peaks appear in the sample with maximum S and CaO contents. The two samples from the least hot position 6 have a weak peak at the position of the most intense reflection of calcite, but the identification is uncertain since no other calcite reflections are detectable.

The XRD-profiles display broad and indistinct first order basal reflections of the smectite (Figure 9-35). A probable explanation for this is that the re-hydration of the smectite was incomplete and variable due to the lack of strict control of humidity. As a consequence, smectite of mixed hydration states occur in the samples.

Both the cation exchange capacity of the bulk samples and the composition of the pool of exchangeable cations (Table 9-11 and Figure 9-35) suggest that the exchange properties of the bentonite from block 16 are essentially the same as those of the reference samples.

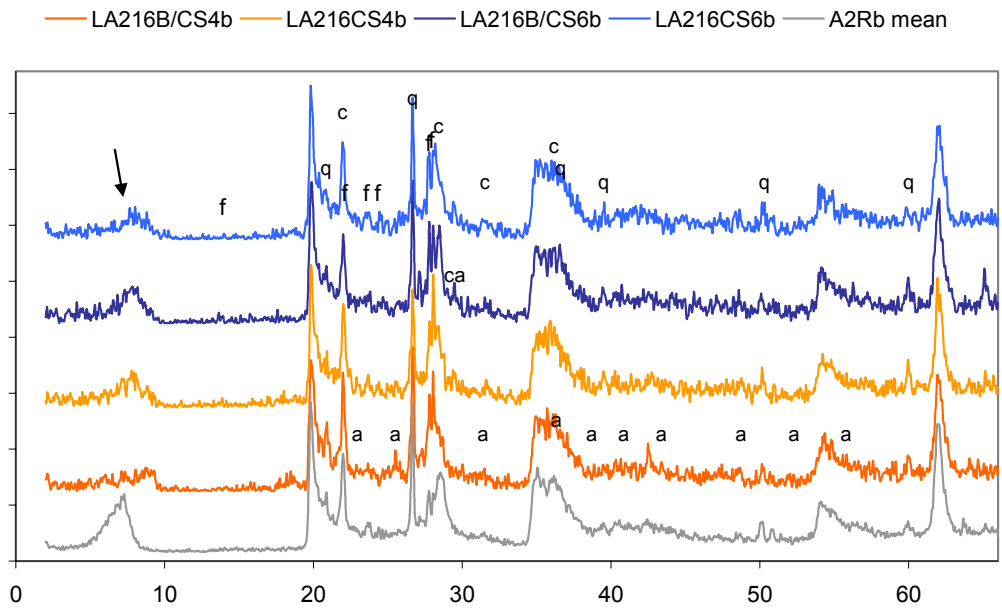

Figure 9-35 XRD-profiles of samples 4 and 6 from block 16 (with additive of K-feldspar) of the LOT A2 parcel. Grey curve: mean XRD-profile of five reference samples. The position of the strongest peaks of the major non-clay minerals is indicated; f=feldspar, q=quartz, c=cristobalite, a=anhydrite ($CaSO_4$). The position of the strongest peak of calcite (ca) is also indicated. Arrow indicates the normal position of the first order basal reflection of smectite (discussed in the text). Random powder of bulk samples; CuKα radiation.

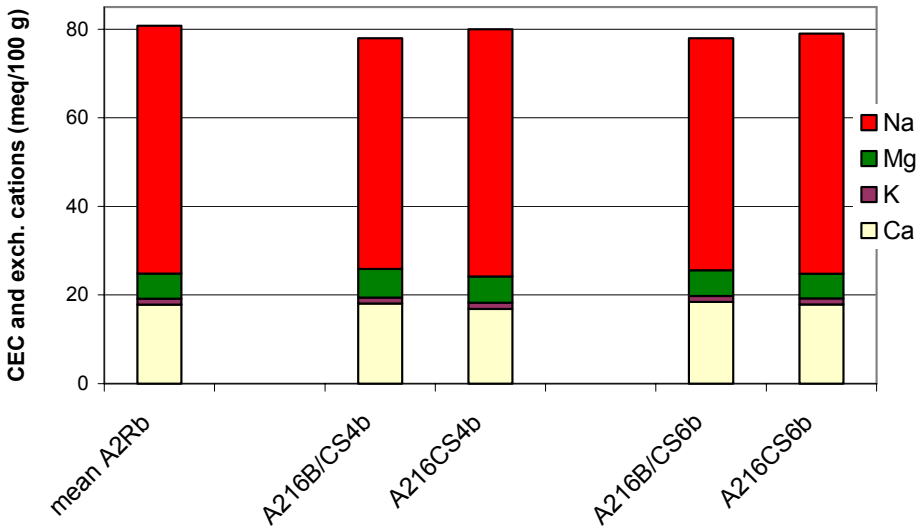

Figure 9-36 Bar graph showing the CEC (meq/100 g dry matter) and the relative distribution of exchangeable Na, K, Ca and Mg in samples from block 16 (additive of K-feldspar) of the LOT A2 parcel. The mean of five reference samples is shown to the left.

Table 9-10 Chemical composition of the bulk bentonite samples from blocks with additives (block 10, 12, 16, 24 and 34) together with five reference samples of the LOT A2 parcel. Major and minor elements by ICP-AES, S and C by evolved gas analysis. SICADA test code LA2EAb.

Sample id	Additive	SiO_2	Al_2O_3	Fe_2O_3	MgO	CaO	Na_2O	K_2O	TiO_2	P_2O_5	MnO	Cr_2O_3	LOI	TOT/C	TOT/S	SUM	Ni	Sc	Cu	Zn	Ba	Co	Nb	Sr	Ta	Zr	Y	Ce
		%	%	%	%	%	%	%	%	%	%	%	%	%	%	%	ppm	ppm	ppm	ppm	ppm	ppm	ppm	ppm	ppm	ppm	ppm	ppm
A210BS2b	$CaCO_3$	63.4	19.51	3.66	2.37	1.39	2.10	0.53	0.14	0.05	0.01	0.002	6.6	0.29	0.25	99.92	5	5	9	107	276	5	35	265	5	189	47	96
A210BS4b	$CaCO_3$	63.3	19.39	3.63	2.31	1.65	2.12	0.53	0.15	0.05	0.01	0.003	6.8	0.29	0.37	100.06	5	6	7	132	361	5	35	393	5	191	46	107
A212BS2b	$CaSO_4$	63.5	19.74	3.68	2.39	1.28	2.15	0.51	0.14	0.05	0.01	0.008	6.5	0.33	0.28	100.06	5	5	7	153	331	5	35	267	10	190	46	103
A212BS4b	$CaSO_4$	62.0	19.00	3.50	2.24	2.70	2.00	0.50	0.14	0.05	0.01	0.004	7.6	0.30	0.87	99.93	5	5	6	110	331	5	37	516	5	187	44	104
A216B/CS4b	K-feldspar	62.9	19.41	3.76	2.25	1.45	2.10	0.54	0.14	0.05	0.01	0.001	7.2	0.36	0.18	99.92	<5	5	<10	80	446	<5	30	318	<20	197	43	84
A216CS4b	K-feldspar	62.9	19.23	3.73	2.26	1.35	2.07	0.55	0.14	0.05	0.01	0.009	7.5	0.34	0.10	99.92	12	5	<10	102	339	<5	26	283	<20	195	44	98
A216B/CS6b	K-feldspar	62.4	18.90	3.70	2.21	1.25	2.06	0.55	0.14	0.05	0.01	0.005	8.5	0.37	0.08	99.93	<5	5	<10	108	315	<5	36	246	<20	183	44	105
A216CS6b	K-feldspar	63.2	19.18	3.77	2.25	1.31	2.07	0.52	0.14	0.04	0.01	<.001	7.4	0.36	0.09	100.06	6	5	12	88	339	<5	32	254	<20	192	43	80
A224B/CS2b	cement	63.6	19.45	3.57	2.34	1.28	2.08	0.5	0.14	0.04	0.01	0.003	6.9	0.38	0.26	100.06	5	5	72	134	282	5	32	304	6	194	46	104
A224CS2b	cement	63.6	19.71	3.64	2.31	1.32	2.12	0.52	0.14	0.05	0.01	0.001	6.5	0.38	0.21	100.07	5	5	63	86	295	5	36	309	5	194	46	105
A224B/CS7b	cement	63.4	19.78	3.71	2.34	1.26	2.19	0.52	0.14	0.04	0.01	0.001	6.5	0.39	0.17	100.06	5	5	6	106	312	5	35	263	5	191	47	109
A224CS7b	cement	63.8	19.70	3.63	2.26	1.26	2.12	0.53	0.14	0.04	0.01	0.001	6.4	0.41	0.18	100.07	5	5	8	91	311	5	36	298	6	186	45	98
A234A/BS5b	cement	61.8	19.27	3.63	3.48	1.57	2.20	0.54	0.14	0.05	0.01	0.006	7.3	0.42	0.16	100.07	5	5	5	118	290	5	32	265	5	189	45	94
A234AS5b	cement	63.8	19.58	3.64	2.16	1.42	2.13	0.51	0.14	0.04	0.01	0.002	6.5	0.39	0.19	100.07	5	5	12	76	296	5	39	293	5	194	45	98
A234A/BS7b	cement	61.9	19.12	3.51	3.58	1.87	2.18	0.55	0.14	0.05	0.01	0.001	7.0	0.42	0.15	100.05	5	5	10	115	309	5	35	258	5	190	45	103
A234AS7b	cement	63.0	19.55	3.64	2.20	1.47	2.16	0.52	0.14	0.05	0.02	0.001	7.2	0.43	0.19	100.06	5	5	9	107	308	6	35	277	5	187	46	107
A2(1-5)Rb	ref	63.5	19.03	3.81	2.38	1.35	2.08	0.55	0.15	0.06	0.01	0.005	7.2	0.38	0.26	100.08	7	5	4	76	442	1	28	289	3	206	46	130
A211Rb	ref	62.8	19.01	3.70	2.30	1.27	2.06	0.51	0.14	0.05	0.01	0.002	8.2	0.36	0.26	100.1	5	5	4	69	240	1	27	270	3	185	47	129
A224Rb	ref	63.4	19.68	3.70	2.39	1.17	2.14	0.51	0.14	0.05	0.01	0.001	6.6	0.37	0.13	99.93	<5	6	<10	74	258	<5	32	275	<20	192	45	94
A233Rb	ref	63.7	19.13	3.74	2.35	1.30	2.09	0.53	0.15	0.05	0.01	0.001	7.1	0.34	0.28	100.1	5	5	4	82	257	1	29	276	3	200	47	135
A234Rb	ref	64.1	19.28	3.64	2.33	1.21	2.09	0.53	0.14	0.04	0.01	0.002	6.4	0.37	0.14	99.93	<5	5	<10	103	395	<5	33	287	<20	187	44	90
Reference mean		*63,50*	*19.23*	*3.72*	*2.35*	*1.26*	*2.09*	*0.53*	*0.14*	*0.05*	*0.01*	*0.002*	*7.10*	*0.36*	*0.21*	*100.0*		*5.2*		*81*	*318*		*30*	*279*		*194*	*46*	*115*

Table 9-11 Exchangeable cations and mean Cu-CEC ($cmol^+/kg$ dry matter) of bulk samples from block 16 (additive of K-feldspar) of the LOT A2 parcel. Data for the mean of five reference samples are also included. Cations extracted by exchange with NH_4^+ in alcoholic solution.

Sample id	Additive	Ca		K		Mg		Na		Sum	mean Cu-CEC
		$cmol^+/kg$	%	$cmol^+/kg$	%	$cmol^+/kg$	%	$cmol^+/kg$	%	$cmol^+/kg$	$cmol^+/kg$
LA216B/CS4b	K-feldspar	18	23	1.4	1.8	6.6	8	53	67	79	78
LA216CS4b	K-feldspar	16	21	1.3	1.7	5.5	7	52	70	75	80
LA216B/CS6b	K-feldspar	19	24	1.4	1.7	6.0	7	54	67	80	78
LA216CS6b	K-feldspar	17	23	1.3	1.7	5.4	7	53	69	77	79
LA2Rb-mean		16	22	1.3	1.7	5.30	7	53	69	76	81

The <2μm fractions of the samples from block 16 have - irrespective of the position relative the feldspar plug – a slightly higher potassium content (ca. 0.02-0.04 % higher) compared to other hot blocks and compared to the references (Table 9-12). Potassium in the clay fraction probably exists mainly in a non-exchangeable form since the clay was saturated with sodium prior to the chemical analysis. Mica/illite and feldspars are the only potassium–bearing minerals that have been identified in MX80 bentonite but their quantities in the <2μm fraction are below the detection limit of the XRD-method, as shown by the XRD-traces in Figure 9-37 and Figure 9-37.

A mixed-layering of the smectite with illitic layers is an alternative source of potassium and if significant enough, mixed-layering will affect the X-ray diffraction characteristics of the clay. The homo-ionic Mg-clays of both block samples and references have a basal spacing of ca. 15 Å when air-dried (relative humidity 50±10%) and expand to 16.9 Å upon ethylene glycol solvation (EG) (Figure 9-37 and Figure 9-37). A close-up of the expanded (001) basal reflections is presented in Figure 9-37. The series of basal reflections of the smectite and the parameter $\Delta 2\theta_{002/003}$ (the difference between the (002) and (003) peaks in degrees 2θ) are indicated in Figure 9-37. Both the rationality of the basal reflections and a $\Delta 2\theta_{002/003}$ value ranging from 5.24 to 5.28 indicate a smectite with virtually no interstratification /Moore & Reynolds 1989/. Thus, the diffraction characteristics give no evidence that the illitic component has increased in block 16. On the other hand, a potassium content of 0.13% K_2O corresponds to ca. 2 % illitic layers at most. Such small a proportion of illitic layers in an I/S structure may not be detectable by routine XRD analysis.

Table 9-12 Chemical composition of the Na-saturated <2µm fraction of samples from blocks with additives (block 16 with K-feldspar, 24 and 34 with cement) together with three reference samples for the LOT A2 parcel. Major and minor elements by ICP-AES (minor elements in reference samples by ICP-MS, which explains differences in detection limits), S and C by evolved gas analysis. SICADA test code LA2EAc.

Sample id	SiO_2	Al_2O_3	Fe_2O_3	MgO	CaO	Na_2O	K_2O	TiO_2	P_2O_5	MnO	Cr_2O_3	LOI	TOT/C	TOT/S	SUM	Ba	Cu	Zn	Ni	Co	Sr	Zr	Ce	Ta
	%	%	%	%	%	%	%	%	%	%	%	%	%	%	%	ppm	ppm	ppm	ppm	ppm	ppm	ppm	ppm	ppm
A216B/CS4c	63.60	20.48	3.76	2.35	0.28	2.23	0.13	0.13	0.02	<.01	0.001	6.9	0.20	<.01	99.95	33	<10	67	<5	5	22	149	111	<20
A216CS4c	64.69	20.33	3.72	2.32	0.07	2.35	0.13	0.13	0.02	<.01	<.001	6.1	0.21	0.01	99.92	37	<10	34	<5	<5	21	150	120	<20
A216CS4c-2	64.66	20.49	3.77	2.33	0.07	2.35	0.14	0.13	0.03	<.01	<.001	5.9	0.22	<.01	99.93	35	<10	35	<5	<5	21	153	93	<20
A216B/CS6c	64.88	20.83	3.72	2.34	0.06	2.37	0.12	0.13	0.02	<.01	<.001	5.4	0.21	<.01	99.93	25	<10	32	6	<5	<20	152	82	<20
A216CS6c	64.47	20.44	3.76	2.33	0.10	2.30	0.12	0.13	0.02	<.01	0.002	6.2	0.19	<.01	99.93	25	<10	53	<5	<5	20	151	81	<20
A224B/CS2c	63.02	20.43	3.64	2.37	0.03	2.37	0.08	0.13	0.02	<.01	0.001	7.8	0.24	<.01	99.93	17	21	32	<5	<5	<20	149	69	<20
A224CS2c	64.28	20.80	3.66	2.36	0.04	2.40	0.08	0.13	0.03	<.01	<.001	6.1	0.26	0.01	99.93	17	22	38	7	<5	<20	148	84	<20
A224B/CS7c	64.51	20.69	3.77	2.39	0.03	2.33	0.10	0.13	0.02	<.01	<.001	5.9	0.33	<.01	99.93	23	10	30	<5	<5	<20	154	97	<20
A224CS7c	64.09	20.36	3.67	2.32	0.03	2.34	0.10	0.13	0.03	<.01	<.001	6.8	0.28	<.01	99.92	19	23	29	<5	<5	<20	154	92	<20
A234A/BS5c	64.21	20.52	3.61	2.49	0.03	2.37	0.10	0.13	0.03	<.01	<.001	6.4	0.27	<.01	99.93	18	<10	22	<5	<5	<20	145	92	<20
A234AS5c	64.61	20.48	3.58	2.35	0.02	2.29	0.10	0.13	0.03	<.01	<.001	6.3	0.33	<.01	99.94	21	15	22	<5	<5	<20	148	96	<20
A234A/BS7c	64.26	20.39	3.64	2.53	0.02	2.29	0.09	0.13	0.02	<.01	<.001	6.5	0.34	<.01	99.91	16	13	20	<5	<5	<20	146	98	<20
A234AS7c	64.72	20.40	3.57	2.33	0.03	2.27	0.11	0.13	0.03	<.01	<.001	6.3	0.28	<.01	99.94	21	<10	23	<5	<5	<20	149	94	<20
A2(1-5)Rc	64.06	21.06	3.56	2.36	0.03	2.18	0.08	0.12	0.03	0.01	0.001	6.4	0.39	0.01	99.93	14	11	27	5	5	13	146	91	5
A211Rc	64.17	20.85	3.62	2.34	0.04	2.21	0.11	0.13	0.03	0.01	0.001	6.5	0.27	0.01	100.1	29	39	32	5	5	15	151	110	6
A233Rc	63.78	21.40	3.67	2.34	0.04	2.21	0.10	0.13	0.03	0.01	0.001	6.3	0.28	0.01	100.1	36	38	35	5	5	13	153	105	5
A233Rc-2	63.88	21.23	3.64	2.35	0.04	2.26	0.11	0.13	0.03	0.01	0.001	6.2	0.27	0.01	99.93	37	41	34	5	5	13	154	89	5
Reference	*63.97*	*21.14*	*3.62*	*2.35*	*0.04*	*2.22*	*0.10*	*0.13*	*0.03*	*0.01*	*0.00*	*6.35*	*0.30*	*0.01*	*100.0*	*29*	*32*	*32*	*5*	*5*	*13.5*	*151*	*99*	*5*

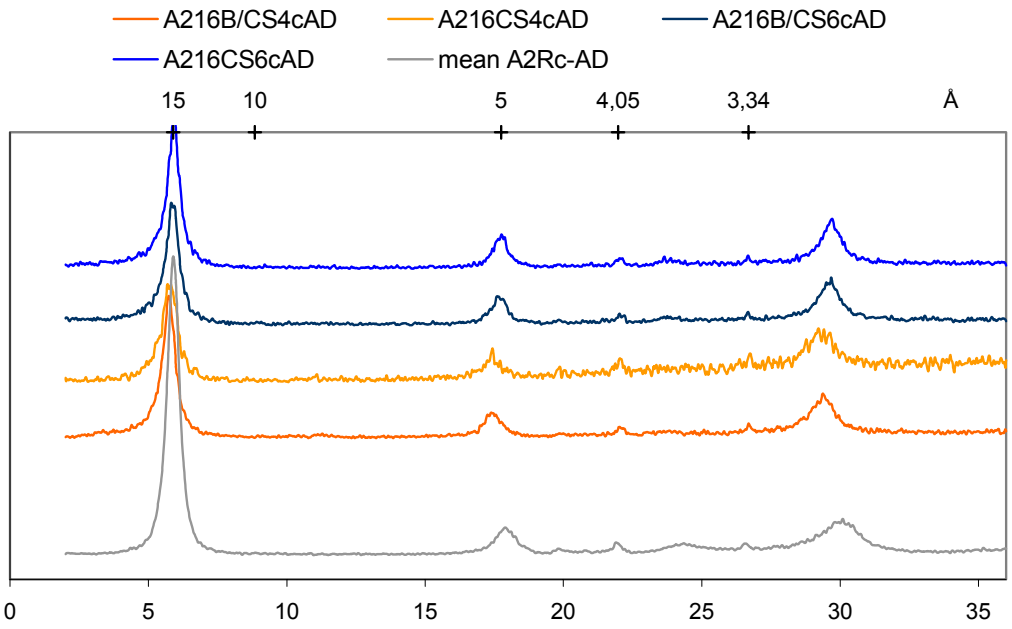

Figure 9-37 XRD-profiles of oriented aggregates of the Mg-saturated, air-dried (AD) clay fraction of samples of block 16 (additive of K-feldspar) from the LOT A2 parcel. Grey curve: Mean XRD-profile of the clay fraction of five reference samples. The positions of the strongest peaks of cristobalite (4.05Å), quartz (3.34Å) and mica/illlite (10Å) are indicated in the upper scale.; CuKα radiation.

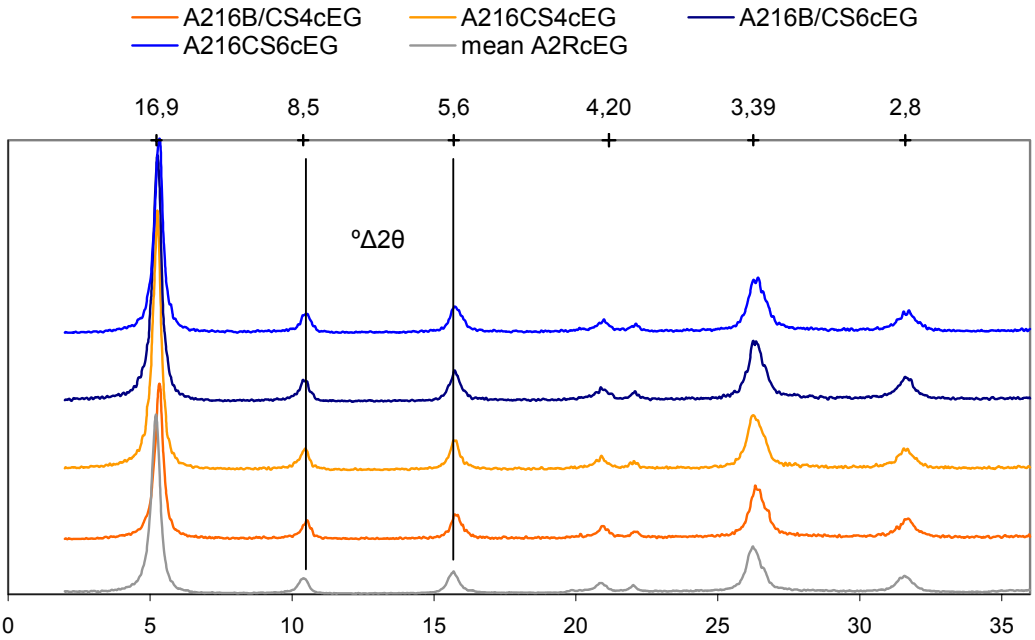

Figure 9-38 XRD-profiles of oriented aggregates of the Mg-saturated, ethylene glycol solvated (EG) clay fraction of samples of block 16 (additive of K-feldspar) from the LOT A2 parcel. Grey curve: mean XRD-profile of the clay fraction of five reference samples. The rational series of smectite reflections is indicated in the upper scale. The measure °Δ2θ is also indicated (cf. text). CuKα radiation.

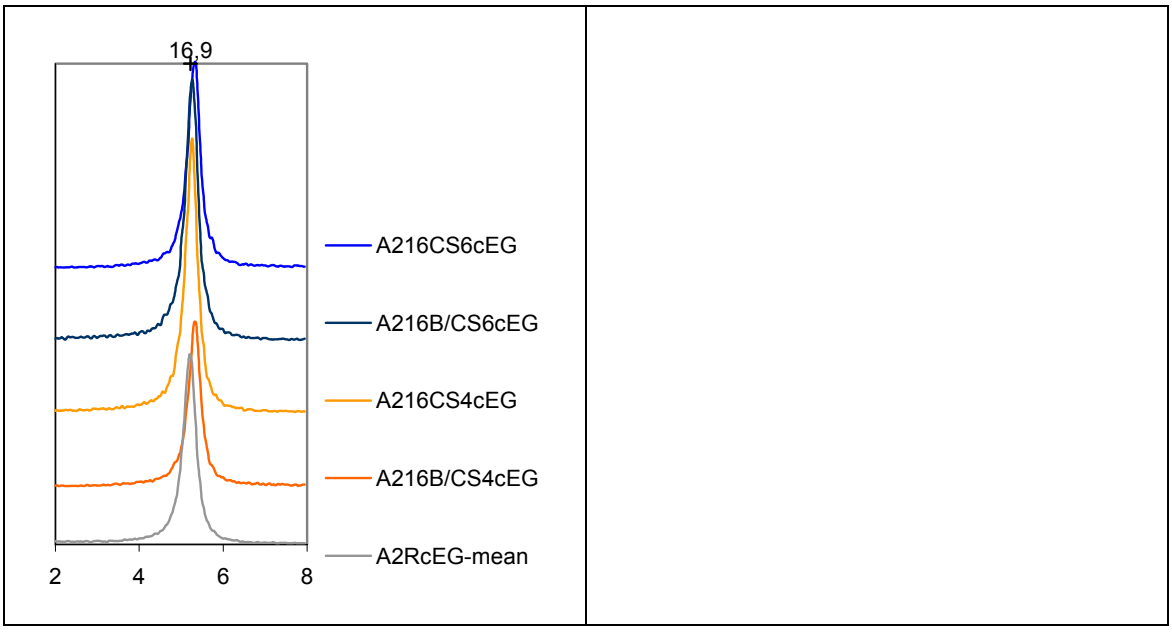

Figure 9-39 Close-up of the 17 Å region of EG-solvated, Mg-saturated clay fractions from block 16 of the LOT A2 parcel. Grey curve: Mean XRD-profile of the reference samples. Cu Kα radiation.

An increase of the fixed interlayer potassium content would also affect the exchange properties of the clay mineral. As shown in Table 12, the CEC values of the clay fractions of samples from block 16 are in the same range as that of the references, but, again, the effect of a gain of less than 0.05 % K_2O on CEC can probably not be detected in any conventional CEC determinations.

9.3.2.3. Blocks 24 and 34 with additive of cement

In fresh cement, extreme pH conditions will develop due to the presence of alkali bases, but pH will stabilize around 12.5 supported by portlandite ($Ca(OH)_2$) in the matured cement. The effects on bentonite of an exposure to these hyperalkaline pore fluids are well-documented e.g. /Karnland et al 2007/, /Savage et al. 2007/, /Trotignon et al. 2007/ and involve dissolution of both the accessory minerals and the clay minerals, which eventually may change fundamental physical and chemical properties of the buffer

Table 9-13 Cation exchange capacity (Cu-CEC) of the <2µm fraction of samples from block 16 and of the reference samples for the LOT A2 parcel.

Sample id	Cu-CEC 1	Cu-CEC 2	Mean Cu-CEC
	$cmol^+/kg$	$cmol^+/kg$	$cmol^+/kg$
A216CS4c	87	88	88
A216B/CS4c	88	85	87
A216CS6c	89	88	88
A216B/CS6c	88	88	88
A2R(1-5)c	87	86	87
A211Rc	86	87	87
A224Rc	88	88	88
A233Rc	87	86	87
A234Rc	88	87	88
Mean reference			*87*

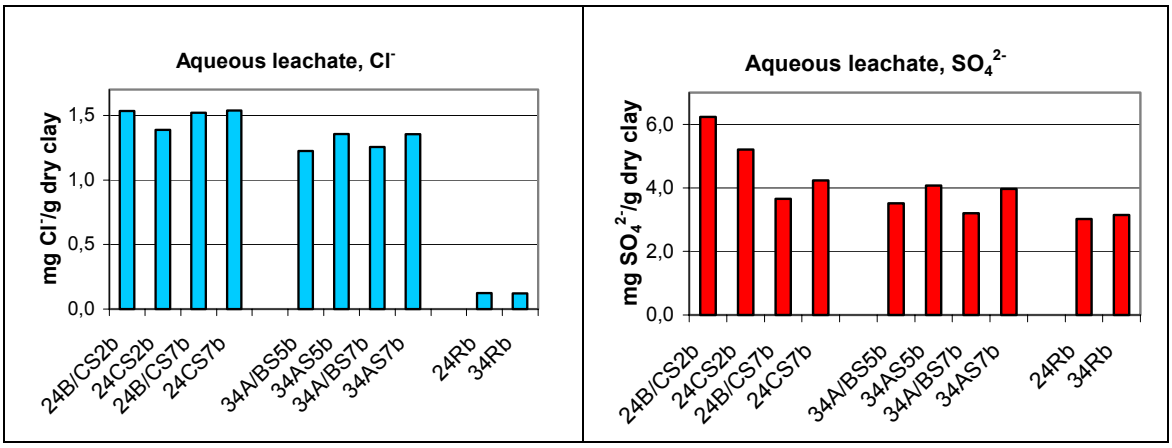

Figure 9-40 The concentration of Cl^- and SO_4^{2-} in water extracts of bulk samples from blocks 24 and 34 (additive of cement) of the LOT A2 parcel. Results for the reference samples for the blocks are shown to the right.

The two blocks 24 and 34 with plugs of Portland cement represent different temperature regimes. Block 24 has been exposed to intermediate temperatures (50-70º C) and the two sampled positions to temperatures in the range 50-60 and 60-70º C, respectively. The sampled positions in block 34 were never exposed to temperatures exceeding 30º C.

The chemical data on non-reactive solutes/water-soluble salts are listed in Table 9-14. Focus is laid on the major anions chloride and sulfate since the concentrations of the cations are strongly affected by the exchange reactions that take place when cations are released from dissolving accessory minerals during the contact with water. In addition, a strong correlation (R^2=0.98) between cations such as Al and Fe suggests that the source are ultra-fine clay particles which the filtering method failed to remove from the solution.

The data for chloride and sulfate are compiled in Fig. 40. Consistent with the results for the standard blocks, the chloride concentration in the bentonite from blocks 24 and 34 has increased significantly due to the saturation with Äspö groundwater.

Also the sulfate distribution in the samples from block 24 and 34 appears to match the distribution pattern in the standard blocks. Thus, the sulfate concentration in the cool block 34 has changed little under the long-term-test conditions, whereas the bentonite 1.5-3.5 cm from the heater in block 24 has gained sulfate and thus appears to correspond to the "zone" of anhydrite precipitation observed in other hot standard blocks. This general pattern is confirmed by the data on total S in the bulk bentonite (Figure 9-41 and Table 9-10) but neither anhydrite nor any other Ca sulfates can be detected in the XRD traces of the samples (Figure 9-42).

Selected chemical data on the bulk samples (Table 9-10) have been re-calculated on a molar, water-free basis and compiled in the bar graph in Figure 9-41, which shows the loss/gain in Ca, Mg, S and C relative to the average reference sample. The most conspicuous alterations are seen in block 34, where both Ca and Mg have increased in the samples proximal to the cement plug, whereas the distal samples are depleted in Mg. Mg has most likely been supplied by dissolution of montmorillonite, which is the main source of Mg in the bentonite.

The samples have gained also some carbon, probably existing as a carbonate phase, but the balance between the cation - anion equivalents is poor, which suggests that other

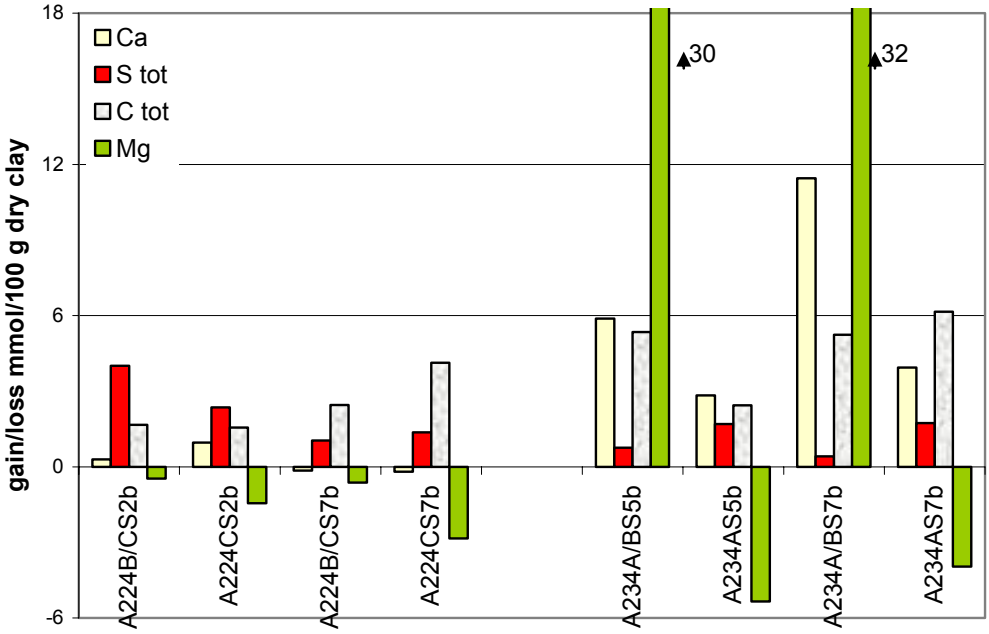

Figure 9-41 Bar graph showing the loss/gain relative to the mean reference in total Ca, Mg, S and C in bulk samples of blocks 24 and 34 (additive of cement) from the LOT A2 parcel.

counter-ions, such as hydroxide, exist. pH in the samples was not measured but a parallel study of the porewater composition in block 24 demonstrates a clear gradient in pH from distal (relative the plug) to proximal positions, as can be expected.

XRD-traces of random powders of the bulk samples are presented in Figure 9-41. The XRD profiles of the contact samples from block 34 display a clear reduction in the peak intensities of cristobalite (marked by arrows in Figure 9-41), indicating dissolution. This is consistent with the results reported by /Karnland et al., 2007/ in an experimental study on the interaction of hyperalkaline solutions with compacted bentonite.

Mg-rich minerals like sepiolite, brucite and hydrotalcite have been reported as potential secondary products of the cement/bentonite interaction, e.g. /Trotignon et al. 2007/, but no neoformed phases serving as sinks for magnesium have been identified with certainty. Several "new" reflections of low intensity appear in the XRD-traces of both blocks and some of these may be produced by cation–disordered, mixed carbonates, the d-values of which show an almost linear relation with composition. Tentatively, the strongest peaks of the magnesium end-member of Ca-Mg carbonates have been indicated in the trace of one of the contact samples from block 34 (Figure 9-41). It should also be emphasized that several of the potential reaction products of the interaction of cement pore fluids with bentonite (e.g. calcium silicate hydrates, CSH) tend to be X-ray amorphous due to poor crystallinity.

Table 9-14 Major anions and cations (mg/g dry clay) extracted by dispersion of bentonite in deionised water in a solid:liquid ratio of 1:100. Data for blocks 24 and 34 from the LOT A2 parcel together with reference samples for the blocks. SICADA test code LA2WA.

Sample id	Additive	Al	Ca	Cu	Fe	K	Mg	Na	S	Si	TotC	TotN	Cl	Br	NO_3-N	SO_4-S
mg/g dry clay																
A224B/CS2b	cement	0.078	0.045	0.001	0.020	0.159	0.021	7.042	2.082	1.151	1.870	0.115	1.535	0.004	0.039	1.864
A224CS2b	cement	0.080	0.042	0.001	0.021	0.123	0.019	5.620	1.737	0.676	1.207	0.112	1.389	0.007	0.037	1.698
A224B/CS7b	cement	0.214	0.046	0.001	0.055	0.123	0.042	6.053	1.219	1.534	1.852	0.112	1.519	0.004	0.040	1.328
A224CS7b	cement	0.094	0.040	0.001	0.024	0.119	0.022	5.672	1.414	0.812	1.499	0.096	1.539	0.008	0.041	1.553
A234A/BS5b	cement	0.236	0.030	0.001	0.057	0.101	0.044	5.051	1.171	1.474	1.226	0.105	1.223	0.007	0.039	1.180
A234AS5b	cement	0.201	0.047	0.001	0.047	0.097	0.037	4.872	1.358	1.195	1.119	0.115	1.357	0.007	0.039	1.386
A234A/BS7b	cement	0.229	0.031	0.001	0.057	0.105	0.047	5.245	1.070	1.592	1.382	0.122	1.254	0.006	0.041	1.182
A234AS7b	cement	0.247	0.046	0.001	0.060	0.110	0.045	4.896	1.324	1.414	1.080	0.112	1.354	0.008	0.038	1.436
A224Rb	ref	0.112	0.026	0.000	0.026	0.089	0.023	3.866	1.008	0.864	1.128	0.096	0.124	0.000	0.042	1.128
A234Rb	ref	0.115	0.024	0.000	0.026	0.084	0.021	3.989	1.050	0.878	1.170	0.107	0.122	0.004	0.042	1.142

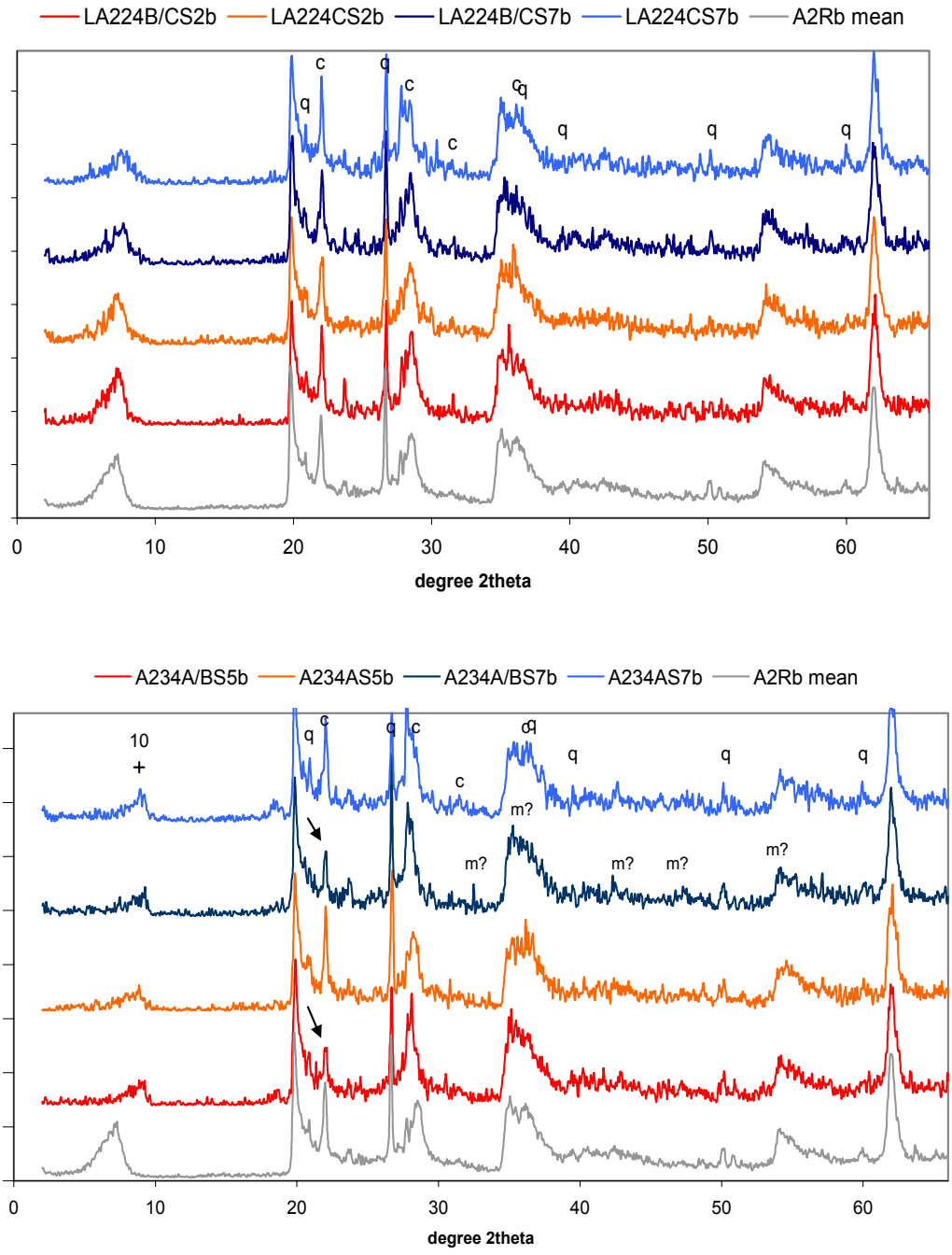

Figure 9-42 XRD-profiles of samples from block 24 (top) and 34 (bottom) of the LOT A2 parcel. Grey curve: mean XRD-profile of five reference samples. The position of the strongest peaks of the major non-clay minerals are indicated; q=quartz, c=cristobalite. Arrows indicate the strongest peak of cristobalite (cf. text). The position of the strongest peaks of magnesium carbonate (m?) is also indicated (cf. text). Random powder of bulk samples; CuKα radiation

Table 9-15 Exchangeable cations and mean Cu-CEC ($cmol^+/kg$ dry matter) of bulk samples from blocks 24 and 34 (additive of cement) of the LOT A2 parcel. The mean of five reference samples are also included. Cations extracted by exchange with NH_4^+ in alcoholic solution.

Sample id	Additive	Ca		K		Mg		Na		Sum	mean Cu-CEC
		$cmol^+/kg$	%	$cmol^+/kg$	%	$cmol^+/kg$	%	$cmol^+/kg$	%	$cmol^+/kg$	$cmol^+/kg$
LA224B/CS2b	cement	15	19	1.5	1.8	6.8	8	58	71	81	78
LA224CS2b	cement	14	18	1.4	1.8	6.3	8	56	72	78	77
LA224B/CS7b	cement	15	19	1.4	1.7	6.9	9	56	71	80	78
LA224CS7b	cement	15	18	1.4	1.7	6.8	8	58	72	81	78
LA234A/BS5b	cement	21	26	1.5	1.8	2.1	2	58	70	83	78
LA234AS5b	cement	18	24	1.4	1.8	2.3	3	54	71	76	78
LA234A/BS7b	cement	24	28	1.5	1.7	2.6	3	58	67	86	79
LA234AS7b	cement	20	26	1.4	1.8	2.4	3	53	69	77	79
LA2Rb-mean		16	22	1.3	1.7	5.30	7	53	69	76	81

Data on the cation exchange capacity of the bulk samples and the exchangeable cations are listed in Table 9-15 and have also been compiled in Figure 9-43. All bulk samples from block 24 and 34 have CEC values that are 2-4 units lower than the mean reference sample. The composition of the pool of exchangeable cations has changed in both blocks but evolved differently. Exchangeable Mg has increased in block 24, whereas an increase of exchangeable Ca is paralleled by a decrease in Mg in block 34.

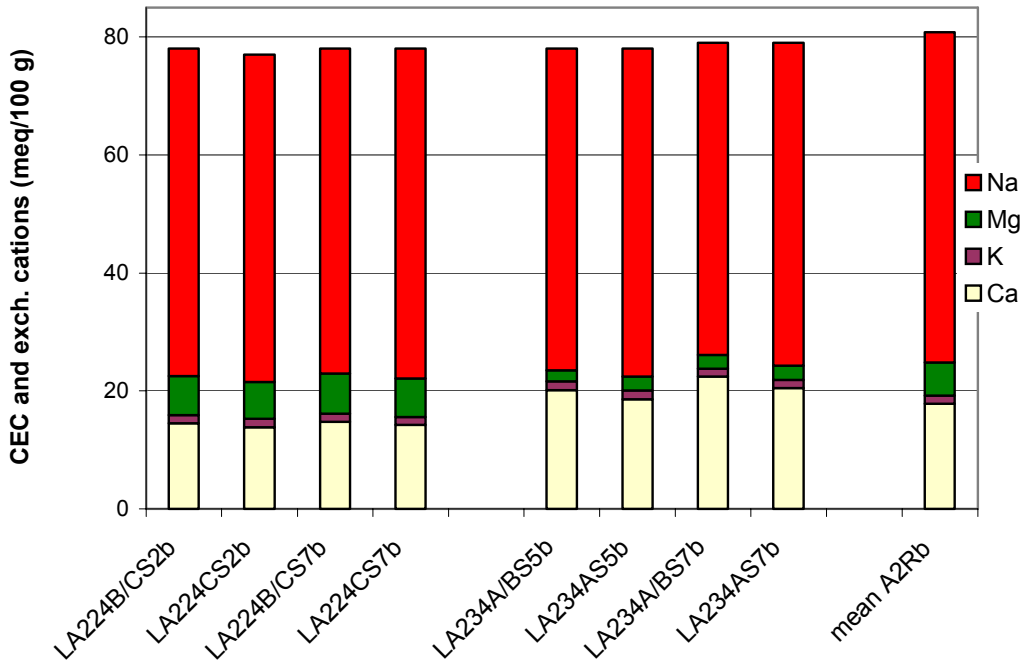

Figure 9-43 Bar graph showing the CEC and the relative distribution of exchangeable Na, K, Ca and Mg in samples from blocks 24 and 34 (additive of cement) of the LOT A2 parcel.

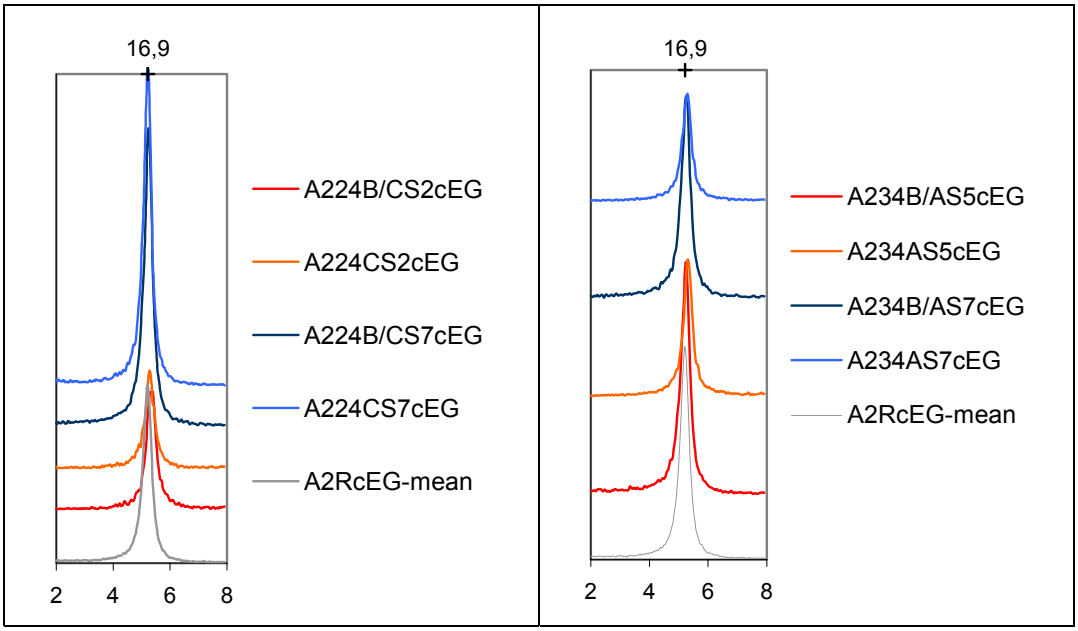

Figure 9-44 Close-up of the 17 Å region of EG-solvated, Mg-saturated clay fractions from block 24 and 34 (additive of cement) of the LOT A2 parcel. Grey curve: Mean XRD-profile of the reference samples. Cu Kα radiation.

The low concentration of exchangeable Mg in block 34 suggests that porewater concentrations were controlled by the precipitation of some Mg-bearing phase(s) of

low solubility. It is evident from the chemical composition of the <2μm fraction (Table 9-12) that the Mg content of the clay fraction from the proximal positions remains augmented despite the pre-treatments prior to the chemical analysis (i.e. removal of carbonates, saturation by Na and dialysis). The source of this extra Mg has not been identified.

XRD-profiles of oriented mounts of the air-dried and EG-solvated clay fractions are shown in Figure 9-45 to Figure 9-458 and a close-up of the expanded first order peak is shown in Figure 9-45.

The diffraction patterns of the air-dried samples from the blocks match the basic features of the pattern of the reference, but the higher order basal reflections of the two contact samples from block 34 are broader and somewhat displaced (Figure 9-457). Both peak broadening and peak displacement may be indications of mixed-layering or small crystallite size. However, the EG-solvated clays produce a rational series of basal reflections and the expansion behavior and d-values are essentially the same as those of the reference, indicating a more or less pure smectite.

Table 9-16 Cation exchange capacity ($cmol^+/kg$ dry matter) of the <2μm fraction of samples from block 24 and 34 with additive of cement from the LOT A2 parcel. The mean of the reference samples for the A2 parcel is included.

Sample id	Cu-CEC 1	Cu-CEC 2	Mean Cu-CEC
	$cmol^+ kg^{-1}$	$cmol^+ kg^{-1}$	$cmol^+ kg^{-1}$
A224CS2c	84	84	84
A224B/CS2c	84	84	84
A224CS7c	83	82	83
A224B/CS7c	83	81	82
A234AS5c	84	85	84
A234A/BS5c	91	92	92
A234AS7c	No data	No data	No data
A234A/BS7c	91	91	91
A2Rc-mean			87

The relative peak intensities are anomalous in some of the samples from both block 24 and 34 (compare, for instance, A224B/C2c and A224B/C7c). The relative intensities of the *00l* reflections are controlled by chemical composition and the positions of atoms in the unit cell but are also affected by properties of the sample preparation, maybe first of all the degree of preferred orientation of the clay minerals. Variations in preferred orientation may arise, for instance, if samples are not equally well dispersed by the pre-treatments applied.

The CEC of the <2 μm fractions (Table 9-15) is generally lower than the CEC of the reference samples. The contact samples from block 34 are exceptions from the trend, having higher CEC than the references. A diminished “dilution” by cristobalite due to dissolution may explain some of the increase in CEC, but more detailed analyses will be required to identify other alteration processes that may have contributed to the increase in charge. The observation reported by /Karnland et al., 2007/ that increasing CEC values were connected to an increased tetrahedral charge, i.e. to a beidellitization of the montmorillonite, may be relevant also in the LOT A2 context.

9.3.3. Summary and conclusions

The mineralogy and chemical composition of bentonite samples from five blocks (blocks 10, 12, 16, 24 and 34) with additives of calcite, gypsum, K-feldspar and cement, respectively, have been studied. The major conclusions of the study are:

- calcium sulfate has been redistributed from the gypsum plug along the thermal gradient and accumulated as anhydrite in the warmer, inner part of the block, although the available data for block 12 are for two block positions only. The re-precipitation has increased the sulfur content in the bentonite volume proximal to the plug by a factor 3-4 compared to the reference bentonite. Accordingly, an increased inventory of soluble sulfates in the bentonite can be expected to give more massive salt accumulations in the warmer parts of the buffer, which will affect the porosity and rheology of the bentonite
- the data for two positions in block 10 with calcite plugs provide no evidence that calcium carbonate has been redistributed in a similar way as calcium sulfate. However, a sampling strategy which allows higher resolution may be necessary to verify the results.
- the addition of K-feldspar to the bentonite of block 16 seems to have had no effect on any of the clay properties investigated. Thus, the exchange properties and the exchange complex as well as the X-ray diffraction characteristics of the clay from the block are essentially the same as those of the references.
- the two blocks with cement plugs (24 and 34) represent different temperature regimes. The most conspicuous chemical alterations are seen in the cool block 34. The XRD profiles display a clear reduction in the peak intensities of cristobalite in the samples proximal to the cement, indicating dissolution. Ca and Mg have increased in the same samples, whereas the samples distal to the cement plug are depleted in Mg. Mg is most likely derived from the main Mg-bearing mineral montmorillonite but the reaction products serving as sinks for magnesium in the proximal samples have not been identified with certainty, possibly because reaction products are of poor crystallinity. The pool of exchangeable cations has changed in both blocks but evolved differently. The clay fraction of the contact samples from block 34 are distinguished also by higher CEC than the references. A diminished “dilution” by cristobalite due to dissolution may explain some of the increase in CEC, but more detailed analyses will be required to identify other alterations that may have contributed to the increase in charge.

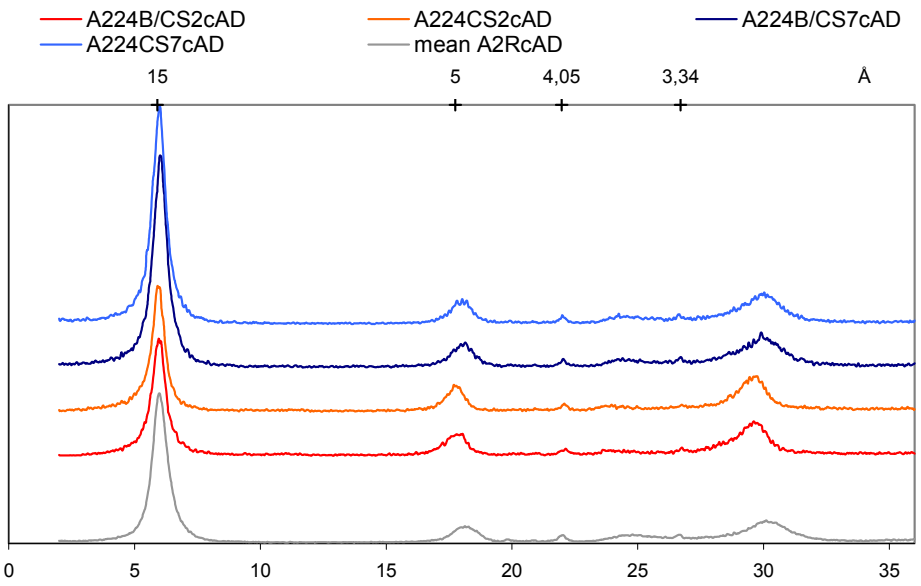

Figure 9-45 XRD-profiles of oriented mounts of the Mg-saturated, air-dried clay fraction of samples of block 24 (additive of cement) from the LOT A2 parcel. Grey curve: mean XRD-profile of the clay fraction of five reference samples. The positions of the strongest peaks of cristobalite (4.05Å), quartz (3.34Å) are indicated in the upper scale; CuKα radiation.

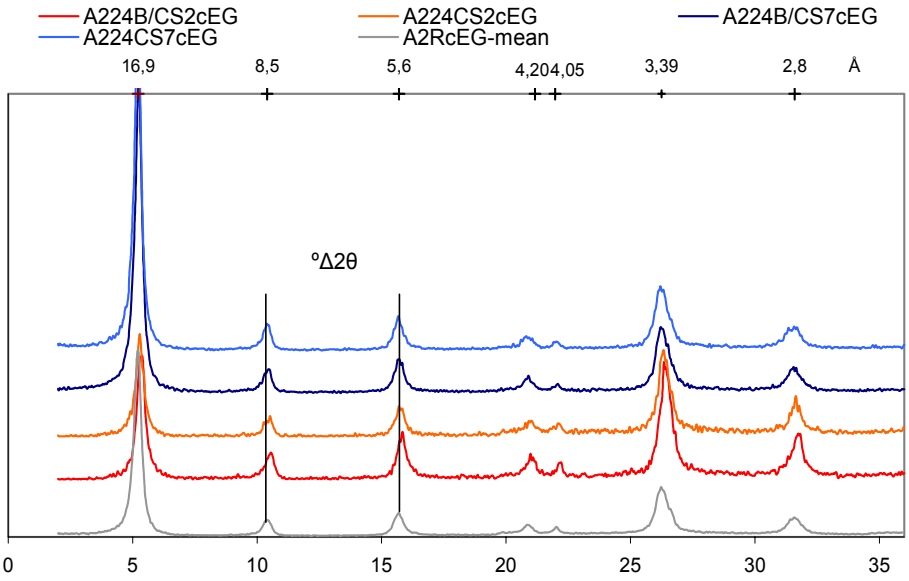

Figure 9-46 XRD-profiles of oriented mounts of the Mg-saturated, ethylene glycol solvated clay fraction of samples of block 24 (additive of cement) from the LOT A2 parcel. Grey curve: mean XRD-profile of the clay fraction of five reference samples. The rational series of smectite reflections is indicated in the upper scale together with the position of the strongest peak of cristobalite (4.05Å). The measure °Δ2θ is also indicated (cf. text). CuKα radiation.

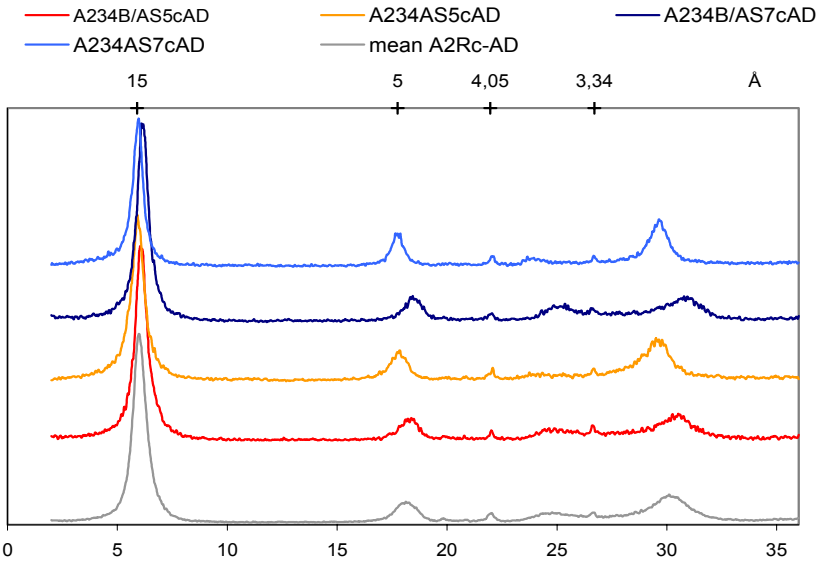

Figure 9-47 XRD-profiles of oriented aggregates of the Mg-saturated, air-dried clay fraction of samples of block 34 (additive of cement) from the LOT A2 parcel. Grey curve: Mean XRD-profile of the clay fraction of five reference samples. The positions of the strongest peaks of cristobalite (4.05Å) and quartz (3.34Å) are indicated in the upper scale.; CuKα radiation.

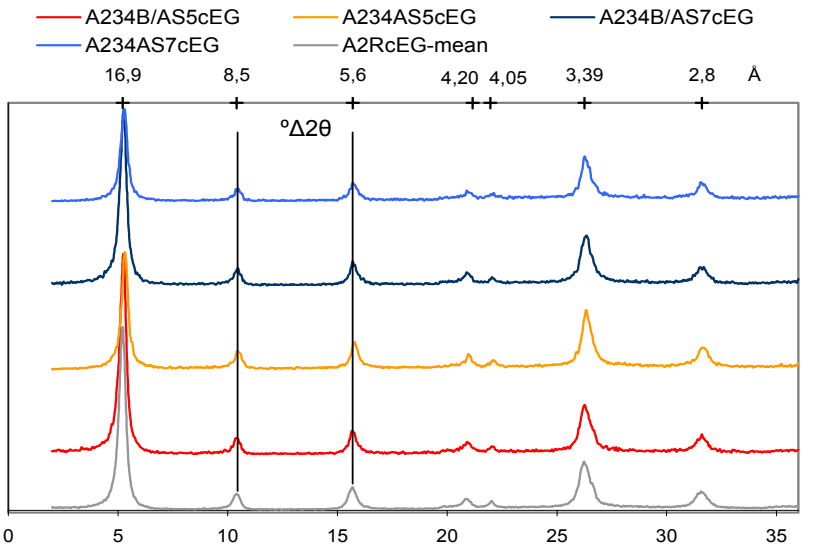

Figure 9-48 XRD-profiles of oriented aggregates of the Mg-saturated, ethylene glycol solvated clay fraction of samples of block 34 (additive of cement) from the LOT A2 parcel. Grey curve: Mean XRD-profile of the clay fraction of five reference samples. The series of smectite reflections is indicated in the upper scale together with the position of the strongest peak of cristobalite (4.05Å). The measure °Δ2θ is also indicated. CuKα radiation.

REFERENCES

Aagard P., Helgeson H.C., 1983. Activity/Composition Relations Among Silicates in Aqueous Solutions II. Clays and Clay Minerals 31 (1983) 207.

Abercrombie H.J., Hutcheon I. E., Bloch J.D. and de Caritat P., 1994. Silica activity and the smectite-to-illite reaction. Geology, v. 22, p 539-542

Ammann, L., Bergaya, F. & Lagaly, G. 2005: Determination of the cation exchange capacity of clays with copper complexes revisited. Clay Minerals 40. 441-453.

Arfvidsson J., Claesson J., Hökmark H., 2000. Method to verify numerical THM-models. SKB TR in print, SKB, Stockholm, Sweden.

Belyayeva, N.I. 1967: Rapid method for the simultaneous determination of the exchange capacity and content of exchangeable cations in solonetzic soils. Soviet Soil Science. 1409-1413.

Birgesson and Karnland 2008

Boles J.R. and Franks S.G., 1979. Clay diagenesis in the Wilcox Sandstones of southwest Texas. J. sed. Petrol. 49, 55-70.

Birgersson, M. & Karnland, O.: Ion concentration discontinuities across bentonite/external solution interfaces. Accepted for publication in Geochimica et Cosmochimica Acta.

Brindley, G.W. & Brown, G. 1980: Crystal Structures of Clay Minerals and their X-ray Identification. Mineralogical Society Mon. No. 5. 495 p.

Börgesson L., Johannesson L.-E., Sandén T., Hernelind J., 1995. Modelling of the physical behaviour of water saturated clay barriers. SKB TR 95-20, SKB, Stockholm, Sweden.

Börgesson L., Johannesson L.-E. 1995. Thermo-hydro-mechanical modelling of water unsaturated buffer material. SKB TR 95-32, SKB, Stockholm, Sweden

Börgesson L., Hernelind J., 1999. Coupled thermo-hydro-mechanical calculations of the water saturation phase of a KBS-3 deposition hole. Influence of hydraulic rock properties on the water saturation phase. SKB Technical Report TR-99-41.

Börgesson L., Johannesson L.-E., Hernelind J., 2003. Earthquake induced rock shear through a deposition hole. Effect on the canister and the buffer. SKB Technical Report TR-04-02.

Chapman, H.D. & Pratt, P.F., 1961. Methods of soil analysis for soils, plants and waters. Div. of Agr. Sci. University of California, Berkeley

Coutour R.A., 1985. Steam rapidly reduces the swelling capacity of bentonite. Nature, 318, 50-52.

Eberl D.D., Velde B. and McCormic T., 1993. Synthesis of illite-smectite from smectite at earth surface temperatures and high pH. Clay Minerals 28, 49-60.

Grauer R., 1986. Bentonite as a backfill material in the high-level wast repository: chemical aspects. NAGRA, Technical Report 86-12E.

Hower J., Eslinger E.V., Hower M.E. and Perry E.A., 1976. Mechanism of burial metamorphism of argillaceous sediments. Geol.Soc. Amer. Bull. 87 725-737.

Huang W.-L., Longo J.M. and Pevear D.R., 1993. An experimentally derived kinetic model for smectite-to-illite conversion and its use as a geothermometer. Clays and Clay Minerals 41, 162-177.

Hökmark H., 1995. Smectite-to-illite conversion in bentonite buffers; application of a technique for modeling degradation processes. SKB Arbetsrapport AR 95-07, Stockholm.

Hökmark H., Fälth B., 2003. Thermal dimentioning of the deep repository. Technical Report, TR-03-09, SKB 2003.

Jackson, M.L. 1975: Soil chemical analysis – advanced course. Second edition. Madison, Wisconsin, 991 p.

Johannesson L.-E., Bögesson L., Sandén T., 1995. Compaction of bentonite blocks. SKB TR 95-19. SKB Stockholm, Sweden.

Karnland O., Pusch R. and Sandén T., 1994. Effects of cyclic hydration/dehydration on Na and K bentonites. SKB Arbetsrapport AR 94-40, Stockholm.

Karnland O., Warfvinge P., Pusch R., 1995. Smectite-to-illite conversion models. SKB AR 95-27. SKB Stockholm, Sweden.

Karnland O. 1995:2. Salt redistribution and enrichment in compacted bentonite exposed to a thermal gradient. SKB AR 95-31, SKB, Stockholm, Sweden.

Karnland O. 1997. Cement/bentonite interaction - Results from 16 months laboratory tests. SKB TR 97-32, SKB Stockholm, Sweden.

Karnland, O., Sandén, T., & Johannesson L-E., Eriksen, T.E., Jansson, M., Wold, S., Pedersen, K., Mutamedi, M. & Rosborg, B. 2000: Long term test of buffer material. Final report on the pilot parcels. SKB Technical Report TR-00-22. Svensk Kärnbränslehantering AB, 131 p.

Karnland, O., Olsson, S., Nilsson, U. & Sellin, P. 2007: Experimentally determined swelling pressure and geochemical interactions of compacted Wyoming bentonite with highly alkaline solutions. Physics and Chemistry of the Earth 32, 275-286.

Karnland O and Birgersson M, 2006. Montmorillonite stability – With special respect to KBS-3 conditions, SKB TR 06-11, SKB, Stockholm, Sweden.

Meier, L.P. & Kahr, G. 1999: Determination of the cation exchange capacity (CEC) of clay minerals using the complexes of copper(II) ion with triethylenetetraamine and tetraethylenepentamine. Clays and Clay Minerals 47, 386-388.

Moore, D.M. & Reynolds, R.C. 1989: X-ray Diffraction and the Identification and Analysis of Clay Minerals. Oxford University Press. 332 p.

Motamedi M., Karnland O. and Pedersen K. 1995. Survival of bacteria in nuclear waste buffer materials - The influence of nutrients, temperature and water activity. SKB Technical Report 95-27. SKB Stockholm, Sweden.

Müller-Vonmoos M., Kahr G., 1983. Mineralogiche Untersuchungen von Wyoming Bentonit MX-80 und Montigel. NTB 83-12, Baden.

Newman, A.C.D. & Brown, G. 1987: The Chemical Constitution of Clays. In Newman, A.C.D. (ed): Chemistry of Clays and Clay Minerals. Mineralogical Society Mon. No. 6. 1-128.

Nilsson A.-C., 1995. Compilation of the groundwater chemistry data from Äspö. Progress Report 25-95-02, SKB, Stockholm.

Perry E.A. and Hower J., 1970. Burial diagenesis in Gulf Coast pelitic sediments. Clays and Clay Minerals 18, 165-178.

Pusch R., Karnland O., Hökmark H., Sandén T., Börgesson L. 1991. Final Report of the Rock Sealing Project- Sealing Properties and Longevity of Smectitic Clay Grouts. SKB TR Stripa Project 91-30. SKB Stockholm, Sweden.

Pusch R., Karnland O., Lajudie A., Bouchet A. 1992. Hydrothermal field test with french candidate clay embedding steel heater in the Stripa mine. SKB TR 93-02. SKB Stockholm, Sweden.

Savage, D., Walker, C., Arthur, R., Rochelle, C., Oda C. & Takase, H. 2007: Alteration of bentonite by hyperalkaline fluids. A review of the role of secondary minerals. Physics and Chemistry of the Earth 32, 287-297.

Trotignon, L., Devallois, V., Peycelon, H., Tiffreau, C. & Bourbon, X. 2007: Predicting the long term durability of concrete engineered barriers in a geological repository for radioactive waste. . Physics and Chemistry of the Earth 32, 259-274.

Weaver C.E., 1959. The clay petrology of sediments. Clays and Clay Minerals 6, 154-187.

Wersin P., Spahiu K., Bruno J. (1994) Kinetic modelling of bentonite-canister interaction. Long-term predictions of coper canister corrosion under oxic and anoxic conditions. SKB Technical Report 94-25. SKB Stockholm, Sweden.

Wersin P., Bruno J., Spahiu K. (1993) Kinetic modelling of bentonite-canister interaction. Implications for Cu, Fe and Pb corrosion in a repository for spent nuclear fuel. SKB Technical Report 94-25. SKB Stockholm, Sweden.